

INAUGURAL - DISSERTATION

Zur Erlangung der Doktorwürde

der Naturwissenschaftlich-Mathematischen
Gesamtfakultät

der

Ruprecht-Karls-Universität

Heidelberg

vorgelegt von

Budhaditya Chatterjee

aus Kalkutta, Indien

Tag der mündlichen Prüfung:

Tunneling Dynamics of Few-Boson Systems in Double-Well Traps

Gutachter:

Prof. Dr. Lorenz S. Cederbaum

Prof. Dr. Peter Schmelcher

Zusammenfassung

Gegenstand dieser Arbeit ist die ab-initio Untersuchung der Tunneldynamik von Wenig-Bosonen-Systemen in einem Doppeltopfpotential mit Hilfe der numerisch exakten "Multi-Configuration Time-Dependent Hartree" Methode (MCTDH). Zunächst studieren wir ein System bestehend aus Bosonen gleicher Spezies mit einer räumlich modulierten Wechselwirkung. Hierbei liegt der Schwerpunkt auf der Rolle von Inhomogenität und deren Einfluss auf das Tunneln. Die Dynamik variiert von Rabi-Oszillationen im Fall ohne Wechselwirkung über stark unterdrücktes Tunneln für mittlere Stärke der Wechselwirkung bis hin zum Wiederauftreten von Tunneln in der Nähe des Grenzwerts für Fermionisierung. Im Regime starker Korrelationen beobachten wir für sehr starke Wechselwirkungsinhomogenitäten Tunneln zwischen höheren Bändern. Für Systeme mit hoher Teilchenzahl wird ein vielseitigeres Verhalten gefunden. In Systemen mit mehr als zwei Bosonen können Tunnelresonanzen erzeugt werden durch die geeignete Wahl der Inhomogenität der Wechselwirkung. Diese Beobachtungen werden auf der Grundlage des Spektrums von wenigen Teilchen und stationären Eigenzuständen erklärt. Als Nächstes wird der geneigte Doppeltopf und sein Wechselspiel mit der Wechselwirkungsasymmetrie diskutiert. Wir zeigen, dass die Effekte der Wechselwirkung durch das Neigen kompensiert werden können, was zu Tunnelresonanzen führt. Danach diskutieren wir die Tunneldynamik von binären bosonischen Mischungen. Der Schwerpunkt liegt auf dem Einfluss der Wechselwirkung zwischen gleichen und unterschiedlichen Teilchenspezies beziehungsweise deren Wechselspiel. Für drei Anfangskonfigurationen wird die Dynamik studiert: vollständiges und teilweises Populationsungleichgewicht und einem phasenseparierten Zustand. Eine Erhöhung der Wechselwirkung zwischen gleichen Teilchenspezies führt zu einem starken Anstieg der Tunnelperiode analog zum "quantum self-trapping" für Kondensate. Abhängig von der Stärke der Korrelationen zwischen gleichen Teilchenspezies und der Anfangskonfiguration kann die Abstossung zwischen den unterschiedlichen Teilchenspezies die Tunnelperiode unterdrücken oder verstärken. Vollständig korreliertes Tunneln zwischen den zwei Teilchenarten und innerhalb der gleichen Spezies werden gezeigt, ebenso wie Mechanismen zur Trennung der unterschiedlichen Teilchenarten und "counterflow". Mit Hilfe des Viel-Teilchen Energiespektrums und der Eigenschaften der beitragenden stationären Zustände werden diese Effekte erklärt.

Abstract

In this thesis, the tunneling dynamics of a few boson system in a double-well is investigated from an ab-initio prospective using the numerically exact Multi-Configuration Time-Dependent Hartree method. We first study a system consisting of single species of bosons with a spatially modulated interaction. The main emphasis is on the role of inhomogeneity and its effect on the tunneling. The dynamics changes from Rabi oscillations in the non-interacting case to a highly suppressed tunneling for intermediate interaction strengths followed by a reappearance of tunneling near the fermionization limit. With extreme interaction inhomogeneity in the regime of strong correlations we observe tunneling between the higher bands. A richer behavior is found for systems with higher particle number. For systems with more than two bosons, the inhomogeneity of the interaction can be tuned to generate tunneling resonances. These observations are explained on the basis of the few-body spectrum and stationary eigenstates. A tilted double-well and its interplay with the interaction asymmetry is discussed next. We demonstrate that the effects of the interaction can be compensated by the tilt leading to tunneling resonances. We then explore tunneling dynamics of binary bosonic mixtures. The focus is on the role of the inter- and intra-species interactions and their interplay. The dynamics is studied for three initial configurations: complete and partial population imbalance and a phase separated state. Increasing the inter-species interaction leads to a strong increase of the tunneling time period analogous to the quantum self-trapping for condensates. The intra-species repulsion can suppress or enhance the tunneling period depending on the strength of the inter-species correlations as well as the initial configuration. Completely correlated tunneling between the two species and within the same species as well as mechanisms of species separation and counterflow are revealed. These effects are explained by studying the many-body energy spectra as well as the properties of the contributing stationary states.

Contents

1	Introduction	1
2	Modeling ultracold bosons in traps	7
2.1	Trapping potential	7
2.1.1	Atom-light interaction	8
2.1.2	Optical lattice	9
2.2	Interactions between the atoms	10
2.2.1	Pseudo-potential approximation	10
2.2.2	The effective one-dimensional description	11
2.2.3	Experimental control of interaction using Feshbach resonances	13
3	Theoretical approaches	17
3.1	Mean field theory and Gross Pitaevskii Equation	17
3.2	Bose-Fermi map	20
3.3	Bose-Hubbard Model	22
3.3.1	Bloch functions and Wannier basis	22
3.3.2	Derivation of Bose-Hubbard Hamiltonian	23
3.3.3	Phases of the Bose-Hubbard Model	25
3.3.4	Two-species Bose-Hubbard model	27
4	Numerical methods	31
4.1	Exact diagonalization	32
4.2	The standard time-dependent method	33
4.3	MCTDH method	34
4.3.1	MCTDH ansatz and equations of motion	34
4.3.2	Implementation	36
4.3.3	Application to few boson systems	38
5	Tunneling dynamics of single species bosonic system	41
5.1	Setup	42
5.1.1	Hamiltonian	42
5.1.2	Interactions	43

5.1.3	Scaling	43
5.2	Tunneling Dynamics for Two Boson System	44
5.2.1	Dynamics from the uncorrelated to the fermionization limit.	45
5.2.2	Analysis	46
5.2.3	Dynamics with varying inhomogeneity	48
5.2.4	Strong interaction inhomogeneity	49
5.3	Multi-Particle Dynamics	50
5.3.1	General behavior and mechanisms	51
5.3.2	Generating tunneling resonances by interaction inhomogeneity	52
5.3.3	Correlations	54
5.4	Asymmetric Double-Well	55
5.4.1	Generating tunneling resonances by a tilt.	55
5.4.2	Spectral Analysis	56
6	Tunneling dynamics of binary bosonic mixtures	59
6.1	Model and setup	59
6.2	Complete population imbalance.	61
6.3	Phase separated initial state.	67
6.4	Partial population imbalanced initial state.	69
7	Summary and outlook	73
A	Density matrices	77
A.1	General properties	77
A.2	One-body density	78
A.3	Two-body density	79
B	The double-well potential	81
B.1	Single particle states	81
B.2	Effective Hubbard model	83

Chapter 1

Introduction

The first experimental realization of Bose-Einstein condensation [1–3] has ushered a period of rapid advancement in the field of the ultra-cold atoms. This has in particular been facilitated by an impressive development in experimental techniques. Cooling methods such as laser or evaporative cooling [4] have enabled researchers to cool atoms to nano-Kelvin temperatures thereby opening the way for the creation of Bose-Einstein condensates (BEC). In this temperature regime, the de-Broglie wavelength is generally larger than the inter-particle distance and thus the quantum mechanical effects become much more prominent. Experiments in ultra-cold atoms thus serve as a tool-box to study an enormous diversity of quantum effects such as superconductivity, superfluidity, tunneling as well as non-linear phenomena like solitons and vortices.

The most important advantage of cold atoms is the high degree of controllability. Sophisticated trapping techniques allow the design external potentials of almost arbitrary geometry and parameters. With suitable combinations of electric and magnetic field and lasers, one can design multi-well potentials, lattices and even ring shaped potentials [5]. Moreover, even the interactions between the atoms can be tuned to arbitrary strengths using Feshbach resonances [6]. Thus it is possible to explore the full range of interactions, from non-interacting to strongly correlated atoms.

The dimensionality plays a crucial role in these studies. Often systems in lower dimensions display unique features thoroughly different from three-dimensional case. For instance, while an ideal Bose-gas does condense to form a BEC in three-dimension, this is not the case for lower dimension [7]. One intriguing effect seen in solely one dimension is a duality between boson and fermion known as the Bose-Fermi map [8]. According to this mapping, there exists a general isomorphy between a system of hard-core i.e. infinitely repulsively interacting boson (also known as Tonk-Girardeau gas) and a system of non interacting fermions and all observable local properties are identical. One can visualize the hard-core interaction as mimicking the exclusion principle and thus this effect is known as *fermionization*. Lieb and Liniger [9] solved the system of untrapped Bose gas in the thermodynamic limit for arbitrary interactions and reproduced

the phenomenon of fermionization in the limiting case of infinite interactions.

Experimentally, the way to achieve an effective one-dimensional system is by having a strong transverse confinement. In a seminal publication, Olshanii showed that under strong transverse confinement such that the particle could only move in the longitudinal direction, the effective one dimensional interaction between the atoms would strongly depend on the strength of the confinement [10]. This phenomenon, known as confinement induced resonance (CIR) provides an extremely useful tool for tuning interaction strength in one dimension and paved the way for the experimental realization of the Tonk-Girardeau gas [11, 12].

The Bose-Einstein condensate generally consists of a large number of atoms ($N \sim 10^5$) and are typically weakly correlated thus satisfying the necessary conditions for use of the Gross-Pitaevskii equation (GPE) [13, 14]. The basic assumptions of GPE are that the interactions are sufficiently low and the number of particles large enough to be able to employ the mean-field approximation. While these approximation hold for many cases, it is no longer valid for strong correlations or for few body systems. Moreover, the GPE treatment is unable to describe effects like fragmentation and thus for a more complete understanding one needs to go beyond the mean-field description.

The Bose-Hubbard model [15, 16] provides a very convenient framework for bosons in optical lattices and has been used to study stationary properties and transitions like superfluid-Mott transitions and predict exotic quantum phases such as Bose glass and Mott shell [17–26]. While, unlike the GPE, it does explain the fragmented condensate, it is also limited to the lowest band approximation and thus cannot describe strongly interacting systems.

To overcome these drawbacks of the theories based of the mean-field or lowest band approximations and understand the true physics without any a priori approximations, one requires to solve the many-body Schrödinger equation. One algorithm that provides a very general and efficient way to solve the Schrödinger equation exactly is the Multi-Configuration Time Dependent Hartree (MCTDH) method [27, 28]. This is designed primarily for distinguishable particles and one requires to modify it suitably for indistinguishable particles. Recently, there has been a development of MCTDH method exclusively for bosons (MCTDHB) [29, 30]. This method incorporates the bosonic permutation symmetry from the onset, and thus is highly optimal for the bosonic systems especially for systems having large number of particles. The MCTDHB has been used to study stationary properties such as fragmentation [31], coherence [32] as well as scattering properties [33] and dynamics [34–36].

The study of few-body systems are especially useful, not only since they are more feasible for ab-initio computations, but also because such systems enables us to understand the microscopic effects and mechanisms and provides a *bottom-up* prospective to the processes occurring in larger systems. Moreover, the few-body systems are not just confined to theoretical studies and recent experimental developments have enabled

persistent miniaturization, such that it is now possible to design and probe very small systems. Nowadays there are various techniques that enable the extraction and transport of few atoms [37, 38], their storage for instance using atom chip [39] as well as their imaging for analysis [37, 40]. This combination of theoretical approaches as well as experimental methods to the few body systems provides a new prospective to the understanding of the fundamental processes and uncover features such as three-body Efimov states [41].

The study of dynamics such as tunneling is especially thrilling and exemplify in particular the quantum nature at a fundamental level. For instance the tunneling dynamics of a Bose-Einstein condensate has been observed to undergo Josephson oscillations [42–44] in which the population simply tunnels back and forth between the two wells. However when the interaction is raised beyond a critical value the atoms remain trapped in one well, a non-linear phenomenon known as self trapping [42, 44, 45].

Theoretical approaches such as mean field Gross-Pitaevskii equation or the Bose-Hubbard model can explain the relevant physics in the low-interaction regime. However, to capture the rich physics present in the stronger interaction regime, we need to go beyond the lowest band approximation. An exact treatment solving the many-body Schrödinger equation is especially useful in understanding the entire crossover from the weakly to strongly interacting systems. For few boson in a double-well a numerically exact calculation reveals a transition from Rabi-oscillations to fragmented pair tunneling via a highly delayed tunneling process analogous to the self-trapping for condensates [46, 47].

While most of the studies focus on symmetric setups, the question of asymmetry is intriguing especially in the context of its role in the dynamics. Asymmetry could be induced in the system through the external potential such a tilted double well or one could have an asymmetry in the internal parameters such as the interaction strength. The former case of asymmetric double-wells has been explored in refs. [46–49]. The second scenario of having an interaction inhomogeneity is the focus of the first part of this thesis where we envision a new approach to asymmetry by introducing an inhomogeneous, i.e., spatially varying interaction strength. This can be achieved experimentally by employing magnetic field gradients in the vicinity of Feshbach resonances or by combining magnetic traps with optically induced Feshbach resonances [50, 51]. Using the numerically exact MCTDH method, we try to understand the role of the interaction inhomogeneity as well as interaction strength on the tunneling dynamics of few bosons [52].

While the single species bosonic system show very exciting and interesting effects, recently there has been a considerable interest in systems consisting of a bosonic mixture. These may correspond to different kinds of atoms or could be hyperfine states of the same atom species. Experimental [53–57] and theoretical [58–67] studies of stationary properties of bosonic binary mixtures reveal interesting effects such as the process

of composite fermionization and phase demixing [59, 60, 64]. Moreover effects such as instabilities [58] as well as new phases such as paired and counterflow superfluidity [68] has been observed.

In the context of dynamics, much of the work has been done in the mean-field level either by solving Gross-Pitaevskii equations or by using the lowest band Bose-Hubbard model [69–76]. These works demonstrate various effects such as macroscopic quantum self-trapping and coherent quantum tunneling [69], observations of collapse and revival of population dynamics [74, 75], symmetry breaking and restoring scenarios [72] as well as dipole oscillations induced pairing and counterflow superfluidity [76]. Although these studies do provide interesting insights into the mechanism of tunneling in mixture, a thorough investigations covering the complete crossover from weak to strong interaction regime promises new effects and mechanisms not present in the mean field description. For instance, referring to the case of two species in a harmonic trap, it has been found that if one species is localized due to its heavy mass then it can act as an effective material barrier through which the lighter component tunnels [77, 78]. The feedback of this material barrier leads to different pairing mechanisms for the light species.

These considerations motivates an ab-initio investigation of the tunneling dynamics of bosonic mixture and is the subject for the second part of this thesis [79]. We study the tunneling dynamics binary mixture of bosonic species in a one-dimensional double-well using the MCTDH method and investigate the crossover from weak to strong interaction regimes. We focus on the interplay between the inter- and intra- species interaction as well as the initial state preparation and understand how they affect the rate and behavior of the tunneling in a non-trivial way.

Overview of this thesis

The thesis is organized as follows.

In Chapter 2 we describe the general setup and modeling of ultra-cold bosonic systems in traps. We start by reviewing the basic mechanism of atom-light interactions and the creation of optical lattices. Then we discuss the interaction between the atoms explaining firstly the effective theoretical model and then describing how one controls the interaction strength experimentally using Feshbach resonances.

Chapter 3 is dedicated to a review of the important theoretical approaches used for solving cold bosonic systems. This consists of discussions about theory and scope of the Gross-Pitaevskii equations, the Bose-Fermi map and the Bose-Hubbard model.

In Chapter 4 we discuss the numerical methods used in the context of cold bosons. This includes a brief review of the time independent method of exact diagonalization and standard time dependent method and a thorough description of MCTDH, the computational method used in the thesis.

In Chapter 5 we present the results for tunneling dynamics of single species bosonic

system. Here, we first explain the system setup and then proceed to present the case for two bosons describing and analyzing the dynamics including the strong inhomogeneity case. This is followed by the study of multi-particle systems as well as understanding the effect of inhomogeneity. A tilted double-well is discussed finally.

In Chapter 6 we present the results for the quantum dynamics of a bosonic mixture consisting of two species. After explaining the relevant setup, we discuss the dynamics focusing on the interplay between the intra and the inter-species interaction. Three initial configurations are discussed and analyzed, each offering unique perspectives to the dynamics.

Finally Chapter 7 is devoted to the summary and outlook of the thesis.

Chapter 2

Modeling ultracold bosons in traps

The general system under consideration for this thesis is ultracold few boson in an external trap. At first modeling the system seems to be rather daunting. Not only do we have to consider the detailed interactions of the atoms between themselves, but also have to account for the interaction between the atoms and the external trapping potentials. However it is always possible to derive an effective model for the system which captures all the essential physics. Generally for cold atoms the two main aspects for an effective model are

- Effective external trapping potential and its interaction with a single atom
- The two-body interactions between the ultracold atoms.

For one dimension, the general Hamiltonian can be written as

$$H_{1D} = \sum_{i=1}^N \left(-\frac{\hbar^2}{2m} \frac{\partial^2}{\partial x_i^2} + U(x_i) \right) + \sum_{i<j} V_{1D}(x_i - x_j), \quad (2.1)$$

where the index i denotes each of the N bosons, where $U(x)$ denotes the external trapping potential and V_{1D} the effective one-dimensional interaction.

2.1 Trapping potential

External trapping potential requires coupling between the potential and the target atoms. Generally in the context of the cold atoms the choice lies between a magnetic trap or an optical trap. In a magnetic trap, the interaction is based on the coupling of the total angular momentum of the atom to the magnetic field vector. For some polarization (which is the case for ultracold atoms), the resultant potential is proportional to the magnetic quantum number. However a magnetic trap suffers from the

disadvantage that a magnetically neutral state cannot be trapped. Moreover, states with different magnetic quantum number feel different potentials creating additional practical difficulties.

Thus in recent times optical traps are the preferred trapping potential used for ultracold atoms. They do not suffer from the above mentioned drawbacks of the magnetic traps and furthermore offer enormous flexibility in terms of intensity, geometry and control parameters. Moreover, a laser is highly controllable compared to that of a magnetic field generator and thus manipulating an optical potential is experimentally more feasible.

2.1.1 Atom-light interaction

The underlying principle of an optical trap is the interaction between the atom and the electromagnetic field. Neutral atoms interact with light in both dissipative and conservative ways. In conservative interaction, the induced dipole moment of the atom interacts with the light field creating a shift in the potential energy in an effect known as the ac-Stark shift. On the other hand, dissipative interaction occurs when the atom absorbs the photon followed by spontaneous emission [80] and is the basic principle for laser cooling technique. For large detuning, spontaneous emission processes is negligible and a thus conservative trapping potential can be created using the ac-Stark shift effect.

The basic mechanism of the ac-Stark shift is the interaction between the induced dipole moment of the atom and the electromagnetic field. When an atom is placed in a light field, the oscillating electric field (of the latter) induces an electric dipole moment in the atom. If the incident light has a much longer wavelength than the typical atomic size, we can apply the dipole approximation which assumes that the spatial variation of the electromagnetic field is small compared with the atomic wave function.

The interaction of the atom and light can then be written as [7]:

$$U(r, t) = -\hat{\mathbf{d}} \cdot \mathbf{E}(r, t) \quad (2.2)$$

where $\hat{\mathbf{d}}$ is the dipole operator and $\mathbf{E}(r, t)$ is the time varying electric field of frequency ω given by

$$\mathbf{E}(r, t) = \mathbf{E}(r)e^{-i\omega t} + c.c \quad (2.3)$$

This interaction induces an electric dipole moment on the atom oscillating with the same frequency as the radiation field. The expectation value of the dipole moment can be written as

$$\langle \hat{\mathbf{d}} \rangle = \alpha(\omega)\mathbf{E}(r, t) \quad (2.4)$$

where $\alpha(\omega)$ is the dipole polarizability of the atom given by

$$\alpha(\omega) = \frac{1}{\hbar} \sum_n |\langle n | \hat{\mathbf{d}} \cdot \mathbf{e} | 0 \rangle|^2 \frac{2\omega_{n0}}{\omega_{n0}^2 - (\omega + i\eta)^2} \quad (2.5)$$

Here, \mathbf{e} is an unit vector in the direction of the electric field, while $|0\rangle$ is the electronic ground state of the atom and the summation is taken over all the excited states $|n\rangle$. $\hbar\omega_{n0}$ is the energy splitting between the ground state $|0\rangle$ and the excited state $|n\rangle$. η is an infinitesimal positive number.

The polarization causes the energy shift due to the ac-stark effect and is given by [81, 82]:

$$\Delta E = -\frac{1}{2}\alpha(\omega)\langle E^2(t) \rangle \quad (2.6)$$

where the bracket denotes the averaging in time over the fast optical oscillations. Here, $\omega = \omega_{n0} + \Delta$, where Δ is the detuning of the light field from the resonant frequency ω_{n0} of the atoms.

The above formula implies that the atom feels an effective optical potential $V_{opt} = \Delta E$ depending on the spatial pattern of the incident light and this is the basis of optical potential and traps. If the light is red-detuned ($\Delta < 0$) then the atoms are attracted towards the maxima (high intensity) of the potential while for blue-detuned ($\Delta > 0$) source, the atoms are attracted towards the minima.

2.1.2 Optical lattice

An optical lattice, is an optical potential with spatially periodic maximum and minimum intensity regions. This can be achieved by creating an optical standing wave by overlapping two counter propagating laser beams. The two counter propagating beams are generally created by retro-reflecting a laser beam so that their coherence is kept under control. The amplitude of electric intensity differs along the axis and thus a one dimensional periodic potential for atoms is created. The resulting potential is given by:

$$V(x) = V_0 \sin^2(kx) \quad (2.7)$$

where $k = 2\pi/\lambda$ is the absolute value of the wave vector of the laser light and V_0 is four times times the depth of a single laser beam without retro-reflection.

For generating higher dimensional lattices, additional counter propagating laser sources are necessary. To avoid the interference between the additional beams, the sources used are of orthogonal polarization. For instance, three pairs of counter-propagating laser beams with orthogonal polarizations will form a 3D optical lattice. This is illustrated in Fig.2.1 which shows a schematic illustration of formation of 2D and 3D optical lattice from counter propagating laser beams.

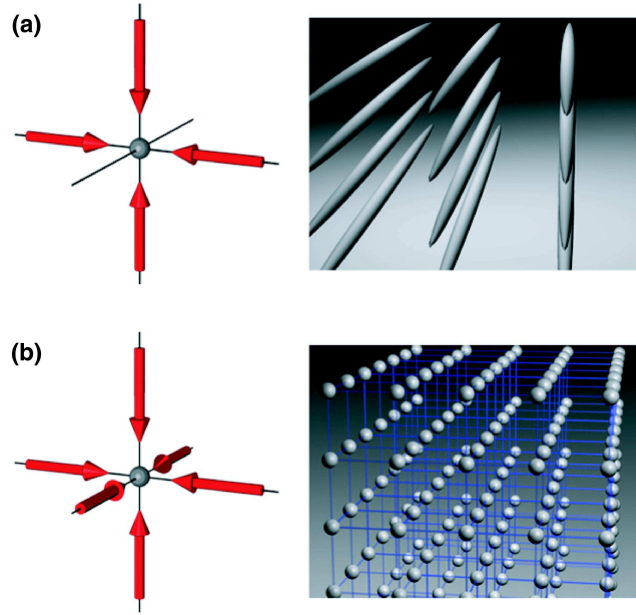


Figure 2.1: Formation of (a) two dimensional and (b) three dimensional optical lattices.(From ref. [5])

2.2 Interactions between the atoms

The computation of the interaction between the atoms in its complete form is an extremely complex task. One has to consider the actual interactions between all electrons and nucleons of the constituent atoms which is practically an impossible task. Thus, it is essential to devise an effective model which captures the essential features of the actual interactions. This is not only useful from computational viewpoint but also gives crucial insights into the effects of the interactions.

2.2.1 Pseudo-potential approximation

A completely detailed derivation of a general effective model is non-trivial and it is not necessary for understanding the physics involved. Therefore for simplicity we highlight the conceptual steps focusing on the two-body interaction which is relevant to our problem. For atom-atom interaction, since the masses of the nuclei is extremely large compared to that of the electrons, their respective kinetic energy scales as well as the time-scales of motions are well separated. This enables us to integrate out the fast electronic motion in the spirit of the *Born-Oppenheimer* approximation and we are left with a Hamiltonian for the nuclear part, depending only parametrically on the electronic structure. The Coulomb interaction between the atoms $V(r = x_i - x_j)$ might still be arbitrarily complicated, making an exact treatment impossible. However, the general form of the interaction potential has a typically a Lennard-Jones type of form. For very

large distances $r \rightarrow \infty$, the interaction potential decays rapidly with distances and the atoms are asymptotically free while for very short distances, there are attractive regions which support the bound states and finally leads to a strong repulsive core as $r \rightarrow 0$.

However, in the ultracold regime, the exact form of the interaction is irrelevant. This is because the thermal de-Broglie wavelength $\lambda = h/\sqrt{2\pi mkT}$ of the particles becomes very large compared to the short range variation of the potential and thus effectively the particles see the average effect of the true potential. This makes it possible to incorporate all the necessary information in a single parameter - the scattering length a_0 .

The formal way to derive an effective interaction in relation to the scattering length is generally by the method of *pseudopotentials* [83]. Here, we assume a hard sphere potential of diameter a , and construct an exact solution via an expansion of partial waves which reproduces the scattering length of the true potential a_0 . This method is analogous to that of multipole expansion in electrostatics. There, the electrostatic potential is calculated by replacing the true charge distribution with a fictitious point source and expanding over multipole terms such that it gives the correct potential asymptotically. Similarly here, the true potential is replaced by an interaction source at the center ($\vec{r} = 0$), such that the asymptotic solution obtained through successive scattering waves yields the same scattering length.

For ultracold temperatures, only the lowest scattering wave (s-wave) contributes and higher terms can be neglected. Then the pseudopotential in three dimensions can be written as

$$V(\vec{r}) = \frac{2\pi\hbar^2 a}{\mu} \delta(\vec{r}) \partial_r r = g \delta(\vec{r}) \partial_r r, \quad (2.8)$$

with $\partial_r r$ being the regularization operator that removes the $1/r$ divergence from the scattered wave.

2.2.2 The effective one-dimensional description

So far we have considered the general pseudopotential in three-dimensions (3D). However in this thesis our focus is on one dimension (1D). Scattering in 3D is considerably different from that in 1D. While the scattering in 3D is radial, in 1D it is linear and the particle can only move back and forth. Thus an effective one dimensional description is required to understand the scattering properties in 1D.

In practice, experimental realization of 1D system is accomplished by using a confining potential to freeze out the transverse degree of freedom (by having the available energy much smaller than the transverse excitation gaps) such that the motion is effectively restricted to the longitudinal direction. This is achieved by tight wave guides or “cigar-shaped” traps.

To have an effective one-dimensional description, one must integrate out the trans-

verse degrees of freedom. This is straightforward for the trapping potential and the kinetic energy terms since they are separable into a transversal and a longitudinal part assuming harmonic confinement:

$$H = \frac{p_x^2 + p_y^2 + p_z^2}{2\mu} + U(x, y, z) + V, \quad U(x, y, z) = \frac{1}{2}\mu\omega_\perp^2(x^2 + y^2) + U_\parallel, \quad (2.9)$$

The two body interaction is much more problematic since the radially symmetric interaction modeled by the pseudopotential $V = g\delta(\vec{r})\partial_r r$ couples transverse and longitudinal modes. The way to achieve this analytically was shown by Olshanii [10] which we present as follows:

Assuming that (i) the incident wave corresponds to a particle in the ground state of the transverse Harmonic oscillator

$$\phi_{inc.} \propto e^{ik_\parallel z} \phi_{0,0}(\rho), \quad (2.10)$$

with $\rho = \sqrt{x^2 + y^2}$.

and (ii) the longitudinal kinetic energy of the incident wave is limited by the energy spacing between the ground and first *axially symmetric* excited state:

$$\frac{\hbar^2 k_z^2}{2\mu} < E_{2,0} - E_{0,0} = 2\hbar\omega_\perp. \quad (2.11)$$

the asymptotic wave function can be written as

$$\psi(z, \rho) \xrightarrow{|z| \rightarrow \infty} \left(e^{ik_\parallel z} + f_{even} e^{ik_\parallel |z|} + \text{sign}(z) f_{odd} e^{ik_z |z|} \right) \phi_{0,0}(\rho), \quad (2.12)$$

where the first term is the incident wave and f_{odd}, f_{even} denote the odd and even scattering amplitudes.

For the zero-range potential of the 3D pseudopotential, the one-dimensional scattering amplitudes can be calculated analytically by expanding the wave function $\psi(z, \rho)$ into a series over the eigenstates of the transverse Hamiltonian, substituting the expansion into the Schrödinger equation and then applying the asymptotic conditions along with the conditions of the continuity of the wave function and its derivative.

This gives the following relation for the scattering amplitudes:

$$f_{odd} = 0 \quad (2.13)$$

$$f_{even} = -\frac{1}{1 + ik_\parallel a_{1D} + O(k_\parallel^3)} \quad (2.14)$$

with the *one-dimensional scattering length*

$$a_{1D} = -\frac{a_\perp^2}{2a} \left(1 - C \frac{a}{a_\perp} \right), \quad (2.15)$$

where a_{\perp} is the transversal confinement length and $C \approx 1.4603$.

For low energies (which is valid for ultracold atoms), the exact scattering amplitude (2.14) can be incorporated into the coupling constant of an effective one dimensional interaction

$$V(x_i - x_j) = g_{1D}\delta(x_i - x_j). \quad (2.16)$$

where the 1D coupling strength $g_{1D} = -\hbar^2/\mu a_{1D}$ indeed encodes all the relevant information of not only the coupling strength g itself, but also the transverse modes, which have been integrated out.

Interestingly, in the limit of $g_{1D} \rightarrow \infty$, the transmission coefficient is

$$|t_{\parallel}|^2 = |1 + f_{\text{even}}|^2 \rightarrow 0 \quad (2.17)$$

and thus the system becomes impenetrable. This physically corresponds to a gas hard-core bosons and is known as the *Tonks-Girardeau gas*. This Tonks-Girardeau limit allows for a remarkable duality with a system of non-interacting fermions and will be discussed in details in Chapter 3 Section 3.2

2.2.3 Experimental control of interaction using Feshbach resonances

Having discussed the procedure of modeling the effective interactions between the atoms, let us briefly describe the most common experimental methods to control the interactions. Experimentally, the most useful method of tuning the interaction strength between the ultracold atoms is by employing *Feshbach resonance* [5, 6]. A Feshbach resonance occurs when the energy of a bound state in a closed channel is resonant with that of the energy of the scattering continuum of an open channel. When this happens, even weak coupling can lead to strong mixing between the two channels. The atoms thus stay for a longer time together since they can be reflected at the potential of the closed channel, leading to a larger scattering length. The most common way to control the energy difference is to use an external magnetic field and the corresponding resonance is known as magnetic Feshbach resonances. If the energy differences are achieved by optical methods and then it is known as optical Feshbach resonance. A schematic representation of the basic process is shown in Fig. 2.2.

A magnetically induced Feshbach resonance can be described by the simple expression for the s-wave scattering length

$$a(B) = a_{\text{bg}}\left(1 - \frac{\Delta}{B - B_0}\right) \quad (2.18)$$

where a_{bg} is the value of the scattering length far from the resonance, B_0 and Δ are position and width of the resonance, respectively.

This expression applies to resonances without inelastic two-body channels which is generally true for magnetically induced Feshbach resonances. In Fig. 2.3 the actual

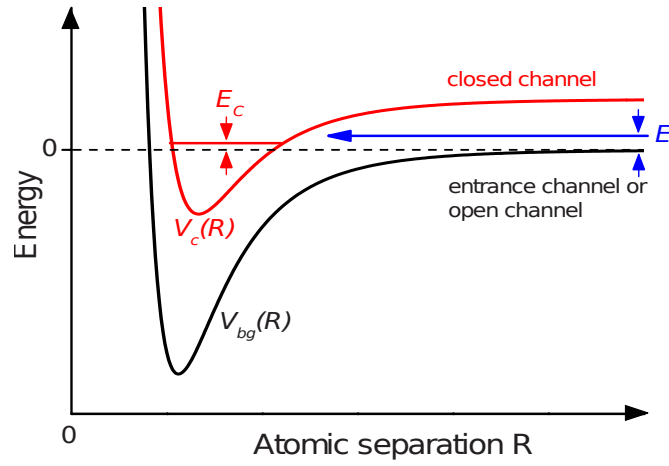


Figure 2.2: The two-channel model for a Feshbach resonance. The threshold energy of the unbound state is indicated by the dashed line and the energy of the bound state E_C by the solid line. When the energies become degenerate, a Feshbach resonance will occur. (From Ref. [6])

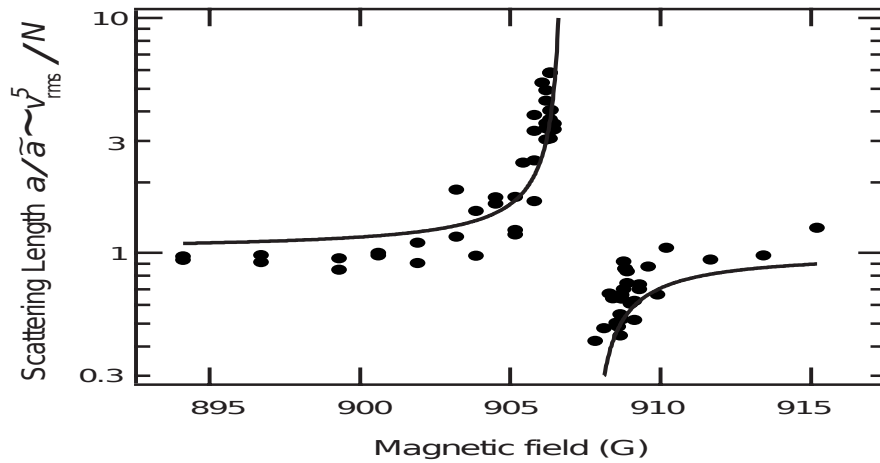


Figure 2.3: Variation the scattering length a for Na atoms near a Feshbach resonance determined experimentally. Here a is normalized to the value of the background scattering length a_{bg} . (From Ref. [84])

experimental variation of the scattering length with magnetic field near Feshbach resonance is shown and compared with the theoretical prediction [84]. We see that in the vicinity of the resonance, the scattering length is highly tunable with small variations of the magnetic field. As explained in the preceding section, since the scattering length is directly related to the effective interactions of the atoms, one can tune the interactions between the atoms using Feshbach resonance.

While Feshbach resonances are valid for all dimensions, in the case of one-dimension with transverse harmonic confinement, one can also control the interaction strength using the *confinement induced resonances* (CIR) [10, 85, 86]. It is essentially a zero-energy Feshbach resonance occurring when the binding energy of the two interacting atoms coincides with the energy spacing between the levels of the transverse harmonic potential. In the vicinity of the CIR, the one dimensional coupling constant g_{1D} can be tuned experimentally from $-\infty$ to ∞ by varying the strength of the confining potential. As a hallmark example, this has led to the experimental realization of the Tonks-Girardeau gas [11].

Chapter 3

Theoretical approaches

While the modeling of the potential and interaction provides the necessary starting point in understanding the physics of bosons in external traps, the actual process of solving the problem is far from trivial. Hardly any system is exactly solvable analytically and thus most theoretical approaches have to rely on approximations to simplify the problem. As a result most of these theories are valid for specific conditions. Before we discuss ways of numerically solving the many-body problem, it would be useful to review some of the theoretical approaches used to understand ultracold bosonic systems.

3.1 Mean field theory and Gross Pitaevskii Equation

The Gross-Pitaevskii equation (GPE) is an effective mean field theory for describing the Bose-Einstein condensate [4, 7]. The basic assumption is that (almost) all particles are condensed i.e. they occupy the same single particle state $\phi(\vec{r})$. The signature for a Bose-Einstein condensate is that this single particle state $\phi(\vec{r})$ has macroscopic occupation. The N (symmetric) many-body wave function for N particles can then be written as

$$\Psi(\vec{r}_1, \vec{r}_2, \dots, \vec{r}_N) = \prod_{i=1}^N \phi(\vec{r}_i), \quad (3.1)$$

with each single particle wave-function $\phi(\vec{r})$ normalized as

$$\int d\vec{r} |\phi(\vec{r})|^2 = 1 \quad (3.2)$$

Strictly speaking, this ansatz is valid only for non-interacting bosons at zero temperature. If there are correlations between the bosons or if the temperature is not zero then there is always a fraction of particles which are not condensed and hence do not occupy the lowest orbital. However, for very small interaction or low temperatures, we can assume that the non-condensed fraction is negligible and thus the above many-body wave-function holds.

Then one can define the wave-function for the condensate state as:

$$\psi(\vec{r}) = \sqrt{N}\phi(\vec{r}), \quad (3.3)$$

with the total number of particles N given by

$$N = \int d\vec{r} |\psi(\vec{r})|^2. \quad (3.4)$$

Considering a general Hamiltonian of the form:

$$H = \sum_{i=1}^N \left[\frac{\vec{p}_i^2}{2m} + V_{ext}(\vec{r}_i) \right] + \sum_{i<j} V(\vec{r}_i, \vec{r}_j), \quad (3.5)$$

where $V_{ext}(\vec{r}_i)$ denotes the external, $V(\vec{r}_i, \vec{r}_j)$ the interaction potential.

the general many-body energy expectation value is given by

$$E = \langle \Psi | H | \Psi \rangle \quad (3.6)$$

Using Eq. 3.1 and 3.3, this becomes

$$E = N \int d\vec{r} \left[\frac{1}{2m} |\vec{\nabla}\phi(\vec{r})|^2 + V_{ext}(\vec{r}) |\phi(\vec{r})|^2 \right] + \frac{N(N-1)}{2} \int d\vec{r}_1 \int d\vec{r}_2 V(\vec{r}_1, \vec{r}_2) |\phi(\vec{r}_1)\phi(\vec{r}_2)|^2. \quad (3.7)$$

Now, in the ultracold regimes one can approximate the actual potential with a contact interaction

$$V(\vec{r}_1, \vec{r}_2) = g\delta(\vec{r}_1 - \vec{r}_2) \quad (3.8)$$

Then the energy equation is given by

$$E = N \int d\vec{r} \left[\frac{1}{2m} |\vec{\nabla}\phi(\vec{r})|^2 + V_{ext}(\vec{r}) |\phi(\vec{r})|^2 + \frac{(N-1)}{2} g |\phi(\vec{r})|^4 \right]. \quad (3.9)$$

This is effectively an energy functional in ϕ . To get the optimal energy expression and the form of ϕ , one needs to perform a minimization of this functional. This is done by introducing the Lagrange multiplier μ (equivalent to the chemical potential) and finding the extremum for $|E - N\mu|$ w.r.t both ϕ and ϕ^* subject to the constraint of a fixed N . Incorporating the condensate wave-function (3.3) and assuming that $N \approx N - 1$ (true for very large N), we obtain the time-independent Gross-Pitaevskii equation:

$$\left(-\frac{1}{2m} \vec{\nabla}^2 \phi(\vec{r}) + V_{ext}(\vec{r}) \phi(\vec{r}) + g(N-1) |\phi(\vec{r})|^2 \right) \phi(\vec{r}) = \mu \phi(\vec{r}). \quad (3.10)$$

The GPE thus represents a Schrödinger equation with an extra non-linear interac-

tion term depending on N and g . Physically the non-linear term represents the effective contribution of the interactions of all the particles. The GPE is exact in the limit of $g \rightarrow 0$ and $N \rightarrow \infty$ with $Ng \rightarrow \text{const}$ [87]. Thus, for systems with high interactions or small number of particles, one would expect significant deviations from an accurate description.

Replacing μ in the right-hand side of Eqn. 3.10 by the operator $i\partial_t$ gives the time-dependent Gross Pitaevskii equation

$$i\partial_t\phi(\vec{r}, t) = \left(-\frac{1}{2m}\vec{\nabla}^2\phi(\vec{r}, t) + V_{ext}(\vec{r})\phi(\vec{r}, t) + g(N-1)|\phi(\vec{r}, t)|^2 \right) \phi(\vec{r}, t). \quad (3.11)$$

An alternative approach to the GPE is to start from the Fock-space prospective. The field operator is a product of the single particle wave-function and the bosonic annihilation operator and is written as:

$$\hat{\Psi}(\vec{r}) = \sum_{i=0} \phi_i(\vec{r})\hat{a}_i, \quad (3.12)$$

The operators $\hat{a}_i^\dagger(\hat{a}_i)$ (creates)annihilates a particle in the state i

$$a_i^\dagger|n_0, n_1, \dots, n_i, \dots\rangle = \sqrt{n_i + 1}|n_0, n_1, \dots, n_i + 1, \dots\rangle \quad (3.13)$$

$$a_i|n_0, n_1, \dots, n_i, \dots\rangle = \sqrt{n_i}|n_0, n_1, \dots, n_i - 1, \dots\rangle \quad (3.14)$$

where n_i denotes the occupation number in the single particle state i .

Separating the condensate fraction ($i = 0$) from the non-condensate portion, we get

$$\hat{\Psi}(\vec{r}) = \phi_0(\vec{r})\hat{a}_0 + \sum_{i=1} \phi_i(\vec{r})\hat{a}_i. \quad (3.15)$$

Now, for very large number of particles, one can approximate $N_0 \approx N_0 + 1$. This allows us to treat the operators \hat{a}_i^\dagger and \hat{a}_i as numbers which, for the lowest mode ($i = 0$), can be approximated as $a_0 = \frac{1}{\sqrt{N}}$.

The above expansion (Eqn. 3.15) can then be written as

$$\hat{\Psi}(\vec{r}) = \Psi_0(\vec{r}) + \delta\Psi(\vec{r}). \quad (3.16)$$

Here $\Psi_0(\vec{r})$ is the expectation value of the field operator $\langle\hat{\Psi}(\vec{r})\rangle$ and represents the condensate fraction. $\delta\Psi(\vec{r})$ describes the non-condensate fraction and is negligible below the transition temperature for Bose-Einstein condensation T_c . We can think the above expansion as an expansion of the operators about its classical (mean-field) value. Plugging this into the second-quantized Hamiltonian gives the energy functional

$$E = \int \left[\frac{1}{2m}|\vec{\nabla}\hat{\Psi}_0|^2 + V_{ext}|\Psi_0|^2 + \frac{g}{2}|\Psi_0|^4 \right] d\vec{r}. \quad (3.17)$$

Then one can apply the standard minimization principle calculation described before to obtain the GPE equation.

This process of assigning mean values to field operators is similar to concept of modeling coherent states in quantum optics. Therefore, the GPE as a lowest order approximation, describes a coherent state [7]. Including the next order in $\delta\Psi(\vec{r})$ leads to the *Bogoliubov equations* which allows small fluctuation about the mean-fields [4].

3.2 Bose-Fermi map

While the Gross Pitaevskii equation is an useful description when the interaction between the atoms are weak, the Bose-Fermi map describes the opposite end of the interaction spectrum namely that of infinite or extremely strong interaction. This was first explained through a seminal paper by Girardeau [8] which demonstrated a general mapping between the same known as the Bose-Fermi map. The principle idea of the Bose-Fermi map is that in one-dimension there exists a one to one mapping between a system of impenetrable hardcore boson and a system of spinless(or spin polarized) non-interacting fermions. To understand this correspondence, let us consider a system of one-dimensional interacting bosons. The general Hamiltonian is given by

$$H = \sum_{i=1}^N h(p_i, x_i) + \sum_{i<j} V(x_i - x_j), \quad (3.18)$$

where $h(p_i, x_i) = \frac{1}{2}p_i^2 + U(x_i)$ is the one-body Hamiltonian containing the kinetic energy and the external trapping potential, and $V(x_i - x_j) = g\delta(x_i - x_j)$ describes an effective one-dimensional short-range interaction with coupling strength g .

The hardcore bosons are realized by letting the contact repulsion go to infinity $g \rightarrow \infty$. This essentially leads to establishing the following boundary condition in the many-body wave-function.

$$\Psi|_{x_i=x_j} = 0, \quad \forall i < j \quad (3.19)$$

This condition separates the Hamiltonian (3.18) into a sum of the single particle terms h_i . The important step now is to recognize that this hardcore boundary condition leads to the same zeros in the wave-function as for fermions (spinless or spin polarized) governed by the same Hamiltonian. However, the permutation symmetries is still different for the two cases. The hardcore boson is still symmetric under permutation while a fermion is anti-symmetric under permutation.

Considering the fundamental domain $\mathbb{D} = \{X \in \mathbb{R}^N \mid x_1 < x_2 < \dots < x_N\}$, one can define an unit anti-symmetric operator which restores the bosonic symmetry [8],

$$A(x_1, \dots, x_N) := \prod_{i < j \leq N} \text{sgn}(x_i - x_j) \quad (3.20)$$

where the function $\text{sgn}(x)$ denotes the algebraic sign of x . The value of A is either $+1$ or -1 , depending on the order of the coordinates x_1, x_2, \dots, x_N being $+1$ when the x_j are arranged in the order $x_1 < x_2 < \dots < x_N$ and picking up an additional minus sign for every permutation in the order of the x_j . This essentially divides the n -dimensional configuration space into $n!$ disjoint regions, with A being constant within these regions and having discontinuities at the boundaries.

For a fermionic wave-function Ψ_F , one can then define a bosonic wave-function Ψ_B such that

$$\Psi_B(x_1, \dots, x_N) = A(x_1, \dots, x_N) \Psi_F(x_1, \dots, x_N), \quad (3.21)$$

The validity of the above equivalence rest on the following arguments:

- $A(x_1, \dots, x_N)$ has discontinuities only at the boundaries $x_i = x_j$ but there $\Psi_F(x_1, \dots, x_N)$ vanishes and hence $\Psi_B(x_1, \dots, x_N)$ is continuous for the whole space.
- Inside the domain $\Psi_B(x_1, \dots, x_N)$ obeys the Schrödinger equation since $\Psi_F(x_1, \dots, x_N)$ also obeys it and $A(x_1, \dots, x_N)$ is just a constant number.
- The LHS of (3.21) is obviously symmetric since it is a product of two anti-symmetric functions.

In the case of periodic boundary conditions (no trap potential, spatially uniform system) one must add the proviso that the boundary conditions are only preserved under the mapping if the number of particles N is odd. The case of N being even is accomplished by imposing periodic boundary conditions on Ψ_F but *anti*-periodic boundary conditions on Ψ_B .

What makes the Bose-Fermi map so useful is the fact that the free fermionic state is just the Slater determinant, that is an antisymmetrized product of single-particle states. This reduces a strongly correlated many-body problem into a single particle problem. In the rare cases where the single particle orbitals are known analytically, a solution in closed form can be obtained, eg. the system for N hardcore boson in harmonic trap where the ground-state is given by [88]

$$\Psi_B(x_1, \dots, x_N) \propto \prod_{i=1}^N e^{-x_i^2/2} \prod_{1 \leq i < j \leq N} |x_i - x_j|. \quad (3.22)$$

Remarks

- For the ground-state the the mapping implies that the wave-function of hardcore bosons is simply the absolute value of the fermionic wave-function

$$\Psi_B(x_1, \dots, x_N) = |\Psi_F(x_1, \dots, x_N)|, \quad (3.23)$$

Thus one can draw analogy between the hardcore repulsion and the Pauli exclusion principle - both effectively preventing the particles from occupying the same position although for different physical reasons. This strong correspondence is the reason why the hard-core limit $g \rightarrow \infty$ is often referred to as **fermionization**.

- The mapping is also valid for excited states and time-dependent states although it is not apparent from the general proof.
- The Bose-Fermi map is valid only in one-dimension. This is due to the fact that in higher dimensions ($d > 1$) the boundary condition $\{x_i = x_j | i < j\}$ fails to give disjoint regions and the configuration space for $d > 1$ is not ordered, and so there is no well-defined unit antisymmetric function A for $d > 1$.
- Since $A^2 = 1$, all local quantities such as their energy spectrum, their probability density $\rho_N = |\psi(x_1, \dots, x_N; x'_1, \dots, x'_N)|^2$, and consequently also their reduced densities $\rho(x)$ and $\rho_2(x_1, x_2)$ will coincide between the hardcore bosons and fermions. However since they still retain their respective permutation symmetries, non-local properties such as the momentum distribution may differ drastically.
- The Bose-Fermi map can also be extended to include infinite attractive interaction [67] as well as mixture of different particle species [63] and spin bosons [89].

3.3 Bose-Hubbard Model

While the GPE and the Bose-Fermi map is not restricted to any specific external potential, the Hubbard model is applicable exclusively for lattice systems [80, 82]. The Fermi-Hubbard model has been used extensively in condensed matter physics to study crystal lattices and has been used to investigate diverse phenomena such as superconductivity and magnetism. Similarly, the bosonic counterpart, the Bose-Hubbard model (BHM) [15] is a very convenient model to study in particular bosons in optical lattices. Moreover, the general theory for the lattice can be used for a system of two lattice points which serve a good approximation to a double-well potential.

3.3.1 Bloch functions and Wannier basis

The periodicity of optical lattices gives rise to band structure in the single particle energy spectrum. For finite lattices, each band consists of m number of discrete levels where m is the number of lattice points. The eigenfunction of the single particle

Hamiltonian are the **Bloch functions** which are essentially a product of a plane wave solution with a periodic function with having the periodicity of the lattice:

$$\phi_q^{(\alpha)}(x) = e^{iqx} u_q^{(\alpha)}(x), \quad (3.24)$$

$$u_q^{(\alpha)}(x+a) = u_q^{(\alpha)}(x), \quad (3.25)$$

where α is the index of the band, a is the lattice period and q is the wave-vector similar to the momentum k in free space, but confined here to the first Brillouin zone $-\pi/a < q \leq \pi/a$.

Although the exact properties of the spectrum and eigenfunctions depend on the details of the corresponding potential, for deep lattices we can incorporate the **tight binding approximation**. The necessary conditions required for applying the tight binding approximation are that the lattice must be deep and the band gaps are large, resulting in a vanishing overlap between spatially neighboring wave functions. For such conditions, one can expand the **Bloch functions** in the basis of **Wannier functions** which are localized in each lattice.

$$w_i^{(\alpha)} = w^{(\alpha)}(x - x_i) = \frac{1}{\sqrt{m}} \sum_q e^{-iqx_i} \phi_q^{(\alpha)}(x), \quad (3.26)$$

where the sum is taken over the first Brillouin zone, and x_i denotes the position of the i^{th} lattice site.

The advantage of the Wannier functions are that they are localized in a single lattice site and thus serve as a very convenient basis for a many-body Hamiltonian of bosons in an optical lattice.

3.3.2 Derivation of Bose-Hubbard Hamiltonian

Consider a system of interacting bosons in an optical lattice. The atom interacts with the lattice potential, any additional external trap potential and also between themselves.

In the second quantized form, the Hamiltonian for the system is given as [16, 80]

$$\begin{aligned} H = \int dx \hat{\Psi}^\dagger(x) \left(\frac{\hbar^2}{2m} \nabla^2 + V_{lat}(x) + (V(x) - \mu) \right) \hat{\Psi}(x) \\ + \int dx dx' \hat{\Psi}^\dagger(x) \hat{\Psi}^\dagger(x') U_{int}(x - x') \hat{\Psi}(x) \hat{\Psi}(x') \end{aligned} \quad (3.27)$$

where $V_{lat}(x)$ is the lattice potential, $V(x)$ is any additional external slowly varying potential, μ is the chemical potential and acts as a Lagrange multiplier to fix the mean number of atoms in the grand canonical ensemble and $U_{int}(x - x')$ is the interaction

potential between two bosons located at x and x' .

$\hat{\Psi}^\dagger(x)$, $\hat{\Psi}(x)$ are the bosonic field operators which creates and annihilates a boson at position x respectively and obey the usual bosonic commutator relations

$$\left[\hat{\Psi}^\dagger(x), \hat{\Psi}^\dagger(x') \right] = \left[\hat{\Psi}(x), \hat{\Psi}(x') \right] = 0 \quad (3.28)$$

$$\left[\hat{\Psi}(x), \hat{\Psi}^\dagger(x') \right] = \delta(x - x') \quad (3.29)$$

To describe the lattice system we can expand the field operator in the basis of the Wannier orbitals

$$\hat{\Psi}(x) = \sum_{i,\alpha} w^{(\alpha)}(x - x_i) \hat{a}_i^{(\alpha)} \quad (3.30)$$

where i denotes the lattice index and α the band index. $\hat{a}_i^{(\alpha)}$ is the bosonic annihilation operator for the lattice site i and band α obeying the canonical bosonic commutation relations.

$$\left[\hat{a}_i^{(\alpha)}, \hat{a}_j^{(\alpha')} \right] = 0, \quad \left[\hat{a}_i^{(\alpha)}, \hat{a}_j^{(\alpha)\dagger} \right] = \delta_{\alpha\alpha'} \delta_{ij}. \quad (3.31)$$

Inserting the expansion (Eq. 3.30) into the many-body Hamiltonian we obtain [82],

$$\begin{aligned} H = & - \sum_{\alpha,\beta,i,j} \left[J_{ij}^{(\alpha\beta)} \hat{a}_i^{(\alpha)\dagger} \hat{a}_j^{(\beta)} + h.c. \right] + \sum_{\alpha,i} V_{i\alpha} \hat{a}_i^{(\alpha)\dagger} \hat{a}_i^{(\alpha)} \\ & + \frac{1}{2} \sum_{i,\alpha,\beta,\alpha',\beta'} \left[U^{(\alpha\beta\alpha'\beta')}(i) \hat{a}_i^{(\alpha)\dagger} \hat{a}_i^{(\beta)\dagger} \hat{a}_i^{(\beta')} \hat{a}_i^{(\alpha')} \right] \end{aligned} \quad (3.32)$$

where

$$J_{ij}^{(\alpha\beta)} = - \int dx w_i^{(\alpha)*}(x) \left(\frac{p^2}{2m} + V_{lat}(x) \right) w_j^{(\beta)}(x) \quad (3.33)$$

represents the effective tunneling coefficient between lattice sites i, j and bands α, β ,

$$U^{(\alpha\beta\alpha'\beta')}(i) = \int dx dx' w_i^{(\alpha)*}(x) w_i^{(\beta)*}(x') V_{int}(x - x') w_i^{(\alpha')}(x) w_i^{(\beta')}(x'). \quad (3.34)$$

is the on-site interaction energy for the lattice i ,

$V_{i\alpha} = V(x_i) - \mu_{i\alpha}$ is an effective lattice chemical potential for site i and band α .

So far we have described the Hamiltonian in its full generality. For simplification, we make the following assumptions:

- Since in the ultracold temperatures the particles generally do not have enough energy to excite the higher states, we can assume that only the lowest band

contributes (hence we can omit the band indices for convenience).

- In the ultracold regime, only the S-wave scattering is relevant and so we can approximate the actual interaction potential between the atoms by the pseudopotential $U_{int}(x - x') = g\delta(x - x')$. This also implies that we rule out long range interaction and hence any interaction energy term for bosons in different sites.
- The overlap between Wannier functions on different lattice sites is small. Thus tunneling is only possible between nearest neighbors $\langle i, j \rangle$.

Applying these assumptions to the general Hamiltonian (Eq. 3.32) we obtain the **Bose-Hubbard Hamiltonian** (BHM) [15, 16]

$$H = -J \sum_{i,j} [\hat{a}_i^\dagger \hat{a}_j + h.c.] + \frac{U}{2} \sum_i \hat{n}_i(\hat{n}_i - 1) + \sum_i V_i \hat{n}_i. \quad (3.35)$$

where $\hat{n}_i = \hat{a}_i^\dagger \hat{a}_i$ is the number operator for the site i .

$$U = g \int dx |w^{(0)}(x)|^4. \quad (3.36)$$

One should note that due to the lowest band approximation, the BHM is valid only when the mean interaction energy per particle U is smaller than the energy gap between the lowest two bands. Although this is valid for many cases in the ultracold regime, if the interaction between the particle gets very strong, higher band contribution becomes more significant and the BHM is unable to describe the systems accurately.

3.3.3 Phases of the Bose-Hubbard Model

The physics of the Bose-Hubbard Hamiltonian is characterized by the competition between the kinetic energy which tries to delocalize the particles and the interaction energy which tries to localize the particles and make the number fluctuations small. At zero temperature the phases of the BHM can be divided into two different regimes. One is the interaction dominated Mott insulator regime, when $J \ll U$, and the other is the kinetic energy dominated superfluid regime when $J \gg U$ where tunneling overwhelms the repulsion between the atoms [5, 80].

Superfluid phase

In the superfluid phase, the kinetic energy term in the Hamiltonian is dominant ($J \gg U$) resulting in a complete delocalization of the particles. In this regime, the quantum correlations can be neglected and one can describe the whole system approximately by a macroscopic wave function. For $U = 0$, the many-body state is a product over identical single particle wave functions, and the ground state is simply a BEC with all bosons in the lowest Bloch band [5]:

$$|\psi\rangle = \frac{1}{\sqrt{N!}} \left(\frac{1}{\sqrt{m}} \sum_i a_i^\dagger \right)^N |0\rangle, \quad (3.37)$$

where m denotes the number of lattice sites and N the number of atoms.

However, due to the presence of the lattice, the effective mass of the particles is increased. Consequently, the critical temperature is lower in the lattice compared to that of a BEC in free space.

The superfluid phase is characterized by a gapless excitation spectrum and infinite compressibility while the filling factor is Poissonian over the entire lattice [91]. The requirement for kinetic energy minimization implies that every atom wants to be at all lattice sites with equal amplitude and thus there is a large probability of finding sites with more than one atom. One characteristic measure for the superfluid phase is long range order, which can be observed in the momentum distribution:

$$\rho(k) \sim |\tilde{w}(k)|^2 \sum_r e^{ikr} \rho_1(r), \quad (3.38)$$

where $\tilde{w}(k)$ denotes the Fourier transformation of the Wannier function and $\rho_1(r)$ is the one-particle density matrix with $r = x - x'$. At $r \rightarrow \infty$, $\rho_1(= n_0)$ approaches a constant value for the superfluid state, hence resulting in a momentum distribution that exhibits peaks at reciprocal lattice vectors [90].

Mott-insulator phase

As interaction between the particles increases, the average kinetic energy required for an atom to hop from one site to the next becomes insufficient to overcome the potential energy cost. Thus, the atoms get more and more localized to the individual sites and the number fluctuations in each site reduces. In the Mott insulator phase ($J \ll U$), the particles are completely localized in the individual sites and tunneling is suppressed. For the $J = 0$ limit, the ground state consists of localized atomic wave functions with a fixed number of atoms per site and is given by the product of local Fock states :

$$|\psi\rangle = \prod_i a_i^{\dagger f} |0\rangle \quad (3.39)$$

with an integer number of atoms per site for a commensurate filling factor f (for a finite lattice size m). For incommensurate fillings however it is impossible to get a complete Mott-insulator phase. For filling factor greater than one, because of the presence of the extra particles (which are delocalized), there is always a SF fraction on top of the MI state. Similar argument holds for holes when the filling factor is less than one [5, 92].

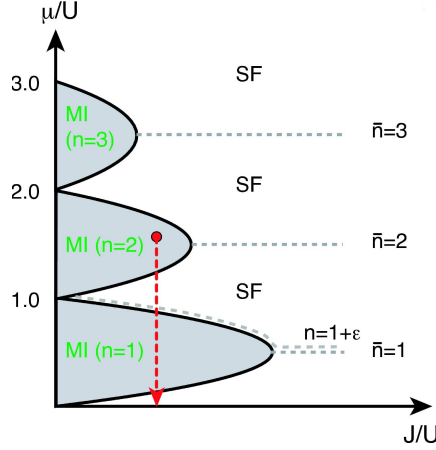


Figure 3.1: Zero temperature schematic phase diagram of the Bose-Hubbard model. The dashed lines of constant density in the superfluid state hit the MI phase at the tips of the lobes at the critical point $(J/U)_c$, which decreases with increasing density. (From ref. [5])

The Mott phase is characterized by the existence of an energy gap in the excitation spectrum which is determined by the energy necessary to create one particle-hole pair. The defining property of the MI phase is the incompressibility of its states: $\partial n / \partial \mu = 0$, as well as vanishing number fluctuations of each site. Moreover, there is an absence of long range order which can be deduced from the Gaussian momentum distribution.

Phase diagram

The phase diagram of the BHM shows lobe like structure in the $\mu - J$ plane (Fig. 3.1) [5, 91, 93]. The area inside the lobe is the Mott-insulator phase while outside is the superfluid phase. Each lobe has a fixed integer density and the area inside the lobe is incompressible, which is the characteristic property of the MI phase. In the Mott phase, keeping J fixed, if one increases μ then at some point the energy of adding an extra particle will balance the interaction energy cost. The resulting extra particle can hop without any energy cost thus inducing the superfluid phase. Same thing happens from reducing μ , with a hole instead of a particle destroying the Mott phase. Thus the Mott phases occurs only on regions of integer densities; non-integer density regions lie entirely in the superfluid phase.

3.3.4 Two-species Bose-Hubbard model

In this thesis, apart from single species bosonic system, we also consider system consisting of two-species bosonic mixture. An equivalent Bose-Hubbard Hamiltonian for such a system can be computed using the techniques described before. The basic formalism for two species BHM is same as that for a single species. However, the presence of the additional species component makes the computation of the Hamiltonian more in-

volved and also provides the possibility for additional quantum phases and an expanded parameter space.

Consider a bosonic binary mixture labeled by A and B . The general Hamiltonian of the composite system is $H = H_A + H_B + H_{AB}$ where H_A , H_B are the individual (single species) Hamiltonian for species A and B while H_{AB} denotes the coupling term between the two species.

In the second quantized form they are given as :

$$H_A = \int dx \hat{\Psi}_A^\dagger(x) \left(\frac{\hbar^2}{2m} \nabla^2 + V_A^{lat}(x) + (V_A(x) - \mu) \right) \hat{\Psi}_A(x) + \int dx dx' \hat{\Psi}_A^\dagger(x) \hat{\Psi}_A^\dagger(x') U_A^{int}(x-x') \hat{\Psi}_A(x) \hat{\Psi}_A(x') \quad (3.40)$$

$$H_B = \int dx \hat{\Psi}_B^\dagger(x) \left(\frac{\hbar^2}{2m} \nabla^2 + V_B^{lat}(x) + (V_B(x) - \mu) \right) \hat{\Psi}_B(x) + \int dx dx' \hat{\Psi}_B^\dagger(x) \hat{\Psi}_B^\dagger(x') U_B^{int}(x-x') \hat{\Psi}_B(x) \hat{\Psi}_B(x') \quad (3.41)$$

$$H_{AB} = \int dx dx' \hat{\Psi}_A^\dagger(x) \hat{\Psi}_B^\dagger(x') U_{AB}^{int}(x-x') \hat{\Psi}_B(x) \hat{\Psi}_A(x') \quad (3.42)$$

$\hat{\Psi}_{A(B)}^\dagger(x)$ is the bosonic field operator for species $A(B)$.

Here, we have assumed for generality that each species feel different lattice and external potential. Moreover, instead of one we have three interaction term each defined by their respective pseudo-potential coupling.

Using the same procedure as in the single-species case and using the same approximations, the two-species BH Hamiltonian can be constructed:

$$H = -J_A \sum_{i,j} [\hat{a}_i^\dagger \hat{a}_j + h.c.] + \frac{U_A}{2} \sum_i \hat{a}_i^\dagger \hat{a}_i^\dagger \hat{a}_i \hat{a}_i + \sum_i V_{iA} \hat{a}_i^\dagger \hat{a}_i - J_B \sum_{i,j} [\hat{b}_i^\dagger \hat{b}_j + h.c.] + \frac{U_B}{2} \sum_i \hat{b}_i^\dagger \hat{b}_i^\dagger \hat{b}_i \hat{b}_i + \sum_i V_{iB} \hat{b}_i^\dagger \hat{b}_i + \frac{U_{AB}}{2} \sum_i \hat{a}_i^\dagger \hat{b}_i^\dagger \hat{b}_i \hat{a}_i \quad (3.43)$$

Here, \hat{a}_i is the annihilation operator at lattice site i for species A while \hat{b}_i the corresponding operator for species B . U_A and U_B denotes the intra-species interaction for species A and B respectively while U_{AB} is the inter-species coupling. J_A and J_B are the respective tunneling coupling.

The possible phases of the two component system are significantly higher than the

single species case as a consequence of the enormity of the possible parameter space. Aside from the usual superfluid- Mott insulator transition which itself shows a much richer behavior, we have formations additional phases. In the deep lattice limit, they include phases such as Z-Neel Mott or x-y Ferro Mott [94]. A detailed discussion of these phases however is beyond the scope of this thesis.

Chapter 4

Numerical methods

Theoretical approaches, like the ones discussed in the preceding chapter, are limited by the assumptions they are based on. To have a complete understanding of the systems, we need to solve the many-body Schrödinger equation. While this might look simple, in practice the computation is far from trivial. Only very few problems are solvable analytically. Thus we have to resort to numerical computations.

For time-independent Hamiltonians, this can be tackled either as a time-dependent or a time-independent problem. The first is an initial value problem of the time-dependent Schrödinger equation

$$-\frac{\hbar^2}{2m}\nabla^2\Psi(t) + V(t)\Psi(t) = i\hbar\frac{\partial\Psi(t)}{\partial t}, \quad (4.1)$$

for a given initial state $\Psi(0)$.

In the second case, the time-independent Schrödinger equation is solved providing the energy eigenstates and eigenvalues. The time evolution of the initial wave function $\Psi(0)$ is then given by

$$\Psi(t) = e^{-iHt}\Psi(0) = \sum_m e^{iE_m t} a_m \Psi_m, \quad (4.2)$$

where E_m and Ψ_m are the eigenstates and eigenvectors of the stationary Schrödinger equation

$$H\Psi_m = E_m\Psi_m. \quad (4.3)$$

In this thesis, our choice of method is the *Multi-Configuration Time Dependent Hartree Method* (MCTDH), which is an ab-initio time dependent method of solving the Schrödinger equation. Before explaining in detail MCTDH method, let us first describe the basic features in some common ab initio approaches to the ultracold bosonic systems focusing on the essential difference between the time-dependent and the time-independent approaches.

4.1 Exact diagonalization

This is the most common and conceptually straightforward time-independent method. The primary approach of the method is to expand the exact wave-function using an orthonormal basis

$$\Psi \approx \sum_{k \leq K} c_k \Phi_k, \quad C = (c_1, \dots, c_K)^T \quad (4.4)$$

The cutoff K depends on the choice of physical problem and also on the convergence of the wave-function. The exact wave-function is recovered in the limit $K \rightarrow \infty$. The Hamiltonian matrix is then computed in the Φ_k basis

$$(H)_{kl} = \langle \phi_k | H | \phi_l \rangle. \quad (4.5)$$

and the problem can then be cast as a matrix eigenvalue problem

$$(E_n - H_{kl})C = 0 \quad (4.6)$$

In the light of the fact that $H \equiv (H)_{kl}$ yields the same spectrum, the essential task to solve the problem is to diagonalize $(H)_{kl}$. Although this is conceptually simple, in practice numerically it is not trivial especially since the dimensions of the matrix can easily get extremely large making computation difficult.

So far the method described is completely with no explicit reference to the many-body nature. That comes from the realization that the many-body states Φ_J , where the multiindex $J = (j_1, \dots, j_f)$ has been introduced for convenience, are generally correlated and can therefore be replaced by a superposition of single-particle states

$$\Phi_J = \phi_{j_1} \otimes \dots \otimes \phi_{j_N}. \quad (4.7)$$

The expansion of the wave function thus reads

$$\Psi(Q) \approx \sum_{J \leq N} c_J \Phi_J(Q) = \sum_{j_1=1}^{N_1} \dots \sum_{j_f=1}^{N_f} c_{j_1 \dots j_f} \prod_{i=1}^f \phi_{j_i}^{(i)}(q_i), \quad (4.8)$$

For identical particles, one either explicitly use symmetric functions ϕ_{j_N} or symmetrizes the coefficients to restore the correct permutation symmetry. The choice of single-particle basis vectors is critical to the numerical efficiency and accuracy. This is especially true since the computation effort grows exponentially with the basis size. A completely arbitrary basis would generally require a large number to converge. Intelligent guesses, energy cutoff, symmetry consideration and various other methods are generally used to reduce the basis size. A different approach is to use variationally

optimal single particle functions. While it reduces the the required basis size, more effort is required in the computation of the Hamiltonian matrix elements.

4.2 The standard time-dependent method

While time-independent method is essentially an eigenvalue problem, time-dependent methods is primarily an initial value problem. In the standard propagation method, the wave function is expanded in an orthogonal product basis set, analogous to the exact diagonalization method but this time it is time-dependent [28]:

$$\Psi(Q, t) = \sum_{J \leq N} c_J(t) \Phi_J(Q) = \sum_{j_1=1}^{N_1} \dots \sum_{j_f=1}^{N_f} c_{j_1 \dots j_f}(t) \prod_{i=1}^f \phi_{j_i}^{(i)}(q_i). \quad (4.9)$$

with the expansion coefficients carrying the time dependence. For convenience, the multiindex $J = (j_1, \dots, j_N)$ has been introduced. As before, for $N \rightarrow \infty$, the exact wave function is recovered. Now, the *Dirac-Frenkel variational principle* [95]

$$\langle \delta\Psi | H - i\partial_t | \Psi(t) \rangle = 0 \quad (4.10)$$

is applied to these wave functions. Essentially this requires variations $\delta\Psi$ of the wave function to be orthogonal $[i\delta_t - H(t)]\Psi(t)$. This can be thought as the “error”, which equals zero for the exact wave function. This leads to equations of motion for the coefficients c_J

$$i\dot{c}_J = \sum_L H_{JL} c_L, \quad (4.11)$$

establishing a linear system of first-order differential equations which is solved to give the time-evolution of the wave-function.

Needless to say, in its fundamental form the standard propagation method is numerically expensive and the computational effort grows exponentially with the number of degrees of freedom f . For the numerically exact solution of (4.11), employing the same number of single particle functions N for each degree of freedom, the effort is proportional to fN^{f+1} (neglecting the effort for computing the matrix representation of H since this has to be done only once at the beginning of the propagation). This scaling behavior generally restricts the standard propagation method to systems with few degrees of freedom. Effort to reduce the computational effort thus rest very much on reducing the required basis function. As before a possible way is to use a variationally optimal, self consistent basis set which may also be time dependent. This consideration leads us into the method of MCTDH.

4.3 MCTDH method

MCTDH is an advancement of the standard method, where instead of using time-independent and therefore static, uncorrelated single-particle functions, one uses a variationally optimal, self-consistent set of basis functions which are explicitly *time-dependent* $\phi_j(q, t)$. Although this does not change the exponential scaling fN^{f+1} , it provides a variationally optimal basis set at each time step of the calculation and therefore a truncated basis, making the problem numerically more feasible.

4.3.1 MCTDH ansatz and equations of motion

As before the basic idea of MCTDH method [27, 28] is to solve the time-dependent Schrödinger equation

$$i\dot{\Psi}(t) = H\Psi(t)$$

as an initial value problem by expanding the solution in terms of Hartree products $\Phi_J \equiv \varphi_{j_1} \otimes \dots \otimes \varphi_{j_N}$:

$$\Psi(Q, t) = \sum_{J \in \Upsilon} A_J(t) \Phi_J(Q, t) = \sum_{j_1=1}^{n_1} \dots \sum_{j_f=1}^{n_f} A_{j_1 \dots j_f}(t) \prod_{i=1}^f \phi_{j_i}^{(i)}(q_i, t), \quad (4.12)$$

N denotes the number of degrees of freedom, with the direct product $\Phi_J = \phi_{j_1}^{(1)} \otimes \dots \otimes \phi_{j_f}^{(f)}$ and the multi-index $J = (j_1, \dots, j_f)$ running over the set $\Upsilon = \{(j_1, \dots, j_f) | j_i \leq n_i\}$.

Note that in the above expansion, both the coefficients A_J and the single particle functions φ_j are explicitly time dependent. The expansion reduces to that of the standard time-dependent method for $n_k = N_k$. Also note that correlations are already incorporated by the virtue of the time-dependence of the single particle functions. The main advantage is that since the single particle functions are optimized in the sense of Dirac-Frenkel variational principle (see below), much less configurations have to be included reducing the computational effort required.

There is however one problem which needs to be taken care of before obtaining the equations of motions. The above wave-function representation (4.12) is not unique. One can linearly transform the single particle functions or the expansion coefficients and still represent the same wave-function. These redundancies induce singularities in the equation of motions. Thus, to get rid of these redundancies and ensure uniquely defined equation of motion, the following constraints are imposed

$$\langle \phi_j^{(i)}(0) | \phi_l^{(i)}(0) \rangle = \delta_{jl} \quad (4.13)$$

$$\langle \phi_j^{(i)}(t) | \dot{\phi}_l^{(i)}(0) \rangle = 0. \quad (4.14)$$

The equation of motion is now obtained by using the the ansatz 4.12 into the *Dirac-Frenkel variational principle*

$$\langle \delta\Psi | H - i\partial_t | \Psi(t) \rangle = 0 \quad (4.15)$$

This yields the following equations:

$$i\dot{A}_J = \sum_L \langle \Phi_J | H | \Phi_L \rangle A_L \quad (4.16)$$

$$i\dot{\phi}^{(i)} = (1 - P^{(i)})(\rho^{(i)})^{-1} \langle \mathbf{H} \rangle^{(i)} \phi^{(i)}. \quad (4.17)$$

Here, $P^{(i)}$ is the projector on the space spanned by the single-particle functions for the i^{th} degree of freedom

$$P^{(i)} = \sum_{j=1}^{n_i} |\varphi_j^{(i)}\rangle \langle \varphi_j^{(i)}|, \quad (4.18)$$

while the term $(1 - P^{(i)})$ assures that the time evolution of the SPFs is orthogonal to the current SPF.

$\rho_{jk}^{(i)}$ is the reduced one-body density matrix in the basis of the single-particle functions, given by

$$\rho_{jk}^{(i)} = \langle \Psi_j^{(i)} | \Psi_k^{(i)} \rangle. \quad (4.19)$$

The coefficients A_J obey the usual Schrödinger equation, as they would in the time-dependent formulation.

The single particle functions $\phi^{(i)}$ on the other hand are not fixed but evolve through an effective Schrödinger equation governed by the mean-field Hamiltonian

$$\langle H \rangle_{jl}^{(i)} = \langle \Psi_j^{(i)} | H | \Psi_l^{(i)} \rangle. \quad (4.20)$$

where

$$\psi_j^{(i)} = \sum_{j_1} \dots \sum_{j_{(i-1)}} \sum_{j_{(i+1)}} \dots \sum_{j_f} A_{j_1 \dots j_{(i-1)} j_{(i+1)} \dots j_f} \varphi_{j_1}^{(1)} \dots \varphi_{j_{(i-1)}}^{(i-1)} \varphi_{j_{(i+1)}}^{(i+1)} \dots \varphi_{j_f}^{(f)}, \quad (4.21)$$

are the **single-hole functions**, a combination of Hartree products of $(f - 1)$ single-particle functions, without the single-particle function for the coordinate Q_i .

In the mean-field Hamiltonian, all but the i^{th} degrees of freedom have been integrated out and thus it acts only on the one-particle space $\mathbb{H}_1^{(i)}$ analogous to the mean fields in Hartree theory.

The system of differential equations (4.16,4.17), is solved self-consistently by starting from a given initial condition $\Psi(0) = \sum_J A_J(0)\Phi_J(Q, 0)$ and integrating iteratively the equations of motion (4.16,4.17) to get the coefficients A_J and the single particle functions ϕ_j and thus obtaining $\Psi(t)$ via Eq. 4.12.

4.3.2 Implementation

Having derived the fundamental working equation of MCTDH, we now set-up general methods for the implementation of its core ideas.

Discrete variable representation(DVR)

The MCTDH method involves evolution of the single particle functions (SPFs) in time. Thus, they have to be represented numerically. This is accomplished by expanding the SPFs in a set of primitive time-independent basis functions:

$$\phi_{j_i}^{(i)}(q_i, t) = \sum_{l=1}^{(N_i)} c_{j_i, l}^{(i)}(t)\varphi_l^i(q_i). \quad (4.22)$$

To obtain the basis one uses the method of **discrete variable representation(DVR)** [28]. The basic idea of a DVR is to use a primitive basis, localized in coordinate representation, which is based on a set of orthogonal polynomials. By diagonalizing the position operator Q in this basis, a set of DVR basis functions φ_α and grid points Q_α are obtained, where the α^{th} function is an approximation to the delta function on the α^{th} point $\varphi_\alpha(Q) = \delta(Q - Q_\alpha)$. The wave function $\phi_j^{(i)}$ is therefore represented by the set of its values at each grid point: $\{\phi_j^{(i)}(Q_\alpha)\}$. Operators local in coordinate space, e.g. the potential energy operator are diagonal on the DVR grid, while non-local operators as the kinetic energy have to be transformed to the **DVR** basis. The **DVR** basis functions are chosen according to the problem and are typically weighted polynomials such as *harmonic-oscillator functions* or *Legendre polynomials*.

Product representation of the potential

To obtain the MCTDH wave-function, one needs to solve the MCTDH equations. However, their exact solutions require computation of the Hamiltonian matrix elements $\langle \phi_J | H | \phi_L \rangle$ and the mean fields at each time step. Their evaluation requires f -fold and $(f - 1)$ -fold integrations which are computationally expensive and thus must be avoided. To circumvent the problem, one require the Hamiltonian to be expressed as a sum of products of single-particle operators h_r :

$$H_R = \sum_{r=1}^s c_r \prod_{i=1}^f h_r^{(i)} \quad (4.23)$$

with expansion coefficients c_r .

The resulting integrals are much more accessible for numerical integration. The kinetic energy usually has the required form already. However, this is not the case for the potential energy since interaction term of the form $V(x_i - x_j)$ are not separable in general. The potential operator is thus transformed to the product form by fitting single-particle operators to the exact Hamiltonian, minimizing the deviation $\|H - H_R\|$. This is to be done before the computation of the problem, using the program **potfit** [28] in the MCTDH package and the fitted potential is then used in the MCTDH run.

Stationary states

MCTDH is inherently a time-dependent method circumventing the detour over the time-independent formalism for energy-conserving problems. However in many cases it becomes necessary to compute the ground-state and also the excited states. Not only do they provide better insights to the system, but also one can verify the dynamics via an expansion over the excited states. The conceptually simplest way to implement this in the MCTDH framework is to propagate the wave function in imaginary time $\tau = it$ [96].

$$\Psi(t) = e^{-iHt}\Psi(0) = \sum_n e^{-\tau E_n} \Psi_n \stackrel{\tau \rightarrow \infty}{\approx} c_0 e^{-E_0 \tau} \left[1 + O\left(e^{-(E_m - E_0)\tau}\right) \right]. \quad (4.24)$$

Thus for an initial state $\Psi(0)$ having a non-zero overlap with the ground-state, contribution from all states are damped out as $\tau \rightarrow \infty$, except that from the exact ground state. To calculate an excited state, one must make the initial state $\Psi(0)$ orthogonal to an underlying eigenstate ($c_m = 0 \forall m < n$). However this algorithm is computationally unstable especially for the calculation of the excited states and thus in practice one relies on a more sophisticated approach, the **improved relaxation** [97, 98].

In this method, one starts from the conventional, *time-independent* variational principle

$$E_0 \leq \frac{\langle \Psi | H | \Psi \rangle}{\langle \Psi | \Psi \rangle}. \quad (4.25)$$

This is then minimized with respect to both coefficients A_J and the orbital φ_j yielding

$$\sum_L H_{JL} A_L = E A_J \quad (4.26)$$

$$\sum_{l=1}^{n_i} \left(\langle H \rangle_{jl}^{(i)} - \epsilon_{jl}^{(i)} \right) \varphi_l^{(i)} = \left(1 - P^{(i)} \right) \sum_{l=1}^{n_i} \langle H \rangle_{jl}^{(i)} \varphi_l^{(i)} = 0 \quad (4.27)$$

These equations simultaneously fulfill the standard eigenvalue problem for the coefficients A_J (4.26) and the *self-consistent* mean field eigenvalue problem for the orbitals

φ_j (4.27), yielding a variationally optimal solution.

The procedure is as follows: First an initial state having some overlap with the required eigenstate is obtained $\Psi(0) = \sum_J A_J(0)\phi_J(0)$. The Hamiltonian H_{JK} is then diagonalized for A_J keeping the orbitals ϕ_J fixed. After the diagonalization, the mean fields $\langle H \rangle^{(i)}$ are built and the SPFs φ_j are relaxed for a short period in imaginary time. The Hamiltonian matrix is then rebuilt in the new configuration and the procedure is repeated until convergence is achieved.

While the convergence for ground-state is generally guaranteed, the same is not the case always for the excited states. The improved relaxation method is very sensitive both on the number of SPFs and also the initial wave-function especially for the excited states. For convergence, the lower states has to be be represented accurately enough which require a large basis of SPFs. The most solid procedure is to start with the computation of the eigenstate in the non-interacting case ($g = 0$). Then, starting from this state as the initial state, the eigenstate for $g \neq 0$ is calculated by an improved relaxation while sieving out the eigenvector closest to the initial state. The resulting eigenstate will then in turn serve as a starting point for an even larger g value, and so on [99].

Moreover, if states are quasi-degenerate then it is extremely difficult to converge via the improved relaxation method unless the basis size is extremely large. These states arises especially in the cases of bosonic mixture and the MCTDH fails to resolve the closely lying states. In those situation one uses the method of *block relaxation* which involves simultaneous relaxation of a whole set of these eigenstates keeping them orthogonal.

4.3.3 Application to few boson systems

So far we have described the MCTDH theory and method in a generic way. However to use it for a system of ultracold bosons, certain specific adjustments need to be made. First is the issue of permutation symmetry. This is especially important since MCTDH is designed at core to treat distinguishable particles and thus it is necessary to adjust so that the correct permutation symmetry is obtained. Second is the requirement to numerically represent the effective interaction in the ultracold regime $V(x) = g\delta(x)$ which is not a smoothly varying function.

Modeling contact potential

The delta potential while a very convenient analytic tool, is problematic numerically since the discontinuity of its derivative leads to numerical inconveniences. However this does not pose a serious problem since for low energies any model potential will suffice which reproduces the right scattering parameters. Thus, throughout in this thesis we

sample the delta function by a narrow Gaussian:

$$\delta_\sigma = \frac{1}{\sqrt{2\pi}\sigma} e^{-x^2/2\sigma^2}, \quad (4.28)$$

yielding the true δ potential in the limit $\sigma \rightarrow 0$.

However it must be ensured that this operator is short-ranged compared to the average inter-particle distance $\sigma \ll L/N_g$ (L being the system's spatial extension). On the other hand the range has to be at least on the order of the grid spacing. Therefore a sufficiently dense grid has to be chosen so that the details of interaction potential V are sampled sufficiently.

Permutation symmetry

MCTDH is designed for distinguishable particles which can be seen from its ansatz

$$\Psi(Q, t) = \sum_J A_J(t) \phi_J(Q, t), \quad (4.29)$$

Indistinguishable particles should have an identical set of single-particle functions $\{\varphi_j\}_{j=1}^n$ for each particle. Clearly, the basis vectors ϕ_J are not necessarily symmetric as one would require for a bosonic system. However this is not a conceptual problem since one can always restore the necessary symmetry by making the coefficients $A_J = A_{P(J)}$ symmetric. For a system of a mixture of different species, the coefficients have to be symmetrized separately for each species: $A_{j_1 \dots n_a}$ and $A_{j_{na+1} \dots n_b}$. While this works sufficiently well for small systems, it becomes highly redundant for large particle numbers $N \gg 1$. In practice this is rarely necessary explicitly since the time evolution of a symmetric initial state does not alter the symmetry of the wave function. However, one has to be careful since numerical instabilities which can occur especially if the number of basis functions is small, can potentially destroy the permutation symmetry.

Technical aspects: Convergence and optimization

The MCTDH run involves adjusting and checking a number of technical parameters to optimize and ensure convergence. Firstly the error tolerance for the integration have to be chosen quite small ($\epsilon \leq 10^{-8}$) since generally MCTDH tends to violate energy conservation during a propagation with strong short-ranged correlations. Secondly, the **grid length \mathbf{L}** has to be sufficiently large to guarantee that the wave function is fully described on the grid. This can be ensured with a vanishing density at the edges of the grid. Moreover the **number of grid points N_g** have to be sufficiently dense to make sure that the short-range potential is well described. This can be tested by simply enhancing the number of grid points and comparing the convergence with increasing N_g . The most important parameter both in the context of convergence and computational effort is the number of *single-particle functions*. For numerical efficiency, the number

has to be kept small since the numerical effort grows exponentially with an increasing number of SPFs. On the other hand, in strongly correlated systems, large numbers of SPF are necessary to ensure convergence. Thus, it is necessary to select the number of SPF judiciously to maintain the balance between computability and accuracy.

One useful way to check convergence is by inspecting the population of the highest natural orbital. The natural orbitals are obtained by the spectral decomposition of the one-particle density matrix

$$\rho_1(x, x') = \sum_i \lambda_i \varphi_i^*(x) \varphi_i(x'), \quad (4.30)$$

where the eigenstates φ_i are denoted the *natural orbitals* and the eigenvalues λ_i reflect their population.

For a converged calculation it has to be ensured that the population of the highest orbital is small. This is because the space spanned by the natural orbitals is equivalent to the one spanned by the SPFs and if the population of the highest natural orbital is low, this has negligible contribution to the wave-function and thus it is converged.

One way to optimize the calculation is to use the *constant mean field integration scheme (CMF)* [28]. Here one exploits the fact that the mean fields $H_{JL} = \langle \Phi_J | H | \Phi_L \rangle$ generally change much slower in time than the coefficients A_J and the SPFs ϕ_j . Therefore, a rougher time discretization can be used for the mean field operators. Effectively, this means that keeping the mean fields constant over several propagation steps for the coefficients and the single particle functions, thus reducing the computational effort.

Chapter 5

Tunneling dynamics of single species bosonic system

The aim of the thesis is to study the quantum dynamics of one-dimensional few boson systems in a double-well trap. A bosonic system in general can comprise of a single species boson or can be a mixture consisting of multi-species component. In this chapter we study the dynamics of the single species few-boson system. We have already seen that systems in lower dimensions which often display unique features such as fermionization. Moreover, quasi-one-dimensional (1D) Bose gases have been prepared experimentally by freezing the transverse degrees of freedom. There it is possible to tune the interaction strength between the atoms by either using confinement induced resonances [10] or magnetic Feshbach resonances [50]. Thus it is possible to study the crossover from a weakly interacting to a strongly correlated regime.

The double well especially serves as a prototype system to study fundamental features of tunneling in great detail. Observations of tunneling dynamics of a BEC in a double well reveal effects such as Josephson oscillations [42–44] and quantum self trapping [42,44,45]. Theoretically the quantum dynamics in the weakly interacting case has been studied using the Bose-Hubbard model assuming the validity of a lowest band approximation [48, 49, 105, 106]. These studies illuminate relevant tunneling mechanisms and resonances. However, to capture the rich physics present in the stronger interaction regime we need to go beyond the Bose-Hubbard limit. Moreover numerically exact calculations of the quantum dynamics for few bosons through a one-dimensional potential barrier [34] or a bosonic Josephson junction [35] reveal deviations from the results obtained with mean-field calculations as well as establish a difference between the dynamics in attractive and repulsive bosonic systems [36]. In a symmetric double well with symmetric interaction, numerically exact quantum dynamical calculations for few bosons reveals a transition from Rabi-oscillations to fragmented pair tunneling via a highly delayed tunneling process analogous to the self-trapping for condensates [46,47].

Most of these works focus primarily on symmetric set-ups. Our primary goal here

is to understand the effect of the asymmetry in the dynamics of few boson system. While the quantum dynamics of asymmetric double-wells keeping a constant interaction strength has been explored in refs. [46–49], in this work we go one step further and envision a new approach to asymmetry by introducing an inhomogeneous, i.e., spatially varying interaction strength. This can be achieved experimentally by employing magnetic field gradients in the vicinity of Feshbach resonances or by combining magnetic traps with optically induced Feshbach resonances [50, 51]. This system enables us to study the role of inhomogeneity as well as the interactions strength and their interplay in the dynamics.

The chapter is organized as follows. In Section 5.1 we discuss our model and setup. Here the many-body Hamiltonian including the model for the spatially modulated interaction strength is introduced. The relevant parameters as well as the scaling is explained. We present and discuss the results for tunneling in a symmetric double well for two atoms in Section 5.2. Here firstly dynamics for a fixed inhomogeneity is presented and compared with the case of symmetric interactions. This is followed by a discussion about the effect of inhomogeneity and finally to the system with high interaction inhomogeneity. Subsequently we present the results for higher atom numbers (Section 5.3). Here, firstly the tunneling with fixed inhomogeneity is studied and contrasted with the results for the reference case of symmetric interactions. This is followed by a discussion about effect of inhomogeneity and tunneling resonances. In Section 5.4 we discuss the case of an asymmetric double well.

5.1 Setup

5.1.1 Hamiltonian

The effective 1D Hamiltonian for N particles is given by

$$H = \sum_{i=1}^N \left[\frac{1}{2} p_i^2 + U(x_i) \right] + \sum_{i < j} V(x_i - x_j) \quad (5.1)$$

The double well trap $U(x) = \frac{1}{2}x^2 + h\delta_\omega(x)$ is modeled as a harmonic potential with a central barrier shaped as a Gaussian $\delta_\omega(x) = \frac{e^{-x^2/2\omega^2}}{\sqrt{2\pi\omega}}$ of width $\omega = 0.5$ and height $h = 8$, in terms of dimensionless harmonic-oscillator units (see Sec. 5.1.3).

As explained in Sec. 2.2, for ultracold atoms only the s-wave scattering is relevant and the effective interaction in 1D can be written as a contact potential:

$$V(x_i - x_j) = g_{1D}\delta(x_i - x_j). \quad (5.2)$$

For transverse harmonic confinement with length $a_\perp = \sqrt{\hbar/m_\sigma\omega_\perp}$ and a 3D scatter-

ing length a_0 , the one-dimensional interaction strength g_{1D} is given by the relation [10]

$$g_{1D} = \frac{2\hbar^2 a_0}{m_A a_\perp^2} \left(1 - C \frac{a_0}{a_\perp}\right)^{-1}, \quad C = \frac{|\zeta(\frac{1}{2})|}{\sqrt{2}} \approx 1.0326. \quad (5.3)$$

However, as explained in Sec. 4.3.3, in the view of numerical difficulty encountered with an actual delta function, we sample it here by a very narrow Gaussian.

We focus in this work is on repulsive interaction ($g_{1D} \equiv g \geq 0$) only.

5.1.2 Interactions

The primary focus of this work is on the role of inhomogeneity of interactions with the modulation depending on the position. More specifically, we model a system where the interaction strength is different in the right and left well of the trap, with both the absolute strength of interaction and their asymmetry depending on controllable parameters.

The interaction coupling is thus modeled as [109] (Fig. 5.1(a))

$$g(R) = g_0[1 + \alpha \tanh(\frac{R}{L})],$$

where $2R = x_i + x_j$ and L is the modulation length which we fix at $L = 1$.

For $R \gg L$, g takes the asymptotic values

$$g_\pm = g_0(1 \pm \alpha).$$

Thus the parameter α regulates the relative difference in interaction strength between the left and the right well,

$$\Delta g \equiv |g_+ - g_-| = 2g_0\alpha,$$

and the corresponding ratio is given by

$$\frac{g_+}{g_-} = \frac{1+\alpha}{1-\alpha}.$$

5.1.3 Scaling

For reasons of universality as well as computational aspects, we will rescale the system to the length scale of the 1D longitudinal system, a_\parallel . This is achieved by making the coordinate transformation $Q' := Q/a_\parallel$, with $Q \equiv (x_1, \dots, x_N)^T$, [109] which leads to

$$\underbrace{H(Q)/\omega_\parallel}_{=: H'(Q')} = \sum_i \left(-\frac{1}{2} \partial_i'^2 + U'(x'_i) \right) + \sum_{i < j} V'(x'_i - x'_j).$$

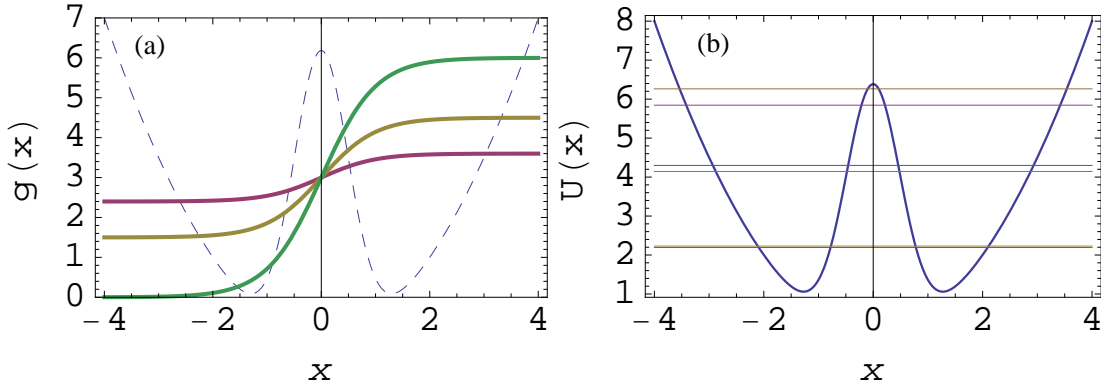


Figure 5.1: (a) Variation of the spatially modulated interaction coupling $g(x)$ plotted for $\alpha = \{0.2, 0.5, 1.0\}$ at $g_0 = 3.0$ shown in the background of the double-well trap (scaled appropriately for visual clarity). (b) Single particle energy spectrum of a double-well with barrier height $h = 8$ and width $\omega = 0.5$.

Here $\omega_{\parallel} \equiv 1/Ma_{\parallel}^2$ defines the energy scale, and $U'(x') := U(x = x'a_{\parallel})/\omega_{\parallel}$ is the rescaled dimensionless potential.

H' is a very convenient Hamiltonian especially for numerical computation and is employed for all the preceding calculations. The primes are left out for convenience.

The scaled 1D interaction term is given by:

$$V'(x') = g'_{\text{1D}}\delta(x'), \quad g'_{\text{1D}} := \frac{4a'_0}{a'^2_{\perp}} \left(1 - C \frac{a'_0}{a'_{\perp}}\right)^{-1}. \quad (5.4)$$

The relevant parameter of the interaction is only the scaled interaction strength which in turn depends on the scaled scattering length $a'_0 = a_0/a_{\parallel}$ and the scaled transverse confinement $a'_{\perp} = a_{\perp}/a_{\parallel}$.

5.2 Tunneling Dynamics for Two Boson System

We first focus on the tunneling dynamics in a symmetric double-well with two bosons initially ($t = 0$) prepared in the left well. This is achieved by adding a tilt or a linear potential dx to the Hamiltonian hence making the left well energetically favorable. Instantaneously, the ground-state is obtained by applying the relaxation method (imaginary time propagation). For reasonably large d , this results in achieving a complete population imbalance between the wells. With this state as the initial state, the tilt is instantaneously ramped down ($d = 0$) at $t = 0$ to study the dynamics in a symmetric double-well. Our aim is to study the impact of the correlations between the bosons on the tunneling dynamics both with respect to the interaction strength as well as the spatial inhomogeneity. For that, we first start by comparing the homogeneous interaction case $\alpha = 0.0$ with the case of a fixed inhomogeneity of $\alpha = 0.2$ and analyzing how the dynamics varies with changing interaction strength g_0 .

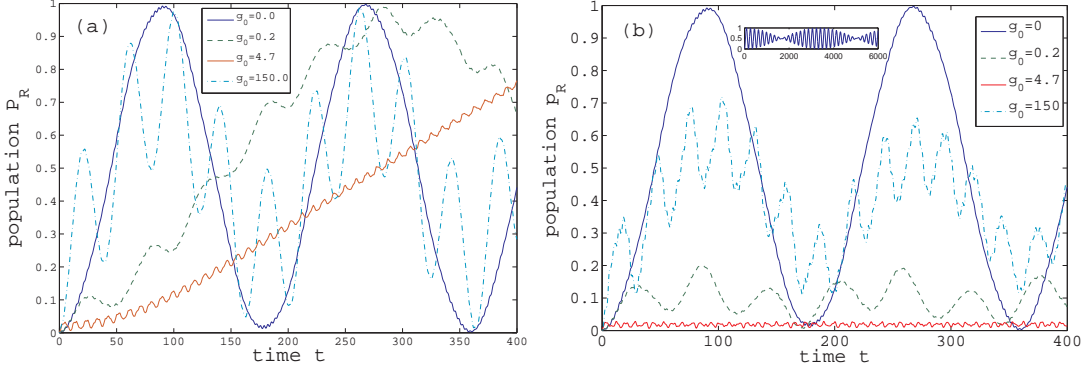


Figure 5.2: Population of the right-hand well over time, $p_R(t)$, for different interaction strengths for (a) $\alpha = 0.0$ and (b) $\alpha = 0.2$ with two bosons. *Inset*: Long time behavior for very low interaction strength $g_0 = 0.005$. Barrier height $h = 8$ and width $\omega = 0.5$ has been used for all calculations. (all quantities are in dimensionless harmonic oscillator units throughout).

5.2.1 Dynamics from the uncorrelated to the fermionization limit.

In the absence of any interaction $g_0 = 0$, the bosons undergo Rabi oscillations between the two wells. This is characterized by complete tunneling of both bosons between the two wells with a single frequency and can be quantified by the time variation of the population of the atoms in the right well

$$P_R(t) = \langle \Theta(x) \rangle_{\Psi(t)} = \int_0^\infty \rho(x; t) dx$$

where ρ is the one-body density. Figure 5.2 shows that P_R oscillates sinusoidally between 0 and 1. If we introduce a very small interaction $g_0 = 0.005$, the Rabi oscillations give way to a beat pattern due to the existence of two very close frequencies (Fig 5.2(b) inset).

Increasing the interaction strength further ($g_0 = 0.2$), we observe a suppression of tunneling for $\alpha = 0.2$ (Fig 5.2(b)), with the maximum population in the right well $P_R^{max} \approx 0.2$. This is a manifestation of the inhomogeneous interaction which drives the tunneling off-resonance and contrasts with that of $\alpha = 0.0$ (Fig 5.2(a)), where we have complete pair-tunneling with an elongated period compared to that of the Rabi oscillations. The dynamics in both cases shows two-mode characteristics, consisting of a slow tunneling envelope, which is modulated by a faster oscillation.

For higher values of interaction strength ($g_0 = 4.7$), the tunneling is completely suppressed for $\alpha = 0.2$ (Fig 5.2(b)). What remains is a fast oscillation with a tiny amplitude. This needs to be differentiated from an apparent suppression in short time-scales seen for $\alpha = 0.0$ (Fig 5.2(a)), which is a consequence of an extremely long tunneling times and is the few body analog of the self-trapping mechanism for condensate [46, 47, 105, 107, 108]. For $\alpha = 0.2$ instead, we observe an actual suppression

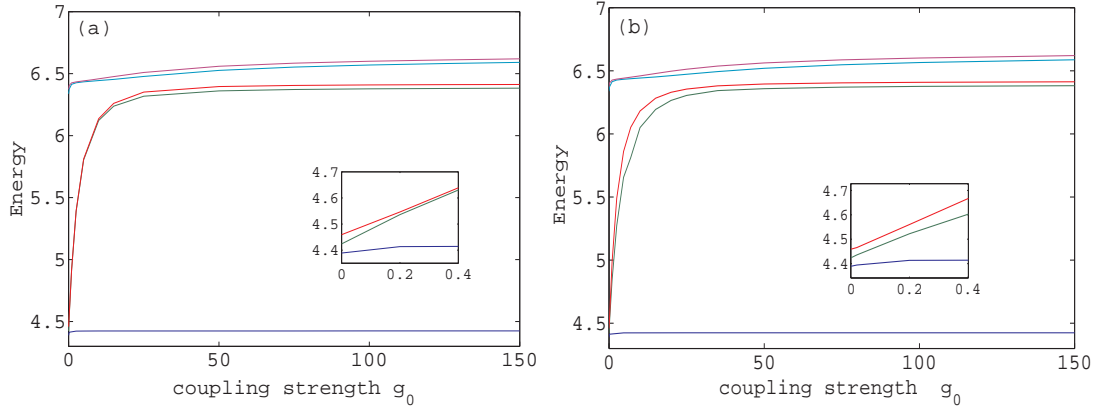


Figure 5.3: Two particle energy spectrum as a function of the interaction strength g_0 for (a) $\alpha = 0.0$ (b) $\alpha = 0.2$. *Inset*: Lowest energy levels for low interaction strength.

of the tunneling amplitude and not so much a delayed process.

However, contrary to the naive intuition a reappearance of tunneling occurs for $\alpha = 0.2$ at larger values of the coupling strength. This is understandable since clearly both for the non- and infinitely interacting limits the inhomogeneity doesn't play a role. Thus for very large g_0 values, the effect of the inhomogeneity α reduces and completely vanishes for $g_0 \rightarrow \infty$. We thus observe a partial restoration of tunneling with $P_R^{max} = 0.7$ for the value $g_0 = 150$ (Fig 5.2(b)), which is close to the fermionization limit. This shows the trend towards the ideal fermionization dynamics which is clearly observed for $\alpha = 0.0$ (Fig 5.2(a)) and is characterized by two frequencies - one very close to the Rabi frequency modulated by a faster oscillation. Ideally at the fermionization limit $g_0 \rightarrow \infty$, the system of hardcore bosons maps to a system of free fermions [8] and all the local properties are identical. Hence in this limit we would have complete two-mode single particle tunneling analogous to tunneling of two free fermions.

Before we move on to analyze in detail the above observations, let us comment briefly on the differences between the behavior observed in our setup having inhomogeneous interaction with a symmetric double-well and the case of an asymmetric double-well with homogeneous interaction. The effects in the low interaction regime are equivalent: The tilt has the same effect as an interaction asymmetry, namely it destroys resonant behavior thereby leading to a suppression of tunneling [48,49]. Nevertheless, our case is fundamentally different and this is evident in the strong interaction regime. Specifically the reemergence of tunneling we observe does not occur in the tilted double-well system.

5.2.2 Analysis

The understanding of the above-described dynamics lies in the variation of the few body spectrum as g_0 is changed from zero to the fermionization limit (Fig.5.3(a)). Considering the wave-function $\Psi(t) = \sum_m e^{-iE_m t} c_m \Psi_m$ with energy E_m corresponding

to the stationary state Ψ_m , the population imbalance $\delta(t) \equiv \langle \Theta(x) - \Theta(-x) \rangle_{\Psi(t)}$ can be computed to be

$$\delta(t) = 4 \sum_{m < n} W_{mn} \cos(\omega_{mn}t) + 2 \sum_m W_{mm} - 1, \quad (5.5)$$

where $W_{mn} = \langle \Psi_m | \Theta(x) | \Psi_n \rangle c_m c_n$ and $\omega_{mn} = E_m - E_n$.

The energy spectrum of both the non-interacting and the fermionization limit can be understood from the single particle energy spectrum of the double well (Fig. 5.1(b)), which is in the form of bands each pertaining to a pair of symmetric and antisymmetric orbitals (see Appendix B for details).

In the uncorrelated limit ($g_0 \rightarrow 0$), the low-lying energies of the spectrum are obtained by distributing the atoms over the symmetric and antisymmetric single particle orbitals in the first band. This leads to $N + 1$ energy levels, N being the number of bosons. $E_m = E_0 + m\Delta^0$ with $m = 0, \dots, N$ where $\Delta^0 = \epsilon_1 - \epsilon_0$ is the energy difference between the two single particle orbitals in the first band. Thus for $g_0 = 0$, the levels are equidistant (Fig.5.3(a) inset) and we see Rabi oscillation with frequency $\omega_{01} = \omega_{12} = \Delta^0$. As the interaction is increased ($g_0 = 0.005$), this equidistance is slightly broken ($\omega_{01} \simeq \omega_{12}$) and we get a superposition of two very close frequencies. This results in the formation of the beat pattern seen in the dynamics for $g_0 = 0.005$.

To understand the dynamics in the low interaction regime, it is instructive to map our system to a two-site Bose-Hubbard Hamiltonian [15, 16]

$$\hat{H} = -J(\hat{c}_L^\dagger \hat{c}_R + \hat{c}_R^\dagger \hat{c}_L) + \sum_{j=L,R} \frac{U_j}{2} \hat{n}_j (\hat{n}_j - 1) \quad (5.6)$$

where J is the tunneling coupling, $U_{L,R}$ is the on-site energy of the left/right well and $\hat{n}_j \equiv \hat{c}_j^\dagger \hat{c}_j$.

Using the B-H Hamiltonian for $U_L, U_R \gg J$, the highest two eigenvalues are approximately U_R and U_L . Whereas in the homogeneous case $\alpha = 0$, these two levels are close to degenerate $U_L \approx U_R$ (Fig.5.3(a) inset), here we have a breaking of the parity symmetry since $U_R > U_L$ (Fig.5.3(b) inset). This is understandable since two particles localized in the left well have lower energy than two particles in the right well leading to the energy level separation seen in Fig.5.3(b) (inset). In terms of the number-state representation in the localized basis $|N_L^{(0)}, N_R^{(0)}\rangle$, the degenerate eigenstates for the homogeneous case read

$$\phi_{1,2} \approx \frac{1}{\sqrt{2}}(|0, 2\rangle \pm |2, 0\rangle)$$

and consequently the dynamics consists of shuffling the probability between the two states corresponding to a complete two particle tunneling.

In the case of sufficiently strong inhomogeneous interaction, the removal of the degeneracy of the energy levels leads to a decoupling of the eigenstates into localized number-states

$$\phi_1 \approx |2, 0\rangle, \phi_2 \approx |0, 2\rangle$$

This implies that the initial state $\psi(t=0) = |2, 0\rangle$ is very close to the first excited state ϕ_1 and, thus, is effectively a stationary state of the system. This results in the suppression of tunneling for corresponding values of g_0

In the fermionization limit ($g_0 \rightarrow \infty$), the system possesses the same local properties as a system of non-interacting fermions due to the Bose-Fermi mapping [8]. Thus, in an ideal case, the inhomogeneity doesn't manifest ($g_{\pm} \rightarrow \infty$) and the tunneling dynamics is identical to a system of free fermions. As an idealization, if we consider the initial state as two non-interacting fermions in the left well, then they would occupy the lowest two orbitals localized in the left well. In terms of the single particle eigenstates of the double well $|n_{a\beta}^{(\beta)}\rangle$ where $n_{a\beta}^{(\beta)}$ denotes the occupation number of the symmetric ($a_{\beta} = 0$) or antisymmetric ($a_{\beta} = 1$) orbital in band β , the tunneling frequencies $\omega_{nn'} = E_n - E'_n$ are given by [47]

$$\omega_{nn'} = \sum_{\beta} \Delta^{\beta} \underbrace{(n_1^{\beta} - n_1'^{\beta})}_{=0, \pm 1} \quad (5.7)$$

where Δ^{β} denotes the energy splitting of the band β , n_1^{β} represents the occupation of the anti-symmetric orbital of the band β . Thus, for two particles the contributing frequencies are the lowest band Rabi frequency Δ^0 and the tunnel splitting of the first excited band Δ^1 . The tunneling dynamics can be pictured roughly as two fermions tunneling independently in the first two bands.

In our system however the finiteness of the g_0 value leads to deviations from the ideal fermionic dynamics. While the homogeneous case $\alpha = 0.0$ is close to the ideal fermionic dynamics, for $\alpha = 0.2$, the inhomogeneity of the interaction still manifests leading to a difference with respect to the localized two-particle energy level in each well, and the tunneling remains incomplete.

5.2.3 Dynamics with varying inhomogeneity

Having analyzed how the dynamics varies with changing interaction strength at a fixed interaction asymmetry and comparing it to the homogeneous case, it is worthwhile to study the dependence of the tunneling dynamics on the strength of the inhomogeneity explicitly. For this, we study the effect of different α values on the tunneling dynamics for a fixed $g_0 = 0.2$.

In Fig.5.4 we observe that for $\alpha = 0$, we have complete tunneling with a two mode dynamics i.e. fast oscillations (ω_{01}) which modulate slower tunneling oscillations (ω_{12}).

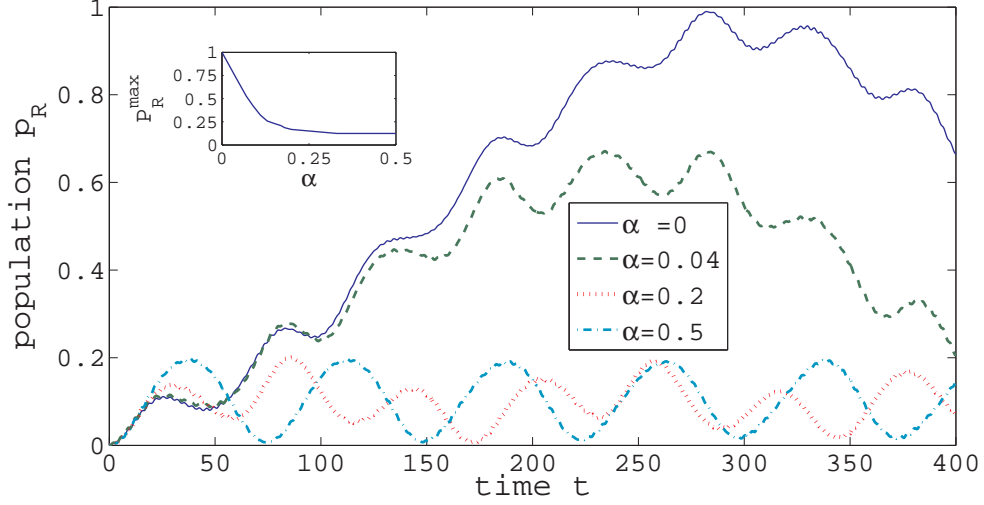


Figure 5.4: Population of the right-well over time, $P_R(t)$, at $g_0 = 0.2$ for different α values. *Inset*: Variation of maximum population of the right well P_R^{max} with α for $g_0 = 0.2$.

When α is increased to a value of 0.04, the tunneling maximum is reduced to roughly 0.7 while still retaining the two-mode character. As α is further increased to 0.2 the tunneling is suppressed as described in Sec. 5.2.2. The characteristic display of fast and slow oscillations arising due to the time-scale difference of the contributing frequencies is not prominent here and for higher interaction asymmetry ($\alpha = 0.5$), we have effectively single mode tunneling with frequency ω_{01} .

The variation of the maximum population P_R^{max} with the inhomogeneity α (Fig.5.4 inset) shows a sharp drop with increasing α before effectively reaching a constant value ~ 0.12 for $\alpha \geq 0.3$. The reader should note that P_R^{max} does not go to zero in the asymptotic limit $\alpha \rightarrow 1$ or $\frac{U_R}{U_L} \rightarrow \infty$. This is due to the fact that with a finite value of g_0 and a finite barrier height the tunneling coupling (J) is not negligible compared to U_R . As a consequence there remains a finite probability of bosonic tunneling between the two wells.

5.2.4 Strong interaction inhomogeneity

An extremely strong inhomogeneity at a high interaction value leads to an interesting higher band tunneling dynamics. We can realize such a system by having $\alpha = 1$ at $g_0 = 25$. This set up effectively makes the bosons fermionized in the right-well and almost non-interacting in the left. Preparing the initial set-up with both bosons in the left well leads to the suppression of tunneling. However if we prepare the initial state with two boson in the right well, then we observe substantial tunneling. In Fig.5.5 (a) we see that the P_R oscillates between 1 and 0.5 indicating a single boson tunneling with a single dominant frequency.

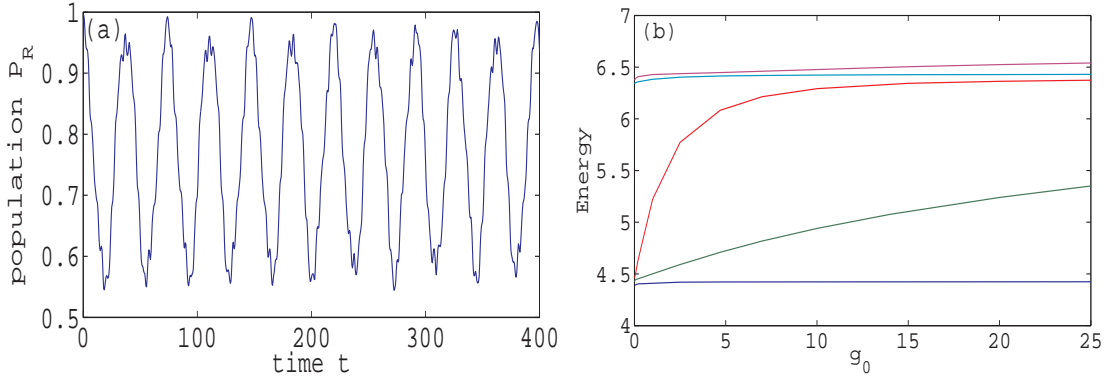


Figure 5.5: (a) Population variation with time $P_R(t)$ at $g_0 = 25$ and $\alpha = 1$ for $P_R(0) = 1$, i.e initially populating the right-well. (b) Energy spectrum for $\alpha = 1$

In order to understand the phenomenon we look at the energy spectrum at $\alpha = 1$ (Fig.5.5 (b)). While the ground-state remains unaffected, what we see is that close to the fermionization regime ($g_0 = 25$), the first excited state decouples from the higher three states, which come closer. The main contribution to the first excited state is the state $|2, 0\rangle$, and its separation from the other states could be understood from the fact that two boson in the left-well is almost non-interacting and thus energetically far off resonant from two effectively fermionized boson in the right-well $|0, 2\rangle$. The consequences of this fact are the following: (i) The initial configuration of $|2, 0\rangle$ becomes a stationary-state resulting in a highly suppressed tunneling, and (ii) the state $|0, 2\rangle$ of the lowest band becomes energetically resonant and couples to the states $|1^1, 1^0\rangle$ and $|1^0, 1^1\rangle$ in the higher bands (where the superscript refer to the ground (0) or excited (1) orbital of the corresponding well). The latter leads to a tunneling dynamics in the higher band states predominantly between the 2nd and the 4th excited eigenstates (see Fig. 5.5 (b)), which have greater overlap with the initial state $|0, 2\rangle$. These orbitals have mostly contributions from the states $|0, 2\rangle$ and $|1^1, 1^0\rangle$, while the other orbital has minimal overlap with the initial state. As a result we get a single-particle tunneling with one dominant frequency given by the splitting of the energy between these two levels. In other words, we effectively have a single boson tunneling between the wells in the excited band. Note that this highly correlated single-particle tunneling scenario is attributed to the high inhomogeneity in the strong interaction regime since the combination of these two factors are responsible for turning the pair-tunneling scenario off-resonance.

5.3 Multi-Particle Dynamics

Having analyzed the tunneling dynamics of two atoms let us now focus on the case of three or more atoms to see the general atom number dependence of tunneling in the presence of spatially modulated interactions.

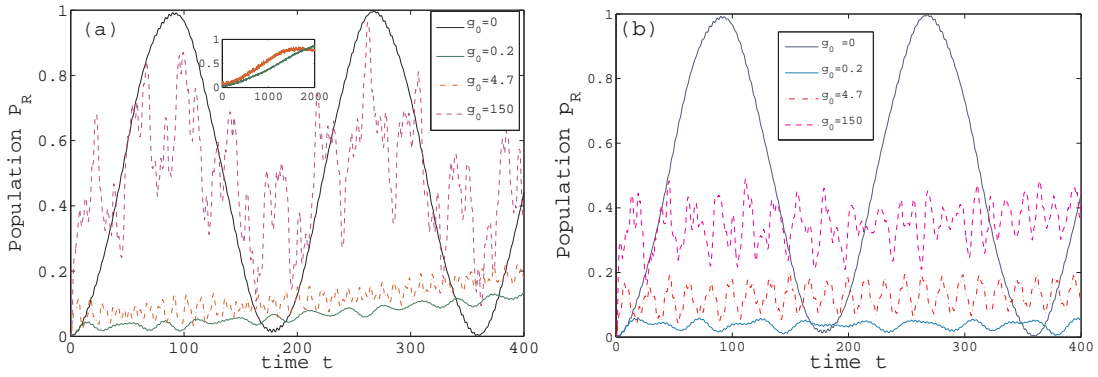


Figure 5.6: Population of the right-hand well over time, $P_R(t)$, for three bosons for different interaction strengths (a) at $\alpha = 0.0$. Inset: Long time behavior for $g_0 = 0.2$ (longer period) and $g_0 = 4.7$ (shorter period) (b) for $\alpha = 0.2$.

5.3.1 General behavior and mechanisms

Like in the two boson case, we start with the initial state of $N = 3$ bosons prepared in the left well. As shown in Fig. 5.6, the main effects are similar to the two-atom case. The dynamics is again governed by frequencies determined by the energy difference of the low lying spectrum. For very small interaction, the nearly equal energy difference gives rise to the beat pattern similar to that of two particles (not shown here). As we increase the interaction strength to $g_0 = 0.2$, there is a elongation of the time period for $\alpha = 0.0$, although we have complete tunneling. On the other hand for inhomogeneous interaction at $\alpha = 0.2$, we observe suppression of tunneling. On further increase of interaction to $g_0 = 4.7$, we observe decrease in the time-period for $\alpha = 0.0$, while for $\alpha = 0.2$, there is a partial restoration of tunneling. A higher amplitude reemergence close to the fermionization limit at $g_0 = 150$ for $\alpha = 0.2$ showing the crossover to fermionization which is recovered more significantly for $\alpha = 0.0$.

The general mechanism for the suppression is the same as for the two particle case. Now, however, in the symmetric case $\alpha = 0$, the contributing nearly degenerate eigenstates are of the form $|N, 0\rangle \pm |0, N\rangle$. Consequently we have a complete N particle tunneling with a frequency given by [105] $\omega \sim 2NU/(N-1)! \times (2\Delta^0/U)^N$ where $U = U_L, U_R$ denotes the on-site interaction energy. The tunnel period thus grows exponentially with N . When the inhomogeneous interaction is introduced, the states decouple to the localized number-states $|N, 0\rangle$ and $|0, N\rangle$ and thus the initial state becomes a stationary one leading to the suppression of tunneling. The important thing to note is that with increasing N , the suppression of tunneling occurs for much smaller values of g_0 . For instance at $g_0 = 0.2$ for $N = 3$ we have almost complete suppression in contrast with $N = 2$ where we still observed significant tunneling (see Fig.5.2) for this value of g_0 . This could be understood from the fact that the contribution of the on-site energy on the cat-state goes as $\sim U_{L,R}N(N-1)/2$, while that of the tunneling

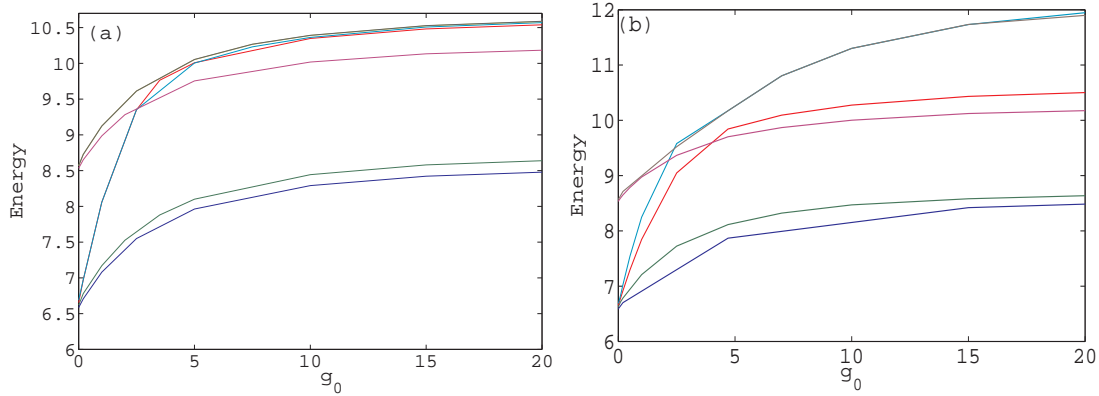


Figure 5.7: Three boson energy spectrum with g_0 at (a) $\alpha = 0.0$ and (b) $\alpha = 0.2$.

term is N independent. This fact is responsible for a significant decoupling of these states at a lower g_0 value leading to faster suppression of tunneling as N increases.

Also unlike that of the two boson case, the spectrum for the three boson case contains crossings between the higher-lying states (see Fig.5.6(b)) and in the vicinity of these crossings there is a partial reappearance of tunneling. This can be seen for instance at $g_0 = 4.7$, where we observe a restoration in the three-particle case whereas for two particles we still observed a significant suppression (see Fig. 5.2). In this regime the higher bands contribute more significantly resulting a decrease of the tunneling period as well as leading to the convoluted dynamics observed. These higher band contributions leads to further recovery with increasing interaction strength towards the fermionization regime although for $\alpha = 0.2$, even for $g_0 = 150$ we do not get the exact fermionic dynamics which is characterized by the tunneling of three independent fermions.

5.3.2 Generating tunneling resonances by interaction inhomogeneity

A very interesting phenomenon for the $N \geq 3$ particle case is that by tuning the asymmetry α , we get a controllable reemergence of tunneling. To observe this, we study how the tunneling dynamics changes with different values of α for $g_0 = 0.2$ (Fig.5.8). The value of g_0 is chosen such that the inhomogeneity effect manifest but is still in the two-mode regime. For three atoms we observe (Fig.5.8(a)) that a complete tunneling for $\alpha = 0$ gives way to suppressed tunneling with increasing α value. However at $\alpha = 0.5$, we observe a reappearance which is in form of a tunneling resonance peaked at $\alpha = 0.5$ with $P_R^{max} \approx 0.6$ corresponding to effective two boson tunneling. In the case of $N = 4$, we see two resonances (fig.5.8(b) *inset*) - the larger one centered on $\alpha = 0.3333$ with an amplitude 0.75, and the smaller one at $\alpha = 0.6667$ with an amplitude 0.5 resulting in the reappearance of tunneling shown in Fig.5.8(b).

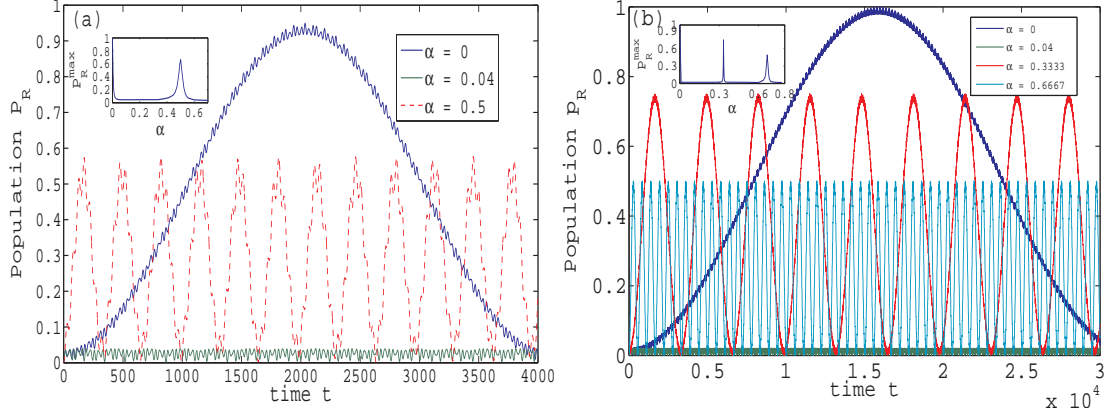


Figure 5.8: Population of the right-well over time, $P_R(t)$, at $g_0 = 0.2$ for different α values for (a) 3-particles and (b) 4-particles. *Inset:* Variation of maximum population of the right well P_R^{max} with α for $g_0 = 0.2$.

In order to understand this we have to study the spectra and the underlying eigenstates for different α (Fig.5.9). In the case of $N = 3$, for no asymmetry $\alpha = 0$, the highest two levels form a doublet (Fig.5.9(a)) and the corresponding eigenstates are degenerate of the form $\frac{1}{\sqrt{2}}(|3,0\rangle \pm |0,3\rangle)$. As α is increased, the parity symmetry is broken, and the doublets separate, and likewise the eigenstates decouple (Fig.5.9(b)). The energy eigenvalues (in the limit of very high g_0) are given by U_L , U_R , $3U_L$ and $3U_R$ with the corresponding eigenstates $|2,1\rangle$, $|1,2\rangle$, $|3,0\rangle$ and $|0,3\rangle$. However, when $U_R \approx 3U_L$ ($\alpha = 0.5$), the first and the second excited eigenstates become near degenerate and form a doublet of the form $\frac{1}{\sqrt{2}}(|1,2\rangle \pm |3,0\rangle)$ (Fig.5.9(c)). Thus, the initial state $|3,0\rangle$ is no longer a stationary state of the system. As a consequence, we get a restoration of tunneling and the dynamics basically involves shuffling atoms between these two number-states. In other words we have tunneling of two particles between the two wells while one particle remains in the left well. This resonant two particle tunneling is what we observe for the $\alpha = 0.5$ case. As α is increased further, this degeneracy is once again broken and the states decouple leading back to the suppressed tunneling dynamics. This is reminiscent of what happens in the asymmetric double-well for homogeneous interactions [48].

In similar consideration, for the 4-particle case the energy eigenvalues are $3U_L$, $6U_L$, $(U_L + U_R)$, $3U_R$ and $6U_R$. Now if $U_R \rightarrow 2U_L$ ($\alpha = 0.3333$), then we have two degeneracies viz $3U_R \rightarrow 6U_L$ and $(U_L + U_R) \rightarrow 3U_L$ corresponding to the eigenstates $\frac{1}{\sqrt{2}}(|4,0\rangle \pm |1,3\rangle)$ and $\frac{1}{\sqrt{2}}(|3,1\rangle \pm |2,2\rangle)$. Since the initial state is $|4,0\rangle$, only the first degeneracy contributes. Thus the dynamics in this case consists of tunneling of three bosons between the wells while one boson remains in the left well. This results in the tunneling amplitude of 0.75. The second tunneling peak occurs for $U_R \rightarrow 5U_L$ ($\alpha = 0.6667$), which leads to $(U_L + U_R) \rightarrow 6U_L$. The corresponding degenerate eigenstates are $\frac{1}{\sqrt{2}}(|4,0\rangle \pm |2,2\rangle)$ and we observe tunneling of two bosons on top of others remaining

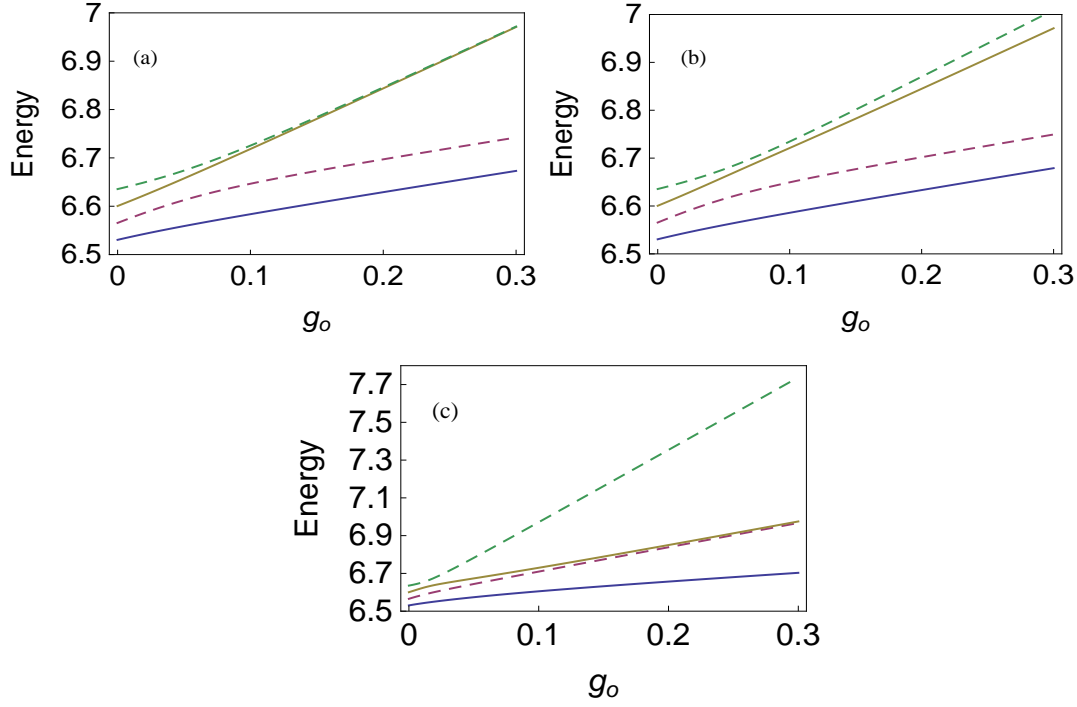


Figure 5.9: Three particle energy levels for $0 < g_0 < 0.3$ for (a) $\alpha = 0$, (b) $\alpha = 0.04$ and (c) $\alpha = 0.5$.

in the left well and thus the tunneling peak of 0.5. The above analysis can be extended generically for N particles where we would have $N - 2$ resonances corresponding to the degeneracies between the eigenstates.

5.3.3 Correlations

In order to study the exact nature of tunneling dynamics, we need to investigate the correlations between the particles. For this we study the temporal evolution of the pair-probability or the probability of finding two particles in the same well defined by

$$p_2(t) = \langle \Theta(x_1)\Theta(x_2) + \Theta(-x_1)\Theta(-x_2) \rangle_t \quad (5.8)$$

and the three-particle-probability or the probability of finding all three particles in the same well defined by

$$p_3(t) = \langle \Theta(x_1)\Theta(x_2)\Theta(x_3) + \Theta(-x_1)\Theta(-x_2)\Theta(-x_3) \rangle_t \quad (5.9)$$

In the case of $N = 3$, for homogeneous interaction $\alpha = 0$ at $g_0 = 0.2$, both p_2 and p_3 oscillate close to unity (Fig.5.10). This implies that all the three particles can be found in the same well or in other words they tunnel together between the wells. This confirms the analysis of the dynamics by the eigenstate analysis in the preceding section

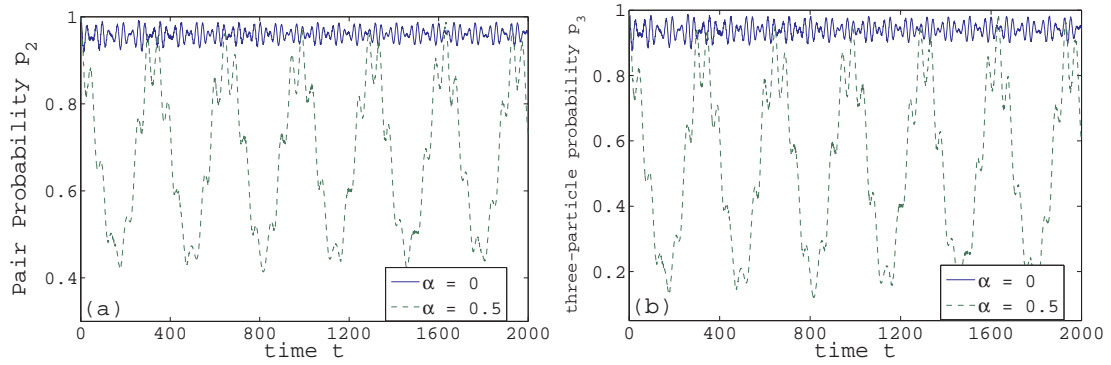


Figure 5.10: Temporal evolution of (a) pair-Probability and (b) three particle probability at $\alpha = 0$ and $\alpha = 0.5$ for $N = 3$ and $g_0 = 0.2$.

as tunneling between $|3, 0\rangle$ and $|0, 3\rangle$ states.

Similarly at resonance ($\alpha = 0.5$), we find that p_3 oscillates from 0.1 and 1 implying that the system oscillates between a three-particle state to a non-three-particle state, namely the pair-state $|1, 2\rangle$ which can be inferred from the variation of p_2 (Fig.5.10(b)). As a result we have pair tunneling on top of a particle remaining in the left-well. (Ideally in the case of B-H model, p_2 should be oscillating between 1 and 0.33 while p_3 between 1 and 0. However in our case the realistic potential and parameter regimes as well as some higher band contributions leads to the some deviations from this behavior).

5.4 Asymmetric Double-Well

Thus far we have investigated the dynamics in symmetric double-well with inhomogeneously interacting bosons. An interesting extension is to study the dynamics in an asymmetric double-well. This gives us the chance to examine the interplay between the interaction inhomogeneity and the tilt. A special interesting consideration would be to see if the tilt could be tuned to offset the inhomogeneity in the interaction and mimic the dynamics of symmetric interaction case or further, if it can generate some new tunneling resonances.

5.4.1 Generating tunneling resonances by a tilt.

In symmetric wells with homogeneous interaction, the localized N particle state $|N, 0\rangle$ has the same energy as that of the state $|0, N\rangle$ resulting in a complete N -particle tunneling between the wells. With the introduction of the inhomogeneity with respect to the interaction, this resonance is broken and the energy of N particles in the right well is higher than that in the left well resulting in the suppression of tunneling as seen before. Now, if we incorporate a tilt in the double well such that the left well is lifted and right well is pushed down energetically in exactly the right amount to make

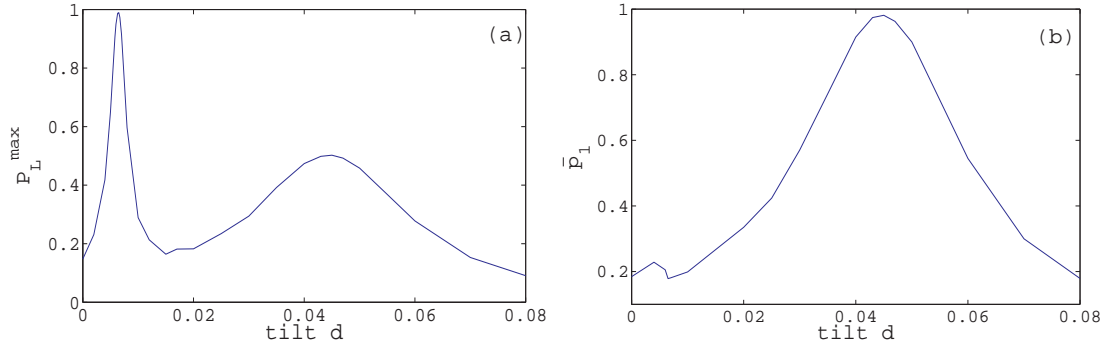


Figure 5.11: Variation of (a) tunneling maximum P_L^{max} with tilt d (b) maximum single particle probability \bar{p}_1 with tilt d for $N = 2$, $g_0 = 0.2$ and $\alpha = 0.2$.

the localized N particle energy levels resonant then we should expect a reemergence of tunneling.

To observe this we prepare the initial state with both particles in the right well $\psi(0) = |0, 2\rangle$ and study the variation of the tunneling maximum P_L^{max} with a tilt d (Fig.5.11(a)) incorporated into the Hamiltonian as a linear term $-dx$. We restrict ourselves to the $\alpha = 0.2$ and $g_0 = 0.2$ cases. We observe a sharp resonance at $d \approx 0.0065$ corresponding to the tilt which exactly balances the localized pair-state energy difference due to inhomogeneous interaction. The result is pair-tunneling between the two wells as we would have it in a completely symmetric set-up.

With higher tilt, the tunneling maximum falls off very sharply as the pair-state becomes off-resonant again, and we get a suppression of tunneling. The next maximum occurs when the tilt is large enough to make the localized pair state $|0, 2\rangle$ resonant with the state $|1, 1\rangle$. This results in a broad tunneling maximum at $d \approx 0.045$ corresponding to single-particle tunneling.

To confirm our analysis of the tunneling mechanism, we look at the variation of maximum single particle probability \bar{p}_1 with tilt (Fig.5.11(b)), defined as $\bar{p}_1 = \max_t(1 - p_2(t))$, which gives the probability of having only one particle in a well. We observe a negligible value at the first resonance $d \approx 0.0065$ confirming that the dynamics is pair-tunneling while a very broad maximum peaked at the second resonance $d \approx 0.045$ corresponds to the maximum probability of finding a single particle, which in our case is the $|1, 1\rangle$ state and the dynamics is a single particle tunneling between the $|0, 2\rangle$ and $|1, 1\rangle$ states.

5.4.2 Spectral Analysis

To understand the effect of the tilt on the tunneling dynamics, we study the energy spectra E with varying tilt d at fixed $g_0 = 0.2$ and $\alpha = 0.2$ (Fig.5.12). At $d = 0$, the eigenstates are basically number-states in the localized basis. With increasing d , the highest two levels $|0, 2\rangle$ and $|2, 0\rangle$ move closer and form a sharp avoided crossing

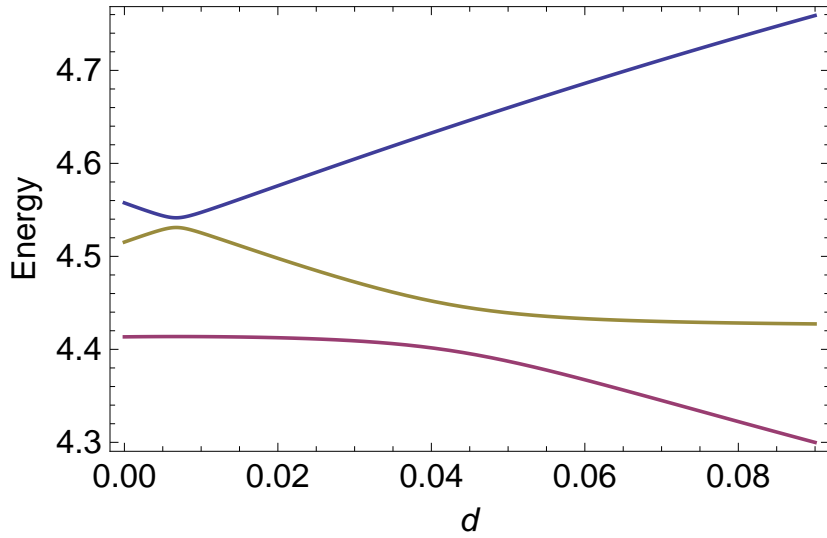


Figure 5.12: Two particle energy spectrum with tilt d for $\alpha = 0.2$ and $g_0 = 0.2$.

at $d \approx 0.0065$ corresponding to the first tunneling resonance. At this point the tilt exactly balances the interaction inhomogeneity and the eigenstate is in form of the cat-state $|2, 0\rangle \pm |0, 2\rangle$. This state is very sensitive to the tilt, and a minute perturbation decouples them into the localized number-state resulting in a very sharp tunneling resonance. The ground-state, which is the $|1, 1\rangle$ state, is insensitive to the tilt since this lowering of one particle and raising another particle keeps the state energetically unaffected within the linear regime. This state forms a broad (anti)crossing with the lower excited state at $d \approx 0.045$ forming the broad single-particle tunneling resonance seen in the dynamics. This behavior seen in the two-particle case can be expected in general for N particles giving N resonances corresponding to the avoided crossings encountered. In particular with increasing tilt, the successive resonances corresponds to a mechanism where one less particle tunnels compared to that of the previous one while the width of the resonances becomes progressively broader.

Chapter 6

Tunneling dynamics of binary bosonic mixtures

In the previous chapter we studied the tunneling dynamics of a single species bosonic system. In this chapter we extend the study of the dynamics to a system of binary bosonic mixtures. A system of bosonic mixture consisting of multiple species of bosons promises a plethora of new possibilities to explore the fundamental processes of bosonic systems.

Investigations into the tunneling dynamics using mean-field approaches or lowest band approximations demonstrate various effects such as macroscopic quantum self-trapping and coherent quantum tunneling [69], observations of collapse and revival of population dynamics [74, 75], symmetry breaking and restoring scenarios [72] as well as dipole oscillations induced pairing and counterflow superfluidity [76]. However these works are confined mainly to the weak interaction regimes.

Here we study the tunneling dynamics of a binary mixture of bosonic species in a one-dimensional double-well investigating the crossover from the weak to the strong interaction regime. We focus on how the interplay between the inter- and intra- species interactions and the initial setup affect the rate and mechanism of the tunneling.

The chapter is organized as follows. In Section 6.1 we introduce our model and setup. Subsequently we present and discuss the results for the quantum dynamics of the mixture with three bosons (two bosons of species A and one of species B). Three initial state scenarios are examined: complete population imbalance in Sec. 6.2, complete phase-separated in Sec. 6.3, and partial imbalance in Sec. 6.4.

6.1 Model and setup

We consider a mixture of two species of bosons labeled by A and B in a one-dimensional double well potential. These may correspond to two different kinds of atoms or could be two hyperfine states of the same atomic species. The fact that there are two different

species induces distinguishability and thus fundamentally alters the physics and in particular the quantum dynamics compared to the case of a single species.

The Hamiltonian for the system reads (see [64] for details)

$$H = \sum_{\sigma=A,B} \sum_{i=1}^{N_{\sigma}} \left[\frac{p_{\sigma,i}^2}{2M_{\sigma}} + U_{\sigma}(x_{\sigma,i}) + \sum_{i<j} V_{\sigma}(x_{\sigma,i} - x_{\sigma,j}) \right] + \sum_{i=1}^{N_A} \sum_{j=1}^{N_B} V_{AB}(x_{A,i} - x_{B,j}). \quad (6.1)$$

where $M_{A,B}$ is the mass for species A and B , respectively.

We assume here that the different species obey the same single particle Hamiltonian, i.e., they possess the same mass and experience the same single-particle potential. In the ultracold scattering limit, one can approximate the interaction (both intra- V_{σ} and inter-species V_{AB}) with an effective contact potential [10]

$$\begin{aligned} V_{\sigma}(x_{\sigma,i} - x_{\sigma,j}) &= g_{\sigma} \delta(x_{\sigma,i} - x_{\sigma,j}) \\ V_{AB}(x_{A,i} - x_{B,j}) &= g_{AB} \delta(x_{A,i} - x_{B,j}) \end{aligned}$$

The different initial configurations are achieved by adding a tilt to the double-well which can be different for the two species depending on the required state. Thus an individual well could be made energetically more favorable (tilted) for a certain species. For instance, to prepare a complete imbalance, the double wells of both species are tilted the same way, while to prepare a phase-separated scenario U_A is tilted opposite to U_B . The ground-state is then computed by the relaxation method and results in the desired initial state. For the study of the dynamics the tilt is instantaneously ramped down to obtain a symmetric double-well at $t = 0$.

The simplest few-body bosonic mixture which exhibits many of the important quantum dynamical processes is that of three bosons - two bosons of species A and one of species B . In this case we have two independent parameters g_{AB} and g_A (since there is only a single boson B species). When the inter-species interaction g_{AB} is zero, the two components are completely decoupled meaning that the single B boson will undergo Rabi oscillations between the wells. The A bosons will then follow a correlated two-particle dynamics regulated by the intra-species interaction g_A (This case is not addressed here but has been discussed in detail in the literature [46,47]. See also Chapter 5). Another case which reduces to that of a single species is $g_{AB} \rightarrow g_A$, where the essentials of the tunneling dynamics is that of three particles of a single species. Our focus is exclusively onto the cases where we expect significant deviations from the single species scenario.

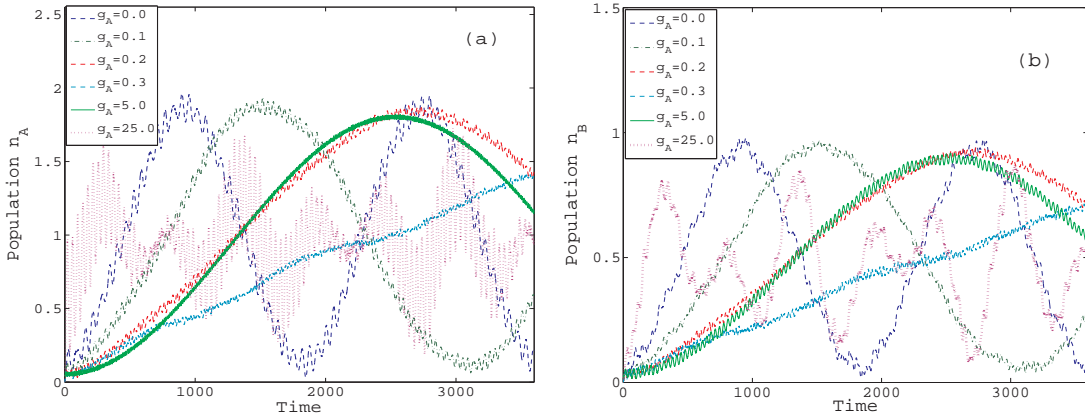


Figure 6.1: Population in the right well (a) n_A of species A and (b) n_B of species B at $g_{AB} = 0.2$ for different g_A values.

6.2 Complete population imbalance.

We first study the dynamics with all the atoms initially loaded into the left well. As observables, we compute the time evolution of the one-particle density of each species and the resulting population in each well. For the right well we have

$$n_\alpha(t) = N_\alpha \int_0^\infty \rho_\alpha(x;t) dx \quad (6.2)$$

where ρ_α is the one-body density of the species $\alpha = A, B$ and we have $n_R = n_A + n_B$

Before we examine the parameter space in detail, let us comment on some general properties we observe with increasing inter-species interaction. For $g_A = 0.0$ for example, increasing g_{AB} results in a strong and monotonic increase of the tunneling period. Specifically $g_{AB} = 0$ provides a period of approximately 10^2 , and for $g_{AB} = 0.2$ the tunneling period becomes of the order of 10^3 (see Fig.6.1). This is counter intuitive since with increasing repulsion between the species initially localized in the same well, one would expect the tunneling to be enhanced. Note that, for short time-scales ($\lesssim 300$) only a minute oscillation of the population between the wells appears. The delayed tunneling is reminiscent of the one found for the case of single species [47, 64] and can be attributed to the degeneracy of states that are related by a permutation (see below section 6.2).

Let us now explore the parameter space step by step, first choosing a weak inter-species interaction strength $g_{AB} = 0.2$. In Fig.6.1, we illustrate the tunneling dynamics for different values of g_A at $g_{AB} = 0.2$ for species A and B by showing the population of the right well n_A, n_B . We observe a long-time envelope behavior modulated by a rapid small amplitude oscillation. The tunneling period (period of the envelope) increases monotonically in this weak intra-species interaction regime with increasing $g_A = 0.0 \rightarrow 0.3$. However this behavior changes as we go beyond the weak interaction

regime where higher bands come into play and we consequently observe a decrease of the tunneling period already for $g_A = 5.0$. Moreover, the two components A and B undergo roughly the same evolution of the oscillation pattern (compare Fig.6.1(a) and (b)) suggesting strong inter and intra-species correlations in the sense that all bosons tunnel together. Near the 'fermionization limit' of species A $g_A = 25$, we obtain an even further reduction of the tunneling period with the dynamics consisting of two primary oscillations. Unlike the previous cases, the dynamics of the two components is not completely identical. The envelope behavior is approximately the same but for species A, the faster modulations are much more prominent than for species B. This indicates, in the line of argumentation provided above, a reduction of the correlations between the two species and attempted single-particle tunneling.

For stronger inter-species interaction $g_{AB} = 5.0$ (Fig.6.2), the interplay between the inter and intra-species interactions lead to a completely different quantum dynamics. Before we enter the corresponding discussion, let us compare the corresponding population evolution of Fig.6.1 and Fig.6.2 for $g_A = 0.0$. We observe that the tunneling period is considerably larger (of the order of 10^4) for $g_{AB} = 5.0$ compared to $g_{AB} = 0.2$. This illustrates the general statement given above that increasing g_{AB} suppresses the tunneling rate. Moreover rapid oscillations on top of the tunneling envelope are less prominent here. A small $g_A = 0.2$ (Fig.6.2(b)) leads to a moderate increase of the tunneling period. For $g_A = 4.0$ (Fig.6.2(c)), we observe a significant reduction of the period thereby approaching the behavior which we would obtain for the case of species with identical parameters $g_{AB} = g_A = 5$. Further reduction of the tunneling period is observed for $g_A = 25.0$.

To understand the degree of correlation between the atoms we need to study the temporal evolution of the pair/triple probability i.e the probability of finding both A atoms (AA), one A and one B atoms (AB) and all of them (AAB) on the same well. When the tunneling is strongly correlated meaning that all the atoms tunnel together, AA, AB and AAB remain close to unity. This is indeed the case for $g_A = 0, 0.2$ and is not shown here. As g_A becomes large, this strongly correlated tunneling reduces and hence the corresponding pair/triple probability also decreases from unity. This can be seen in Fig.6.2(e),(f) where we presents the temporal evolution of the pair/triple probability for $g_A = 4.0$ and 25.0 respectively. As we can observe, there is a substantial decrease from unity signifying that the process of single-particle tunneling becomes more relevant for this case.

The effects observed with increasing g_A at $g_{AB} = 5.0$ (Fig. 6.2) are even more pronounced for $g_{AB} = 25.0$ (see Fig.6.3). For $g_A = 0.0$ (Fig.6.3(a)), the dynamics is characterized by a tunneling with an extremely long period $\sim 10^5$ and the envelope is modulated by faster oscillations which are more prominent than for the case $g_{AB} = 5.0$ (see with Fig.6.2). A small interaction $g_A = 0.2$ (Fig.6.3(b)), leads to a reduction of the tunneling period and a pronounced two-mode behavior. At $g_A = 5.0$ (Fig.6.3(c)), the

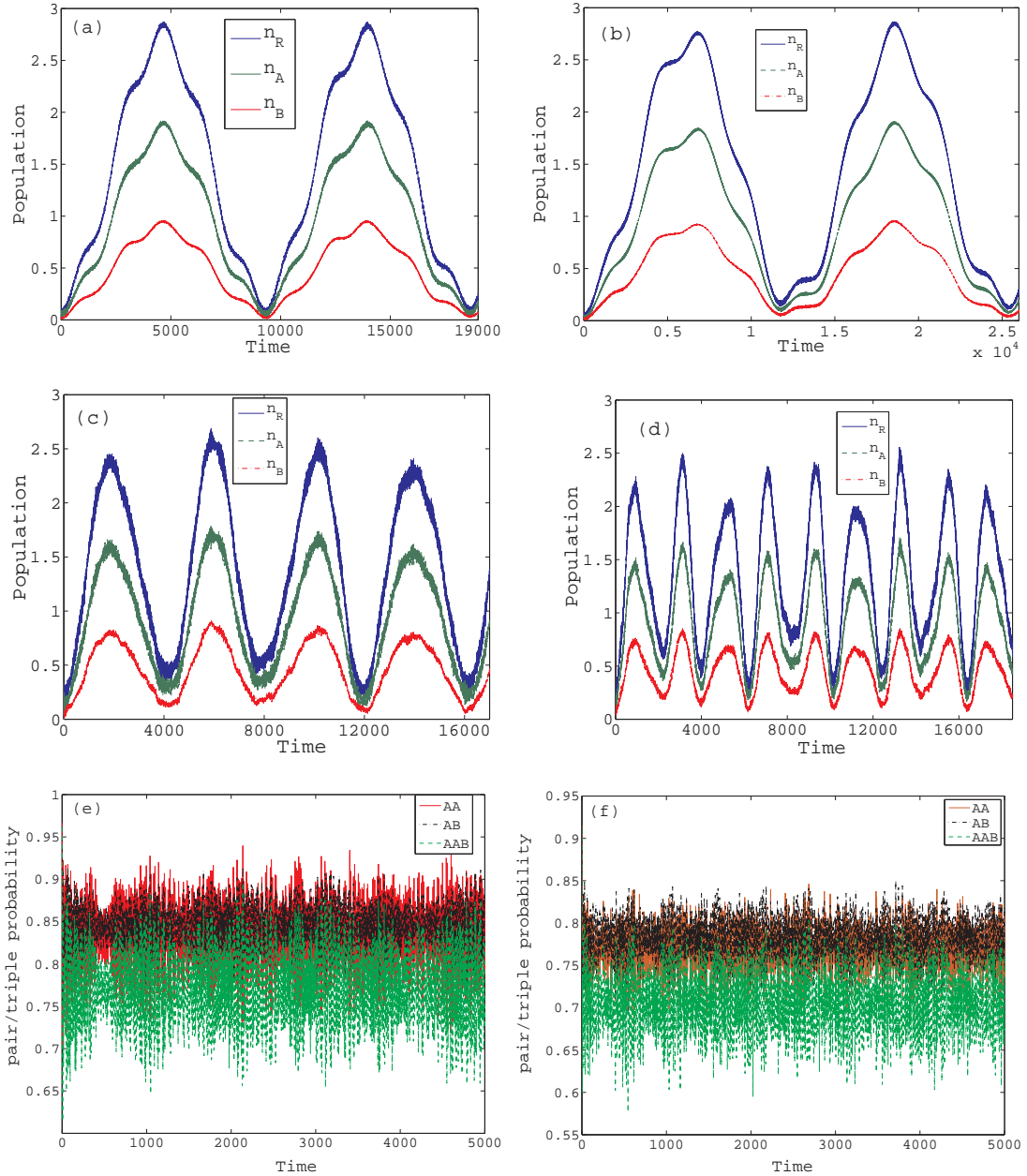


Figure 6.2: Total population in the right well n_R and population of the individual species n_A , n_B for $g_{AB} = 5.0$ for (a) $g_A = 0.0$, (b) $g_A = 0.2$, (c) $g_A = 4.0$ and (d) $g_A = 25.0$. (e) and (f) show the pair/triple probability corresponding to the cases (c) and (d). AA, AB and AAB correspond to the probability of finding AA, AB and AAB particles in the same well respectively.

smooth two-mode dynamics changes into a combination of broad tunneling envelope with period a of the order of 3×10^4 and irregular small amplitude oscillations on top of it. Finally for the onset of the fermionization limit $g_A = 20.0$ (fig.6.3(d)), the separation of the time-scales is strongly reduced. For $g_A = g_{AB} = 25.0$ (not shown here), we would recover the dynamics of fermionized bosons which correspond to uncorrelated

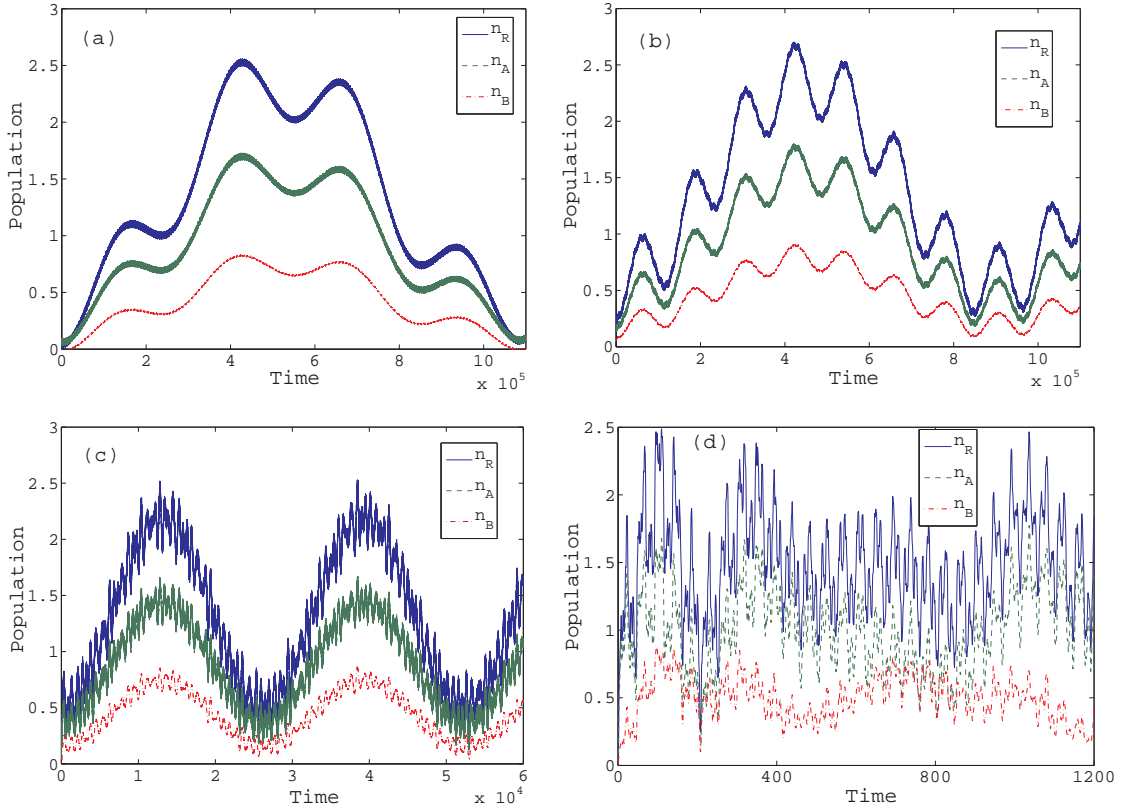


Figure 6.3: Population in the right well of total n_R and the individual species n_A , n_B for $g_{AB} = 25.0$ for (a) $g_A = 0.0$, (b) $g_A = 0.2$, (c) $g_A = 5.0$ and (d) $g_A = 20.0$.

oscillations of the individual atoms.

An understanding of the preceding observations requires an examination of the many-body stationary states and the energy spectrum of the system. As shown in Fig.6.4, the energy spectrum of the mixed system is characterized by a series of near degenerate levels arising from the inherent permutation symmetries of the system. For weak inter-species interactions (Fig.6.4(a) inset) the levels split and for somewhat larger $g_{AB} \geq 0.1$ tend to form doublets. Exact crossings are observed in this regime of the spectrum. For very strong $g_{AB} \gtrsim 10$, the states come close in energy again forming bundles of near degenerate states (Fig.6.4(a)). For a completely localized initial state, it is only the energetically highly excited states that possess a significant overlap with it. Moreover by symmetry two quasi-degenerate permutationally symmetric states share almost the same overlap with the initial state and thus contribute primarily to the dynamics. The long time tunneling period is given by the splitting of these two states and since the latter is very small, the corresponding tunneling period is very large.

Concerning the impact of changing g_A , let's analyze first the state-decomposition and evolution of the lowest eigenstates in the weak interaction regime where only the lowest band contributes. There are six eigenstates of the first band which can be obtained

as linear combinations of localized number-states of the individual species which are $|AAB, 0\rangle$, $|AA, B\rangle$, $|A, AB\rangle$, $|0, AAB\rangle$, $|B, AA\rangle$ and $|B, AB\rangle$ where e.g. $|AA, B\rangle$ denotes two atoms of species A in the left well and one atom of species B in the right well. In the non-interacting case ($g_A = g_{AB} = 0$), the eigenstates have contributions from all these number-states. As we increase g_{AB} , the lowest two eigenstates gradually acquire a 'species separated profile' of the form $|AA, B\rangle \pm |B, AA\rangle$ meaning that this superposition is the dominant contribution to the eigenvector. This holds as long as $g_A \leq g_{AB}$. At $g_A = g_{AB}$ the lowest two states form an avoided crossing with the next two upper levels (see Fig.6.4(b) inset). With further increasing g_A , it is energetically more favorable to have separated A bosons instead of separated A and B bosons. Consequently, the energetically lowest two states have the profile $|AB, A\rangle \pm |A, AB\rangle$, while the next two excited levels have the species separated profile of the form $|AA, B\rangle \pm |B, AA\rangle$. The highest two states of the sextet are well separated from the other states and become increasingly closer to degeneracy with increasing g_A . These two states are of the form $\phi_{5,6} \approx \frac{1}{\sqrt{2}}(|AAB, 0\rangle \pm |0, AAB\rangle)$. Since our initial state is characterized by a complete population imbalance $|AAB, 0\rangle$, the latter two states possess a maximal contribution to the following dynamics. Thus with increasing g_A , the tunneling period increases strongly. However as g_A increases even further, higher lying states contribute and the previously near degenerate states, which is the main contributing doublet to the dynamics, split (Fig.6.4(b)). This splitting leads to a decrease of the tunneling period as seen for $g_A = 5$ and more significantly for $g_A = 25$ where the A bosons are close to the fermionization limit.

For $g_{AB} = 5.0$ (Fig.6.4(c)), the tunneling dynamics possesses higher band contributions for any value of g_A . However the basic behavior is similar to the case $g_{AB} = 0.2$. The lowest two states have a dominant contribution by the species separated configurations up to the point $g_{AB} = g_A$, where we encounter an avoided crossing (see inset of Fig.6.4(c)) while the energetically highest states have contributions from the completely imbalanced states. However for $g_{AB} = 5.0$ increasing g_A starting from zero leads to a minor splitting of the states relevant to the dynamics. As a consequence a decrease of tunneling times is observed. Finally, in the fermionization limit at $g_{AB} = g_A = 25.0$ the tunneling period corresponds roughly to the Rabi frequency.

Let us provide an intuitive physical picture for the decrease of the tunneling period which occurs in certain regimes of increasing intra-species interaction strength. As g_A increases, the repulsion of the A bosons increases and thus the corresponding wave-function and density profile broaden. This broadening leads to a greater overlap between the left and the right well 'localized' wave functions of A atoms and this in turn increases the effective tunneling coupling and the corresponding tunneling rates. This effect can be seen in Fig.6.5 where we show the one-particle density $\rho_{A,B}$ for the dominant eigenstate contributing to the dynamics (Note that there are actually two dominant contributions with near identical density profiles). At $g_A = 0$, the local-

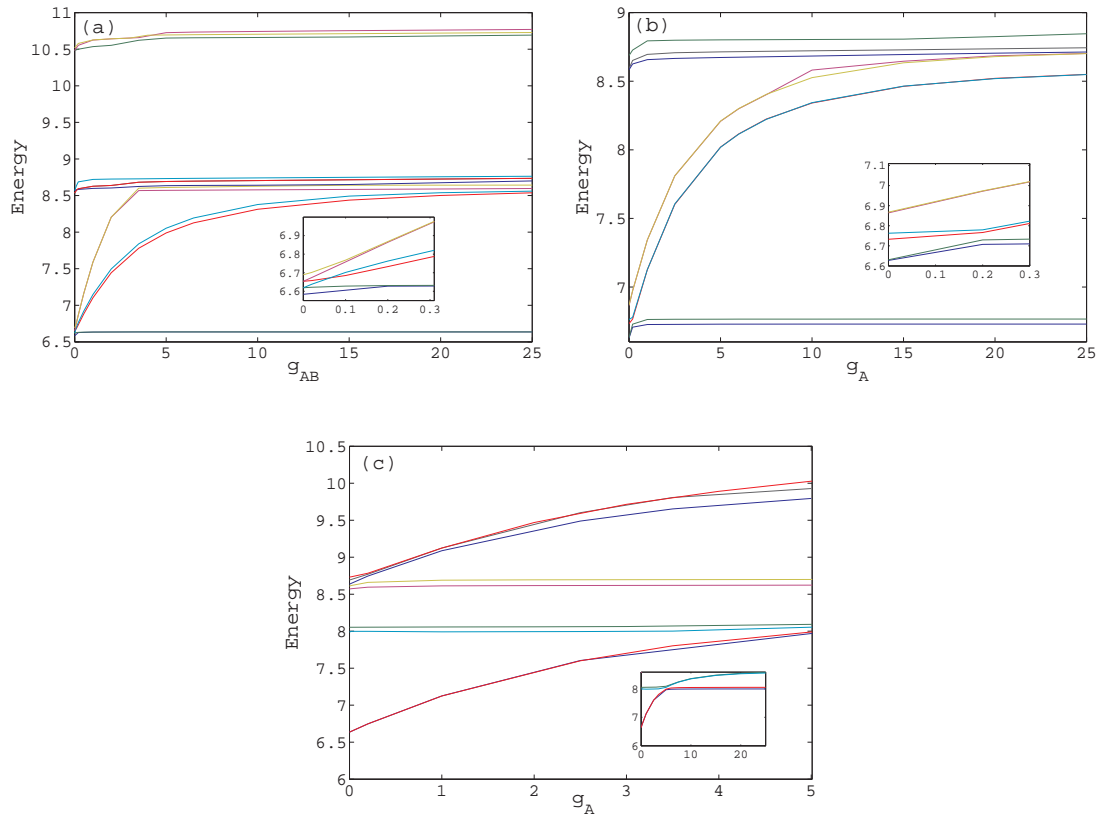


Figure 6.4: Variation of the energy spectrum with (a) g_{AB} for $g_A = 0.0$ (Inset: magnification for small interaction strengths), (b) g_A for $g_{AB} = 0.2$ (Inset: Magnification for small interaction strengths), (c) g_A for $g_{AB} = 5.0$ (Inset: anti-crossing lower states).

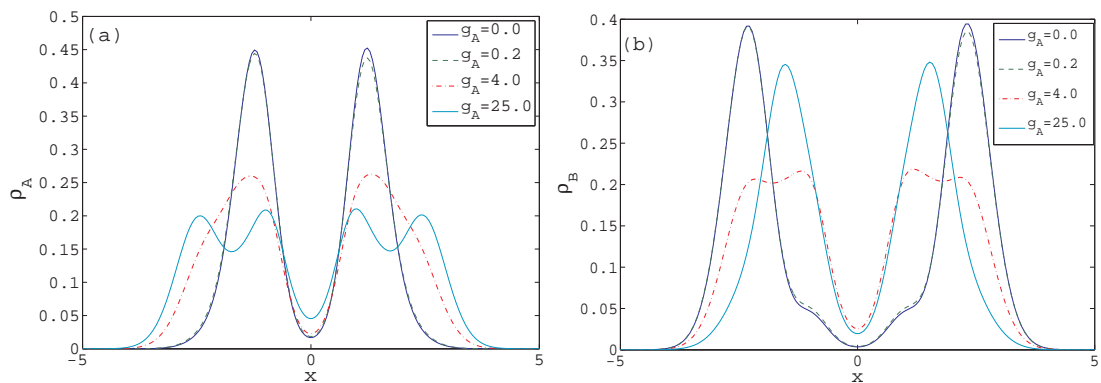


Figure 6.5: One-particle density as obtained by taking into account the most important eigenstates contributing to the initial state for (a) species A and (b) species B for $g_{AB} = 5.0$.

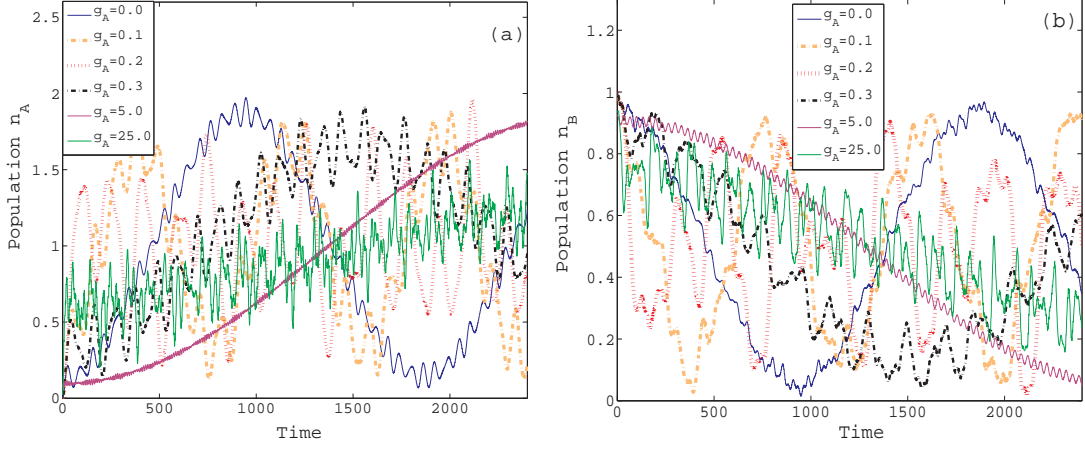


Figure 6.6: Population in the right well (a) n_A of species A and (b) n_B of species B at $g_{AB} = 0.2$ for different values of g_A for a phase separated initial state.

ized densities ρ_A and ρ_B are spatially separated in each well as a consequence of the repulsion between the species. Note that the density of the B boson possesses its maximum for larger values of $|x|$ thereby 'sandwiching' the A boson population. This arises from the fact that due to the unequal number ($N_A > N_B$), it is energetically favorable to shift the density of the B species to larger values of $|x|$. As g_A is increased, the two localized densities ρ_A, ρ_B in the two wells gain an increasing overlap which can be observed as a vertical upward shift of the density profile at $x = 0$ which becomes progressively stronger with increasing g_A . This mechanism, also present for other contributing states, leads to an overall increase of the tunneling coupling and consequently to an increase of the tunneling frequency.

6.3 Phase separated initial state.

Let us now consider the initial state for which the two species are localized in different wells. The basic mechanism concerning the dynamics will be similar but since the two species are initially separated, we expect essential differences from the preceding case. We consider an initial state with the A bosons being localized in the left well and the B boson in the right well.

For $g_{AB} = 0.2$ and $g_A = 0.0 - 0.3$, only states in the first band will contribute to the dynamics. However unlike the previous case of complete imbalance, the phase separated initial state is constituted by the eigenstates belonging to the energetically lowest two doublets. Also, since the species are separated initially, their individual dynamics is out of phase meaning that when A bosons move to the right well the B boson moves to the left and vice versa. For $g_A = 0$ (Fig.6.6), the dynamics is a two-mode oscillation similar to what was observed in the completely imbalanced case. However with increasing g_A ,

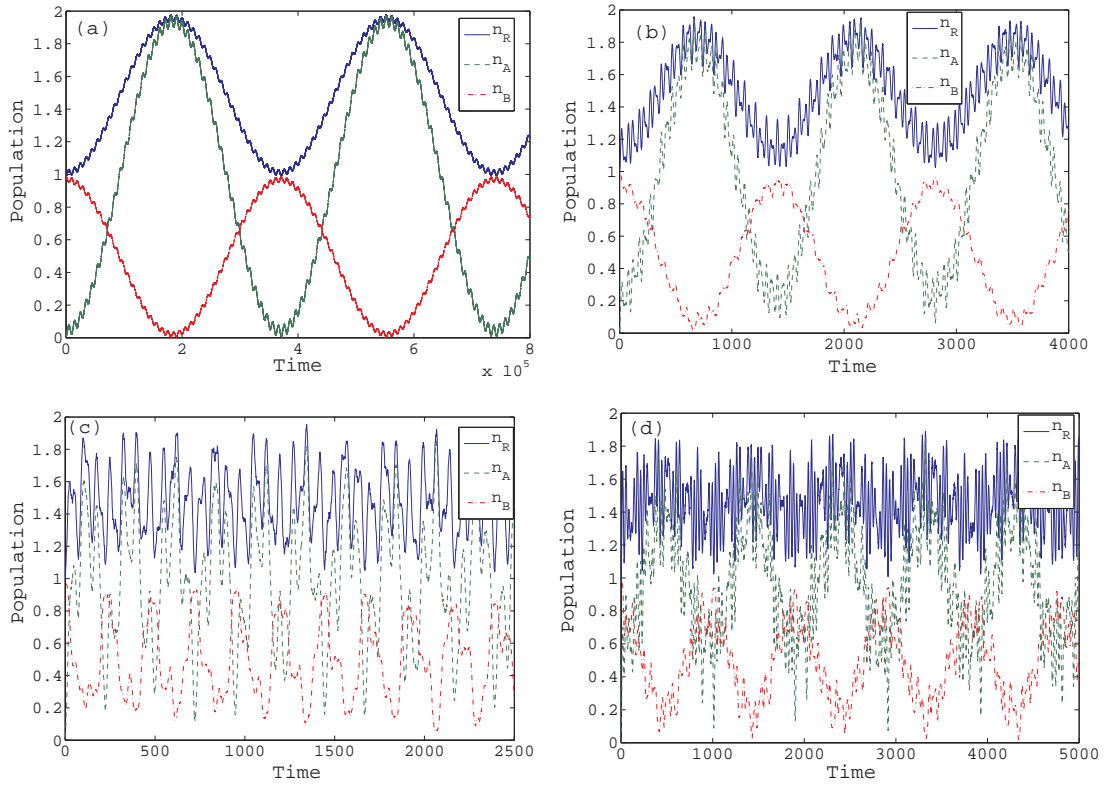


Figure 6.7: Population in the right well n_R , n_A and n_B for (a) $g_{AB} = 5.0$, $g_A = 0.0$, (b) $g_{AB} = 5.0$, $g_A = 4.0$, (c) $g_{AB} = 5.0$, $g_A = 25.0$ and (d) $g_{AB} = 25.0$, $g_A = 20.0$ for the phase-separated initial state.

the tunneling period decreases reaching a minimum at $g_A \approx 0.2$. Upon further increase, the tunneling period increases monotonically as long as we remain within the first band (Fig.6.6). This behavior can be analyzed and understood via the energy spectrum (Fig.6.4(b)). Since as mentioned above, the lower eigenstates contribute, the impact of the avoided crossing is observed in the corresponding dynamics for low interaction strengths, which was not the case for the state of complete imbalance (see previous section). Increasing g_A from zero, the energetically lowest two levels, which are the main contributing states split (Fig.6.4(b) inset) and this leads to an increase of the tunneling rates seen for $g_A \leq 0.2$. For larger g_A , it is the energetically excited doublets which represent the main contribution. The two levels of the doublet come closer in energy as g_A increases further leading to a smaller tunneling frequency. For very high values of interaction ($g_A = 25.0$) additional states contribute to the dynamics leading to the high frequency 'noise' observed.

For higher g_{AB} (Fig.6.7), the lowest two eigenstates represents an entangled linear superposition of phase separated number-states $|AA, B\rangle \pm |B, AA\rangle$ which is the minimal energy configuration. Since the initial configuration is also phase separated, the dynamics consist of shuffling between the two number-states. The energy gap between

these two quasi-degenerate states is exceedingly small and gets progressively smaller as g_{AB} increases leading to extremely long tunneling periods. Indeed the tunneling period is greater (of the order of 10^5) than for the case of a completely imbalanced initial state. This behavior is in accordance with the intuitive physical picture: due to the strong inter-species repulsion, the initially separated bosonic species prefer to stay separated in each well and are reluctant to tunnel to the other well as that would require them to overcome the repulsive energy of the other species. Again a substantial increase of g_A not only reduces the tunneling period but also induces small amplitude oscillations and noise due to the contribution of higher excited states (see Fig.6.7(b),(c)). The dynamical behavior for $g_{AB} = 5$ and $g_{AB} = 25$ is similar for all parameter regimes of g_A , except for very strong intra-species couplings close to fermionization (see Fig.6.7(c),(d)). We underline here that for this phase separated initial state, the higher the inter-species interaction g_{AB} is, the more restricted the dynamics is to the lower part of the energy spectrum and to the shuffling between number-states $|AA, B\rangle$ and $|B, AA\rangle$. Therefore, for $g_{AB} = 25$, g_A should be very large too, in order to observe substantial fast oscillations resulting from higher excitations (see Fig.6.7(d)).

As a last remark on the dynamics of the phase separated initial state we would like to comment on the degree of correlation of the tunneling. Since the tunneling consists here in principle of a shuffling between $|AA, B\rangle$ and $|B, AA\rangle$, the two species spent most of the time in different wells. Therefore the probability to find B and A species in the same well remains always close to zero, while the A particles tunnel as a pair. Similar to the previous section this behavior ceases to exist in general for strong g_A where single particle tunneling for the A species via excited states is induced. Note that for the so-far discussed cases of initial states, the destruction of the correlated tunneling behavior, (three bosons staying together; the two species remaining separated), results from a strong increase of the intra-species interaction which drives the system beyond the simple number state dynamics ($|AAB, 0\rangle \Leftrightarrow |0, AAB\rangle$ or $|AA, B\rangle \Leftrightarrow |B, AA\rangle$). We show next that such strong deviations from the initial state configuration can also be achieved for the situation of a partially population imbalanced initial state but for a different reason.

6.4 Partial population imbalanced initial state.

A novel tunneling mechanism is encountered if the initial state is prepared such that the two wells share an equal population of A atoms while the B atom is on the left well. This initial state we call *partially population imbalanced* state. The behavior observed above namely the increase of the tunneling period with increasing g_{AB} and its decrease with increasing g_A can still be observed here. However, a major difference compared to the preceding cases arises in terms of the evolution of the different states which reflects itself in the corresponding time-evolution of the populations.

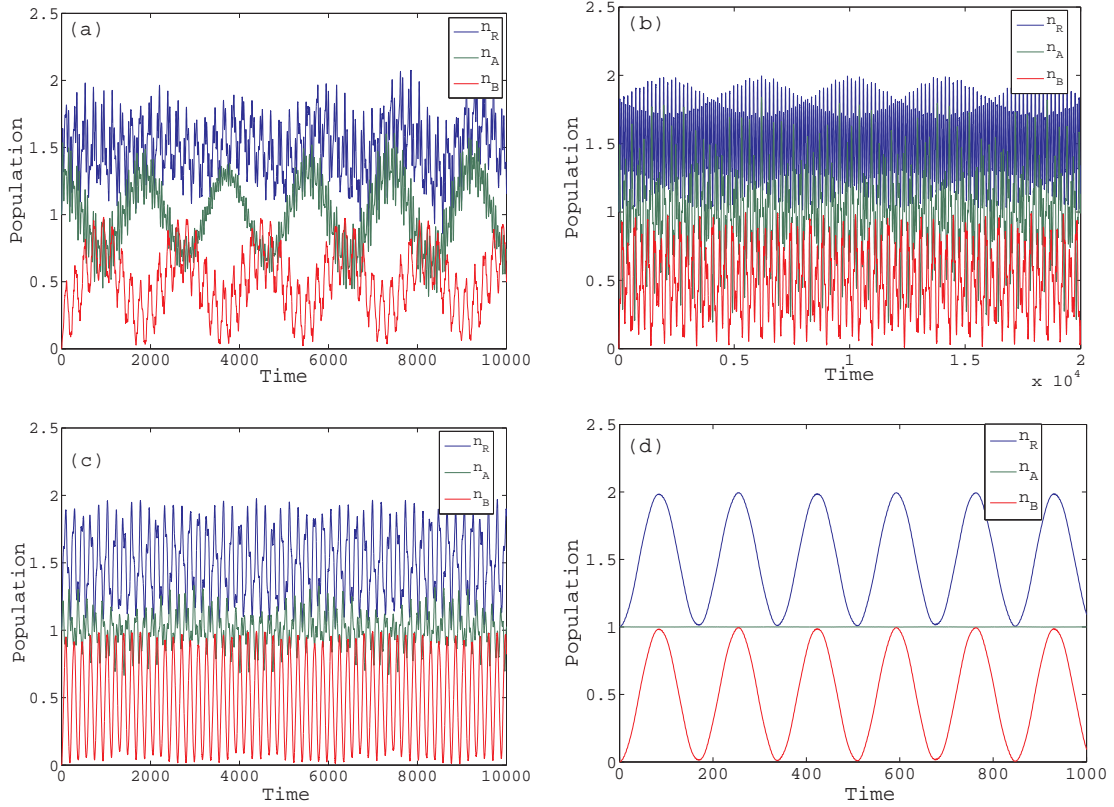


Figure 6.8: Population in the right well n_R , n_A and n_B for $g_{AB} = 0.2$ for (a) $g_A = 0.0$, (b) $g_A = 0.2$, (c) $g_A = 0.3$ (d) $g_A = 5.0$.

In Fig.6.8 we show the populations n_A , n_B and n_R for $g_{AB} = 0.2$. Naively, one would expect that the B boson will undergo Rabi-oscillations on the background of the A bosons which should remain with equal population in each well. However this does not happen for $g_{AB} > g_A$. The envelope behavior of the A particle population i.e n_A in Fig.6.8(a) for $g_A = 0$ first increases then decreases, indicating that the single A atom in the right well tunnels partially to the left well thus decreasing the population of the A particles in the right-well. The B boson on the other hand tunnels completely to the right well. This process is retained thereafter and is overall periodic. The envelope behavior is modulated by high frequency oscillations of significant amplitude involving a rapid tunneling between the two wells. As g_A is increased from 0 to 0.2 the pattern becomes more irregular consisting mainly of a constant envelope showing rapid oscillations. The amplitude of the oscillation of n_A remains large. When the intra-species interaction strength $g_A = 0.3$ becomes larger than the inter-species coupling $g_{AB} = 0.2$ (Fig.6.8(c)), the tunneling of A bosons is strongly suppressed. For even higher interactions $g_A = 5.0$ (Fig.6.8(d)), the A bosons are completely localized while the B boson undergoes Rabi oscillations between the two wells as one would expect intuitively since the highly repulsive species A are initially in different wells.

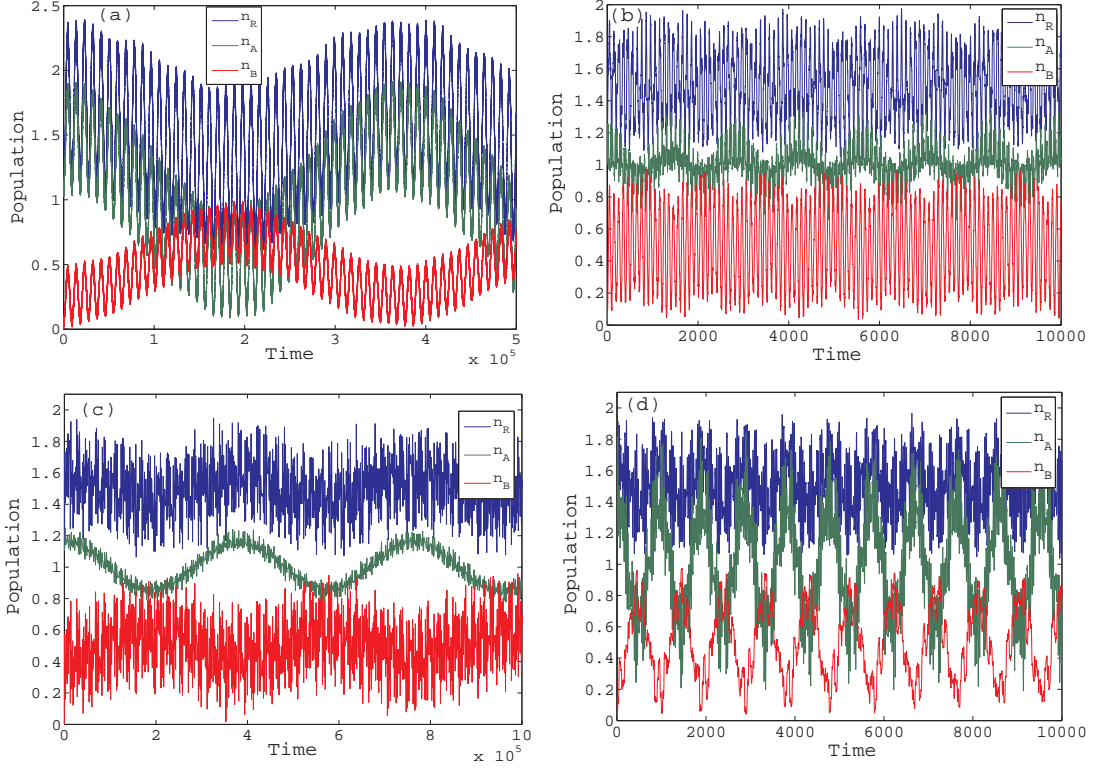


Figure 6.9: Population in the right well n_R , n_A and n_B for (a) $g_{AB} = 5.0$ and $g_A = 0.0$, (b) $g_{AB} = 5.0$ and $g_A = 4.0$, (c) $g_{AB} = 25.0$ and $g_A = 5.0$ (d) $g_{AB} = 25.0$ and $g_A = 20.0$.

The evolution of the dynamics shows further characteristics for stronger interspecies interactions. Fig.6.9 presents the results for $g_{AB} = 5.0$. For $g_A = 0.0$ (Fig.6.9(a)), there are two distinct oscillations for both n_A and n_B : a fast fluctuation with significant amplitude for n_B coupled to a large amplitude motion of n_A . Intuitively one can understand this behavior (seen also in the previous case) for large g_{AB} as follows: the tunneling of the B boson to the right well pushes the A bosons to the left well due to the strong repulsion and vice versa leading to a counterflow type of dynamics. The fast oscillation of considerable amplitude for n_A involves tunneling of a 'complete' A boson and partial tunneling of a B boson between the wells. The origin of these oscillations can be understood via the number state decomposition of the initial state as will be explained below. Opposite to this, for $g_A = 4.0$ (Fig.6.9(b)), the tunneling of A boson is considerably suppressed and the B boson undergoes a rapid oscillation between the wells. For even higher g_A as before we get an almost complete suppression of the A boson tunneling while the B boson executes the same very fast oscillations.

For very strong inter-species interaction $g_{AB} = 25.0$, a similar pattern is seen for low g_A (not shown) albeit with a much longer period. For quite strong $g_A = 5.0$ there is a tendency for suppression of the tunneling of the A boson (Fig.6.9(c)) which still oscillates but with a small amplitude. Unlike $g_{AB} = 5.0$, increasing the interaction to

$g_A = 20.0$ (Fig.6.9(d)) does not reduce the tunneling of the A bosons but increases it approaching a 'fermionization' type behavior of the dynamics.

To understand the underlying dynamical mechanisms of the above results, we first note that the initial state in this case is not necessarily a pure number-state $|AB, A\rangle$ but is a linear combinations of the number states: $|AAB, 0\rangle$, $|AB, A\rangle$ and $|B, AA\rangle$ maintaining the required population balance of the initial state (equal population of A bosons in each well and the B boson in the left).

For this initial setup the tunneling dynamics consists of shuffling between the initial state and the number states $|0, AAB\rangle$, $|A, AB\rangle$ and $|AA, B\rangle$. For $g_{AB} \gg g_A$, the evolution is dominantly to the state $|AA, B\rangle$ since this represents the number state with minimal energy. As a result we have a tunneling of the B boson to the right well and of a single A boson to the left well which we can observe in the envelope behavior of n_A and n_B of Fig.6.8(a) and more prominently in Fig.6.9(a). The faster oscillations are the result of the contributions from the states $|0, AAB\rangle$ and $|A, AB\rangle$. For $g_{AB} \approx g_A$, we have contributions of approximately the same magnitude from almost all the number states leading to Josephson like oscillations. However, for $g_{AB} \ll g_A$, the system shuffles between the initial state and the state $|A, AB\rangle$ since this number state now has the minimal energy. Therefore the A bosons are effectively localized while the B bosons undergo Rabi oscillations between the wells.

Chapter 7

Summary and outlook

In this thesis we have investigated the tunneling dynamics of few boson systems in one-dimensional double-well. This was done using the numerically exact MCTDH method thus allowing us to explore the whole range of the interaction spectrum- from the non-interacting to the fermionization limit.

We first studied the dynamics for single species bosonic system. The focal point of the study was the role of asymmetry in the dynamics. For that purpose, we envisioned a new approach to asymmetry by considering spatially varying interaction. More specifically, we modeled the system such that we have two different interaction strengths in the two wells. We observed that the inhomogeneity of interaction leads to a suppression of tunneling. The reason for this suppression can be attributed to the breaking up of the doublet structure in the energy spectrum leading to a decoupling of the eigenstates into the localized number-state. Increasing the interaction to the fermionization limit leads to a reappearance of the tunneling, although the presence of the interaction inhomogeneity leads to deviation from the ideal fermionic behavior. In the fermionization limit, similar to the homogeneous case, the dynamics is governed by the band splitting of the first two bands. For a very pronounced interaction inhomogeneity in the strong interactions regimes, we observed single particle tunneling between the localized excited bands of the double-well. These basic considerations was extended to understand the multi-particle system. A richer tunneling behavior was seen for the three-boson system. We observed a more severe suppression of tunneling for even lower interaction values. A partial restoration of tunneling in the intermediate interaction range was observed which is a consequence of exact crossings in the energy spectrum. Interestingly, for $N \geq 3$ atoms, one can generate tunneling resonances by tuning the interaction asymmetry. These resonances occur as a result of the formation of degeneracies between different many-body eigenstates. For three particles, the exact tunneling mechanism at the resonances was investigated using the evolution of the pair-probability and the three-particle probability. These studies revealed that we get correlated pair and triplet tunneling and an absence of single particle tunneling.

Finally, we explored the dynamics in a asymmetric double-well and investigated the interplay between the interaction inhomogeneity and the tilt. We observed that the tilt can be tuned to offset the effects of the interaction inhomogeneity leading to tunneling resonances. These effects were explained through the spectral analysis in terms of avoided crossings between the energy levels.

We then extended the study of the tunneling dynamics to a system of bosonic binary mixture in a double-well. Our focus was the interplay between the inter-species and intra-species interactions and their impact on the dynamics. We considered three initial configurations - complete population imbalance, phase separated state and partial population imbalance. A generic effect we observed was that the tunneling period increases drastically as the inter-species interaction g_{AB} increases, which is due to quasi-degenerate permutationally symmetric states contributing primarily to the dynamics. This effect is quite general and was observed for different initial configurations. The intra-species coupling g_A had a different impact on the behavior of the dynamics, depending on the strength g_{AB} as well as on the initial state. The general trend is that for large g_A , the overlap of localized wave functions of contributing states becomes larger and thus the effective tunneling coupling is increased leading to higher tunneling frequencies. For low interactions though different behavior is encountered for different setups. For a completely imbalanced initial state, for instance, we observed that for small values of g_{AB} , the tunneling period increases as we increase g_A in the weak interaction regime. However for larger values of g_A , the tunneling period reduces with increasing g_A . This behavior is not seen for the phase-separated initial condition. In the latter case, we observed a minimal period at $g_A = g_{AB}$, which is a manifestation of an avoided crossing in the spectrum. For the partially population imbalanced case, although one would intuitively expect that the A particles remain in different wells due to their initial preparation in opposite wells this happens only if the interaction between them is considerably large. In the other cases the A particles undergo oscillations and the initially mixed state where an A and a B boson coexist in the same well can turn into separated state for which the A and B species reside in different wells.

This investigation of the tunneling dynamics of few bosons is by no means complete but rather is a small step towards the exploration of the fascinating physics in these systems. From the methodological point of view, while we have tackled the problem through ab-initio calculations, an interesting prospective would be to try to describe the presently found effects in the context of a generalized Bose-Hubbard model, where the on-site energies and the coupling constants would be site, occupation number and time-dependent [110–112]. Similarly, while we have restricted ourselves to the few-boson systems, a study of the crossover from few to many-body systems is interesting especially in the context of understanding the microscopic mechanisms occurring in large systems. Although, using the MCTDH method, it is extremely difficult to treat systems with large number of bosons, the developments of MCTDHB (where the bosonic

permutation symmetry is incorporated directly into the MCTDH algorithm) has made it possible to treat such systems and compare with other theoretical approaches [33–36].

The tunable inhomogeneity of interactions and asymmetry in external potential especially in the context of dynamics can be used to design schemes for selective transport of particles between different wells and/or reservoir systems [113,114]. The multi-species system in particular could be used to realize systems such as bosonic transistors as well as for studies of entanglement and statistical properties of mixed ensembles. Further extension of the study of quantum dynamics to multi species and multi-well systems [115] could reveal new mechanisms of tunnelings. One could also consider systems with time-dependent interaction modulations and study the possible excitation dynamics or effects like coherent destruction of tunneling [116,117] in high interaction regimes. Extension to higher dimensions can be interesting as well as challenging, both conceptually and computationally. One could also consider long range interactions such as dipolar interactions and observe their effects as well as their interplay with the short range interactions. In all, there promises to be multiple directions, which one can take forward, in this fascinating area.

Appendix A

Density matrices

A.1 General properties

The density matrix formalism is a very convenient tool to study and analyze many-body problem. The general theory of density matrices and their application is comprehensively discussed in standard textbook of quantum mechanics e.g. [102] and so is omitted here. In this section instead, we highlight and discuss some aspects which are useful in the context of few boson systems.

In general, the knowledge of the many-body wave-function Ψ is equivalent to that of its density matrix, defined as

$$\hat{\rho}_N := |\Psi\rangle\langle\Psi|. \quad (\text{A.1})$$

$\hat{\rho}_N$ thus can be thought as the quantum mechanical analog of classical probability distribution and is Hermitian and positive and normalized to unity through $\text{tr}(\hat{\rho}_N) = 1$. For any operator \hat{A} , the expectation value is given by:

$$\langle\hat{A}\rangle = \langle\Psi|\hat{A}|\Psi\rangle = \text{tr}(\hat{\rho}_N\hat{A}). \quad (\text{A.2})$$

In the case of an n -body operator defined as $\hat{A}_n = \frac{1}{n!} \sum_{i_1 \neq \dots \neq i_n}^N \hat{A}_{i_1, \dots, i_n}$, the expectation value can be written as

$$\langle\hat{A}_n\rangle = \binom{N}{n} \text{tr}(\hat{\rho}_n\hat{A}), \quad (\text{A.3})$$

where $\hat{\rho}_n$ is the reduced density matrix (RDM) of n^{th} order obtained by integrating out all degrees of freedom $f > n$:

$$\hat{\rho}_n = \text{tr}_{n+1, \dots, N}(\hat{\rho}_N). \quad (\text{A.4})$$

Note that for identical particles, owing to the permutation symmetry of the wave-function, it does not matter which particles are integrated out.

From the Fock-space prospective the expectation value of operator is given by:

$$\langle \hat{A}_n \rangle = \frac{1}{n!} \int \int dX_n dX'_n \langle X_n | \hat{A}_n | X'_n \rangle \langle \hat{\Psi}^\dagger(x_1) \dots \hat{\Psi}^\dagger(x_n) \hat{\Psi}(x'_1) \dots \hat{\Psi}(x'_n) \rangle, \quad (\text{A.5})$$

where $\hat{\Psi}^\dagger(x_n)(\hat{\Psi}(x_n))$ are the bosonic creation (annihilation) operators creating (annihilating) a particle at position x_n .

Comparing with Eq. A.3, the general RDM then can be written as:

$$\hat{\rho}_n(X_n, X'_n) = \frac{(N-n)!}{N!} \langle \hat{\Psi}^\dagger(x_1) \dots \hat{\Psi}^\dagger(x_n) \hat{\Psi}(x'_1) \dots \hat{\Psi}(x'_n) \rangle. \quad (\text{A.6})$$

A.2 One-body density

For $n = 1$, Eq.(A.6) gives the one-body density matrix

$$\hat{\rho}_1(x, x') = \frac{1}{N} \langle \hat{\Psi}^\dagger(x) \hat{\Psi}(x') \rangle. \quad (\text{A.7})$$

The diagonal elements gives the *one-body density*

$$\hat{\rho}_1(x) := \hat{\rho}_1(x, x) = \frac{1}{N} \langle \hat{\Psi}^\dagger(x) \hat{\Psi}(x) \rangle. \quad (\text{A.8})$$

which is the probability of finding a particle at position x .

The off-diagonal elements in the one-body density matrix $\rho_1(x, x')$ can be generally complex and so is not an observable in its own right. Nevertheless, one can compute all one-particle non-local quantities from it. One such example is the one-body momentum distribution which can be obtained by a Fourier transformation

$$\tilde{n}(k) = \int dx \int dx' e^{-ik(x-x')} \rho_1(x, x'). \quad (\text{A.9})$$

To get some intuitive physical insights, it is useful to expand the one-body RDM in terms of its eigenfunctions:

$$\rho_1(x, x') = \sum_i \lambda_i \varphi_i^*(x) \varphi_i(x'). \quad (\text{A.10})$$

The eigenvalues are positive $\lambda_i \in [0, 1]$ and are normalized through $tr(\rho_1) = \sum_i \lambda_i = 1$. The eigenfunctions φ_i are called natural orbitals and the corresponding eigenvalues λ_i represents their population. These natural orbitals also serve to define Bose-Einstein condensation as well as fragmentation in interacting systems. If the population of the lowest natural orbital is of the order of the number of particle then the system is said to be condensed [103] while on the other hand if there are more than one natural orbital which have population of the order of the total particles then the system is said to be

fragmented [104].

A.3 Two-body density

The two-body density matrix depends on four variables

$$\rho_2(x_1, x_2, x'_1, x'_2) = \frac{1}{N(N-1)} \langle \hat{\Psi}^\dagger(x_1) \hat{\Psi}^\dagger(x_2) \hat{\Psi}(x'_2) \hat{\Psi}(x'_1) \rangle. \quad (\text{A.11})$$

and thus does not readily provide for an visualization.

It is more convenient and intuitive to study its diagonal kernel

$$\rho_2(x_1, x_2) := \rho_2(x_1, x_2, x_1, x_2) \quad (\text{A.12})$$

This represents the probability of finding one particle located at position x_1 and any second one at x_2 and is thus also called *pair-distribution* or *two-body correlation function*.

Using the one-body RDM and the $\hat{\rho}_1$ and the two-body RDM one can compute all quantities of a Hamiltonian containing only one- and two-body operators $H = \sum_i h_i + \sum_{i<j} V_{ij}$. In particular the exact many-body energy is given by

$$E = N \text{tr}(\hat{\rho}_1 h) + \frac{N(N-1)}{2} \text{tr}(\hat{\rho}_2 V), \quad (\text{A.13})$$

Moreover, using the corresponding bosonic commutation relation for the field operators, ρ_2 can be related to the density-density correlations:

$$\langle \hat{n}(x_1) \hat{n}(x_2) \rangle = \rho_2(x_1, x_2) + \delta(x_1 - x_2) n(x_1). \quad (\text{A.14})$$

This gives the fluctuations of the atom number in a certain spatial region over repeated measurements, and thus provide useful analysis tool to understand effects such as the Superfluid to Mott-Insulator transitions.

Appendix B

The double-well potential

In this thesis, the double-well trap has been used as the external potential to study the dynamics of the bosons. In this section we discuss some basic essential properties of the double well trap. The general double-well trap is characterized by having two minimas separated by a barrier and can be modeled in a variety of ways. The model we adopted for all computations is a Gaussian barrier at the center of a harmonic trap $U(x) = \frac{1}{2}x^2 + h\delta_\omega(x)$

We stress here that for sufficiently deep wells, the properties are generic and doesn't depend of the details of the model adopted.

B.1 Single particle states

To understand the properties of the single particle states, let us first consider the (solvable) toy model of a harmonic trap split in the center by a delta potential.

$$U(x) = \frac{1}{2}x^2 + h\delta(x) \tag{B.1}$$

This model is thus equivalent to a double-well with infinitely thin barrier and thus shares many common features with an ordinary double well. The following analysis is based on Ref [99, 100]

The single-particle 1D Hamiltonian can be written as

$$H = -\frac{1}{2}\partial_x^2 + \frac{1}{2}x^2 + h\delta(x) \tag{B.2}$$

The delta potential at the center imposes the following boundary condition on the wave-function $\psi(x)$ at $x = 0$:

$$\psi'(0^+) - \psi'(0^-) = 2h\psi(0), \tag{B.3}$$

with prime denoting differentiation with respect to x . This condition can be ob-

tained by integrating the time-independent Schrödinger equation over an infinitesimal interval

$$\lim_{\epsilon \rightarrow 0} \int_{-\epsilon}^{\epsilon} dx \psi''(x) - \lim_{\epsilon \rightarrow 0} 2h \int_{-\epsilon}^{\epsilon} dx \delta(x) \psi(x) = \lim_{\epsilon \rightarrow 0} \int_{-\epsilon}^{\epsilon} (x^2 - 2E) \psi(x). \quad (\text{B.4})$$

The RHS is zero and thus in the limit $\epsilon \rightarrow 0$, we obtain the relation B.3.

The procedure to solve this problem is thus to solve the unperturbed problem and then incorporate the boundary condition imposed by the delta function at the center.

To solve the unperturbed part, it is convenient to rescale the coordinates $\tilde{x} = \sqrt{2}x$ and the time-independent Schrödinger equation for energy E and wave-function ψ is given by:

$$\left[-\partial_{\tilde{x}}^2 + \frac{1}{4}\tilde{x}^2 - 2E \right] \psi = 0. \quad (\text{B.5})$$

The solutions to Eqn.B.5 are the *parabolic cylinder functions* [101]

$$U(-\tilde{E}, \tilde{x}); \quad V(-\tilde{E}, \tilde{x}),$$

with $\tilde{E} = 2E$.

The condition of square-integrability as $|r| \rightarrow \infty$ implies that the solution $V(-\tilde{E}, \tilde{x})$ is unphysical and thus we are left with the solution

$$\psi = cU(-\tilde{E}, \tilde{x})$$

To apply the boundary condition B.3, we require the explicit form of the functions which are given by [101]

$$U(-\tilde{E}, 0) = \frac{\sqrt{\pi}}{2^{-\frac{1}{2}\tilde{E} + \frac{1}{4}} \Gamma(\frac{3}{4} - \frac{1}{2}\tilde{E})} \quad (\text{B.6})$$

$$\pm U'(-\tilde{E}, 0^{\pm}) = -\frac{\sqrt{\pi}}{2^{-\frac{1}{2}\tilde{E} - \frac{1}{4}} \Gamma(\frac{1}{4} - \frac{1}{2}\tilde{E})}. \quad (\text{B.7})$$

Plugging the boundary conditions B.3 on the above equations gives the general dependence of the energy eigenvalues and the barrier height h , through the transcendental equation

$$h = -\sqrt{2} \frac{\Gamma(\frac{3}{4} - \tilde{E}(h)/2)}{\Gamma(\frac{1}{4} - \tilde{E}(h)/2)}, \quad (\text{B.8})$$

Recasting in terms of an effective quantum number $\nu(h) = \tilde{E}(h) - \frac{1}{2}$

we get

$$h = -\sqrt{2} \frac{\Gamma(\frac{1-\nu}{2})}{\Gamma(\frac{\nu}{2})}, \quad (\text{B.9})$$

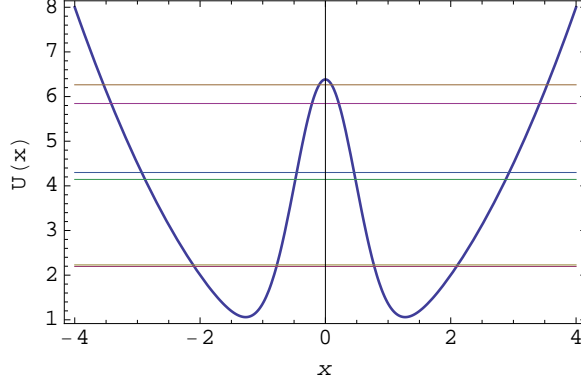


Figure B.1: Single particle energy spectrum of a double-well with barrier height $h = 8$ and width $\omega = 0.5$.

The wave-function for the even states are given by:

$$\psi_\nu(x) = ce^{-x^2/2}U\left(-\frac{\nu}{2}, \frac{1}{2}, x^2\right) \quad (\text{B.10})$$

while the odd states are simply the unperturbed harmonic oscillator states

$$\psi_n(x) = \frac{1}{\sqrt{\sqrt{\pi}2^n n!}} \exp(-x^2/2)H_n(x) \quad (\text{B.11})$$

The nature of the single particle spectrum can be understood as follows:

For no barrier ($h = 0$), the states are simply the harmonic oscillator states and the energy spectrum is equidistant $E_n = n + 1/2$. With the introduction of the barrier, the odd states are unaffected since they have node at $x = 0$. The even states on the other hand will acquire a notch at the center because of the barrier causing the energy level to shift. The energy spectrum thus acquires a doublet structure each doublet comprising of a pair of symmetric and anti-symmetric states (Fig. B.1). This is the characteristic feature of a double well spectrum for barrier with finite width also. For infinite barrier height ($h \rightarrow \infty$), the even states becomes degenerate with the next odd state.

B.2 Effective Hubbard model

In order to quantify the above observation regarding the nature of the states, one can model the double well into an effective two-site Bose-Hubbard Hamiltonian.

Consider the lowest band which consists of a pair of symmetric ψ_0 and anti-symmetric ψ_1 states. The linear combination of these states in the form of

$$\psi_{L,(R)} = \frac{1}{\sqrt{2}} (\psi_0 \pm \psi_1) \quad (\text{B.12})$$

is localized in the left (right) well due to the symmetry properties of the states.

The states ψ_L and ψ_R can thus be used as the equivalent Wannier orbitals for the double-well.

Using these effective Wannier function, one can follow the similar procedure used to derive the general Bose-Hubbard model for lattices and obtain the two-site Bose-Hubbard Hamiltonian.

$$\hat{H} = -J(\hat{c}_L^\dagger \hat{c}_R + \hat{c}_R^\dagger \hat{c}_L) + \frac{U}{2} \sum_{j=L,R} \hat{n}_j (\hat{n}_j - 1) \quad (\text{B.13})$$

with the tunneling coupling J and the on-site energy U . The number operator is defined by $\hat{n}_j \equiv \hat{c}_j^\dagger \hat{c}_j$.

The parameters U and J are given by the usual relations of the Bose-Hubbard Hamiltonian for lattices.

The double-well potential however allows for some simplification for the tunneling coupling. For the single particle Hamiltonian h , the tunneling coupling J is given by

$$J = \langle \psi_L | h | \psi_R \rangle = \frac{1}{2} (\langle \psi_1 | h | \psi_1 \rangle - \langle \psi_0 | h | \psi_0 \rangle) = \frac{1}{2} (\epsilon_1 - \epsilon_0) \quad (\text{B.14})$$

Thus the tunneling coupling is given by the splitting of the symmetric and the anti-symmetric levels of first band and is equal to the frequency of Rabi oscillations for non-interacting bosons.

Bibliography

- [1] M. H. Anderson, J. R. Ensher, M. R. Matthews, C. E. Wieman, and E. A. Cornell, *Science* **269**, 198 (1995).
- [2] C. C. Bradley, C. A. Sackett, J. J. Tollett, and R. G. Hulet, *Phys. Rev. Lett.* **75**, 1687 (1995).
- [3] K. B. Davis, M.-O. Mewes, M. R. Andrews, N. J. van Druten, D. S. Durfee, D. M. Kurn, and W. Ketterle, *Phys. Rev. Lett.* **75**, 3969 (1995)
- [4] C. J. Pethick and H. Smith, *Bose-Einstein condensation in dilute gases* (Cambridge University Press, Cambridge, 2008).
- [5] I. Bloch, J. Dalibard, and W. Zwerger, *Rev. Mod. Phys.* **80**, 885 (2008).
- [6] C. Chin, R. Grimm, P. Julienne and E. Tiesinga *Rev. Mod. Phys.* **82**, 1225 (2010).
- [7] L. Pitaevskii and S. Stringari, *Bose-Einstein Condensation* (Oxford University Press, Oxford, 2003).
- [8] M. Girardeau, *J. Math. Phys.* **1**, 516 (1960).
- [9] E. H. Lieb and W. Liniger, *Phys. Rev.* **130**, 1605 (1963).
- [10] M. Olshanii, *Phys. Rev. Lett.* **81**, 938 (1998).
- [11] T. Kinoshita, T. Wenger, and D. S. Weiss, *Science* **305**, 1125 (2004).
- [12] B. Paredes *et al.*, *Nature* **429**, 277 (2004).
- [13] E. P. Gross, *Nuovo Cimento* **20**, 454 (1961).
- [14] L. P. Pitaevskii. *Soviet Physics JETP* **13**, 451 (1961).
- [15] M. P. A. Fisher, P. B. Weichman, G. Grinstein, and D. S. Fisher, *Phys. Rev. B.* **40**, 546 (1989).
- [16] D. Jaksch, C. Bruder, J. I. Cirac, C. W. Gardiner, and P. Zoller, *Phys. Rev. Lett.* **81**, 3108 (1998).

- [17] G. G. Batrouni, V. Rousseau, R. T. Scalettar, M. Rigol, A. Muramatsu, P. J. H. Denteneer, and M. Troyer, *Phys. Rev. Lett.* **89**, 117203 (2002).
- [18] H. P. Büchler, G. Blatter, and W. Zwerger, *Phys. Rev. Lett.* **90**, 130401 (2003).
- [19] G. K. Campbell, J. Mun, M. Boyd, P. Medley, A. E. Leanhardt, L. G. Marcassa, D. E. Pritchard, and W. Ketterle, *Science* **313**, 649 (2006).
- [20] B. Damski, J. Zakrzewski, L. Santos, P. Zoller, and M. Lewenstein, *Phys. Rev. Lett.* **91**, 080403 (2003).
- [21] V. A. Kashurnikov, N. V. Prokofev, and B. V. Svistunov, *Phys. Rev. A* **66**, 031601(R) (2002).
- [22] D.-S. Lühmann, K. Bongs, and D. Pfannkuche, *J. Phys. B* **42**, 145305 (2009).
- [23] A. M. Rey, G. Pupillo, C. W. Clark, and C. J. Williams, *Phys. Rev. A* **72**, 033616 (2005).
- [24] M. Rigol, G. G. Batrouni, V. G. Rousseau, and R. T. Scalettar, *Phys. Rev. A* **79**, 053605 (2009).
- [25] P. Sengupta, M. Rigol, G. G. Batrouni, P. J. H. Denteneer, and R. T. Scalettar, *Phys. Rev. Lett.* **95**, 220402 (2005).
- [26] S. Wessel, F. Alet, M. Troyer, and G. G. Batrouni, *Phys. Rev. A* **70**, 053615 (2004).
- [27] H.-D. Meyer, U. Manthe, and L. S. Cederbaum, *Chem. Phys. Lett.* **165**, 73 (1990).
- [28] M. H. Beck, A. Jäckle, G. A. Worth, and H.-D. Meyer, *Phys. Rep.* **324**, 1 (2000).
- [29] O. E. Alon, A. I. Streltsov, and L. S. Cederbaum, *Phys. Rev. A* **77**, 033613 (2008).
- [30] O. E. Alon, A. I. Streltsov, and L. S. Cederbaum, *Phys. Rev. A* **76**, 062501 (2007).
- [31] A. I. Streltsov, O. E. Alon, and L. S. Cederbaum, *Phys. Rev. Lett.* **100**, 130401 (2008).
- [32] O. E. Alon, A. I. Streltsov, and L. S. Cederbaum, *Phys. Lett. A* **373**, 301 (2009).
- [33] A. I. Streltsov, O. E. Alon, and L. S. Cederbaum, *Phys. Rev. A* **80**, 043616 (2009).
- [34] A. U. J. Lode *et al.* *J. Phys. B: At. Mol. Opt. Phys* **42**, 044018 (2009).
- [35] K. Sakmann, A. I. Streltsov, O. E. Alon, and L. S. Cederbaum, *Phys. Rev. Lett.* **103**, 220601 (2009)

- [36] K. Sakmann, A. I. Streltsov, O. E. Alon, and L. S. Cederbaum, Phys. Rev. A **82**, 013620 (2010)
- [37] S. Kuhr, W. Alt, D. Schrader, M. Müller, and D. Gomer, V. and Meschede, Science **293**, 278 (2001).
- [38] S. Nussmann, M. Hijlkema, B. Weber, F. Rohde, G. Rempe, and A. Kuhn, Phys. Rev. Lett. **95**, 173602 (2005).
- [39] R. Folman, P. Krüger, J. Schmiedmayer, J. Denschlag, and C. Henkel, Adv. At. Mol. Opt. Phys. **48**, 263 (2002).
- [40] T. Gericke, C. Utfeld, N. Hommerstad, and H. Ott, Laser Phys. Lett. **3**, 415 (2006).
- [41] T. Kraemer *et al.*, Nature **440**, 315 (2006).
- [42] M. Albiez *et al.*, Phys. Rev. Lett. **95**, 010402 (2005).
- [43] G. J. Milburn, J. Corney, E. M. Wright, and D. F. Walls, Phys. Rev. A **55**, 4318 (1997).
- [44] A. Smerzi, S. Fantoni, S. Giovanazzi, and S. R. Shenoy, Phys. Rev. Lett. **79**, 4950 (1997).
- [45] T. Anker *et al.*, Phys. Rev. Lett. **94**, 020403 (2005).
- [46] S. Zöllner, H.-D. Meyer, and P. Schmelcher, Phys. Rev. Lett. **100**, 040401 (2008)
- [47] S. Zöllner, H.-D. Meyer, and P. Schmelcher, Phys. Rev. A **78**, 013621 (2008).
- [48] L. D. Carr, D. R. Dounas-Frazer and M. A. Garcia-March, EPL **90**, 10005 (2010).
- [49] D. R. Dounas-Frazer, A. M. Hermundstad, and L. D. Carr, Phys. Rev. Lett. **99**, 200402 (2007).
- [50] T. Köhler, K. Góral, and P. S. Julienne, Rev. Mod. Phys. **78**, 1311 (2006).
- [51] D. M. Bauer *et al.*, Nature Physics **5**, 339 (2009).
- [52] B. Chatterjee, I. Brouzos, S. Zöllner and P. Schmelcher, Phys. Rev. A **82**, 043619 (2010)
- [53] C. J. Myatt *et al.*, Phys. Rev. Lett. **78**, 586 (1997).
- [54] D. S. Hall *et al.*, Phys. Rev. Lett. **81**, 1539 (1998).
- [55] P. Maddaloni *et al.*, Phys. Rev. Lett. **85**, 2413 (2000).
- [56] G. Modugno *et al.*, Phys. Rev. Lett. **89**, 190404 (2002).

- [57] J. Catani *et al.*, Phys. Rev. A **77**, 011603 (2008).
- [58] M. A. Cazalilla and A. F. Ho, Phys. Rev. Lett. **91**, 150403 (2003).
- [59] O. E. Alon, A. I. Streltsov, and L. S. Cederbaum, Phys. Rev. Lett. **97**, 230403 (2006).
- [60] T. Mishra, R. V. Pai, and B. P. Das, Phys. Rev. A **76**, 013604 (2007).
- [61] T. Roscilde and J. I. Cirac, Phys. Rev. Lett. **98**, 190402 (2007).
- [62] A. Kleine, C. Kollath, I. P. McCulloch, T. Giamarchi, and U. Schollwöck, Phys. Rev. A **77**, 013607 (2008).
- [63] M. D. Girardeau and A. Minguzzi, Phys. Rev. Lett. **99**, 230402 (2007).
- [64] S. Zöllner, H.-D. Meyer, and P. Schmelcher, Phys. Rev. A **78**, 013629 (2008).
- [65] Y. Hao and S. Chen, Eur. Phys. J. D **51**, 261 (2009).
- [66] Y. Hao, Y. Zhang, X.-W. Guan, and S. Chen, Phys. Rev. A **79**, 033607 (2009).
- [67] E. Tempfli, S. Zöllner, and P. Schmelcher, New J. Phys. **11**, 073015 (2009).
- [68] A. Hu, L. Mathey, I. Danshita, E. Tiesinga, C. J. Williams, C. W. Clark, , Phys. Rev. A **80**, 023619 (2009).
- [69] L-M. Kuang and Z-W Ouyang, Phys. Rev. A **61**, 023604 (2000).
- [70] X. Q. Xu, L. H. Lu, Y. Q. Li, Phys. Rev. A **78** , 043609 (2008).
- [71] G. Mazzarella, M. Moratti, L. Salasnich, M. Salerno, F. Toigo, J. Phys. B: At. Mol. Opt. **42**, 125301 (2009).
- [72] I. I. Satija, R. Balakrishnan, P. Naudus, J. Heward, M. Edwards, C. W. Clark, Phys. Rev. A **79**, 033616 (2009).
- [73] B. Julia-Diaz, M. Guilleumas, M. Lewenstein, A. Polls, A. Sanpera, Phys. Rev. A **80**, 023616 (2009).
- [74] B. Sun, M. S. Pindzola, Phys. Rev. A **80**, 033616 (2009).
- [75] A Naddeo, R Citro, J. Phys. B: At. Mol. Opt. Phys **43**, 135302 (2010).
- [76] A. Hu, L. Mathey, E. Tiesinga, I. Danshita, C. J. Williams, C. W. Clark, arXiv:1103.3513v2 (2011)
- [77] A.C. Pflanzner, S. Zöllner and P. Schmelcher, J. Phys. B (FT) **42**, 231002 (2009).
- [78] A.C. Pflanzner, S. Zöllner and P. Schmelcher, Phys. Rev. A **81**, 023612 (2010).

- [79] B. Chatterjee, I. Brouzos, Lushai Cao and P. Schmelcher, arXiv:1105.3850v1 (2011)
- [80] A. M. Rey. *Ultracold bosonic atoms in optical lattices*. PhD thesis, University of Maryland at College Park, 2004.
- [81] O. Morsch, and M. Oberthaler, Rev. Mod. Phys. **78**, 179 (2006).
- [82] M. Lewenstein, A. Sanpera, D. Bogdan, A. Sen(De), and U. Sen, Adv. Phys. **56**, 243 (2007).
- [83] K. Huang and C. N. Yang. Phys. Rev. **105**, 767 (1957).
- [84] S. Inouye, M. R. Andrews, J. Stenger, H.-J. Miesner, D. M. Stamper-Kurn, and W. Ketterle, Nature **392**, 151 (1998).
- [85] T. Bergeman, M. G. Moore, and M. Olshanii, Phys. Rev. Lett. **91**, 163201 (2003)
- [86] J. I. Kim, V. S. Melezhik, and P. Schmelcher, Phys. Rev. Lett. **97**, 193203 (2006).
- [87] E. H. Lieb and R. Seiringer, Phys. Rev. Lett. **88**, 170409 (2002).
- [88] M. D. Girardeau, E. M. Wright, and J. M. Triscari, Phys. Rev. A **63**, 033601 (2001).
- [89] F. Deuretzbacher et al., Phys. Rev. Lett. **100**, 160405 (2008)
- [90] N. W. Ashcroft and N. D. Mermin. *Solid State Physics*. Brooks Cole, USA, 1976.
- [91] M. Greiner, O. Mandel, T. Esslinger, T. W. Hänsch, and I. Bloch, Nature **415**, 39 (2002).
- [92] I. Brouzos, S. Zöllner and P. Schmelcher, Phys. Rev. A **81**, 053613 (2010).
- [93] T. D. Kühner and H. Monien, Phys. Rev. B. **58**, 14741 (1999).
- [94] E. Altman, W. Hofstetter, E. Demler, and M. D. Lukin, New J. Phys. **5** , 113, (2003).
- [95] P. A. M. Dirac. Proc. Cambridge Philos. Soc. **26**, 376, (1930).
- [96] R. Kosloff and H. Tal-Ezer, Chem. Phys. Lett. **127**, 223 (1986).
- [97] H.-D. Meyer and G. A. Worth, Theor. Chem. Acc. **109**, 251 (2003).
- [98] H.-D. Meyer, F. L. Quéré, C. Léonard, and F. Gatti, Chem. Phys. **329**, 179 (2006).
- [99] S. Zöllner, *One-dimensional Few-boson Systems in Single- and Double-well Traps*. PhD thesis, Ruperto-Carola University of Heidelberg, 2008.

- [100] M. A. Cirone, K. Góral, K. Rzazewski, and M. Wilkens, *J. Phys. B* **34**, 4571 (2001).
- [101] M. Abramowitz and I. A. Stegun. *Handbook of Mathematical Functions*. Dover, New York, 1972.
- [102] J. J. Sakurai, *Modern Quantum Mechanics*. Addison-Wesley, New York, 1994.
- [103] O. Penrose and L. Onsager, *Phys. Rev.* **104**, 576, (1956).
- [104] P. Nozieres, D. Saint James, *J. Phys. (Paris)* **43**, 1133 (1982);
- [105] A. N. Salgueiro *et al.*, *Eur. Phys. J. D* **44**, 537 (2007).
- [106] L. Wang, Y. Hao, and S. Chen, *Eur. Phys. J. D* **48**, 229 (2008)
- [107] A. P. Tonel, J. Links, and A. Foerster, *J. Phys. A* **38**, 1235 (2005).
- [108] C. E. Creffield, *Phys. Rev. A* **75**, 031607 (2007).
- [109] S. Zöllner, H.-D. Meyer, and P. Schmelcher, *Phys. Rev. A* **74**, 053612 (2006).
- [110] S. Will *et al.*, *Nature* **465**, 197-201 (2010).
- [111] P. I. Schneider, S. Grishkevich, and A. Saenz, *Phys. Rev. A* **80**, 013404 (2009).
- [112] K. Sakmann, A. I. Streltsov, O. E. Alon, and L. S. Cederbaum, *New J. Phys.* **13**, 043003 (2011)
- [113] T. Ernst, T. Paul and P. Schlagheck, *Phys. Rev. A* **81**, 013631 (2010).
- [114] P. Schlagheck, F. Malet, J. C. Cremon and S. M. Reimann, *New J. Phys.* **12**, 065020 (2010).
- [115] A. I. Streltsov, K. Sakmann, O. E. Alon, and L. S. Cederbaum , *Phys. Rev. A* **83**, 043604 (2011).
- [116] F. Grossmann et al., *Phys. Rev. Lett.* **67**, 516 (1991).
- [117] J. Gong, L. M-Molina, and P. Hanggi, *Phys. Rev. Lett.* **103**, 133002 (2009).

Acknowledgements

Many people have directly or indirectly helped me with my PhD and I take this opportunity to thank them.

Firstly, I would like to thank Prof. Dr. Lorenz S. Cederbaum and Prof. Dr. Peter Schmelcher, for providing me the opportunity to work in this fascinating field and providing active support throughout my PhD. My sincere thanks to all my group members past and present who provided a wonderful company and working environment. In particular, I would like to thank the people of my sub-group - Yiannis Brouzos and Lushai Cao with whom I had great time together with many useful discussions and collaborations. My sincere thanks to all my friends and roommates in Heidelberg and Hamburg. Their company in a big way helped me adjust to the life in a foreign country. My biggest thanks is to my parents. Even while being far away, they have been a source of constant support and encouragement throughout the course of my work.

Eidesstattliche Erklärung

Ich erkläre hiermit, dass ich die vorgelegte Dissertation selbst verfasst und mich keiner anderen als der von mir ausdrücklich bezeichneten Quellen und Hilfen bedient habe.

Heidelberg, den 31.05.2011

Budhaditya Chatterjee